Lattice Boltzmann Method in Theory and in Application to Coupled Problems

Master Thesis

Daniel Heubes

supervising
Prof. Dr. Michael Günther
Dr. Andreas Bartel

University of Wuppertal
Faculty of Mathematics and Natural Sciences

Chair of
Applied Mathematics / Numerical Analysis
Prof. Dr. Michael Günther

July 2, 2010

Declaration of Authorship

I declare that I have authored this thesis independently, that I have not used other than the declared sources, and that I have explicitly marked all material which has been quoted either literally or by content from the used sources.

Wuppertal, July 2, 2010

(Daniel Heubes)

Contents

List of Figures

List of Tables

Introduction and Overview

Flows are in general described by the Navier-Stokes equations. When simulating real physical processes where fluid flows play a major role, one is especially interested in solving the Navier-Stokes equations. Unfortunately, analytical solutions of the Navier-Stokes equations are in general not present. Finding an approximation of the solution numerically is a common procedure in the cases when no analytical solutions are present. Several possibilities to do this are known, conventional methods in computational fluid dynamics solve the Navier-Stokes equations directly. In recent years, an alternative approach for finding approximating solutions of the Navier-Stokes equations appeared. This approach is based on solving the discrete Boltzmann equation and is known as the lattice Boltzmann method. The Boltzmann equation describes phenomena of the fluid microscopically based on particle densities and collisions. Using the lattice Boltzmann method to simulate fluid flows means to not solve the Navier-Stokes equations directly, instead one uses the aspect that from the Boltzmann equation the Navier-Stokes equations can be recovered in a hydrodynamic limit. Since this method was mentioned for the first time, the lattice Boltzmann method becomes increasingly popular especially as an approach for simulating flows through complex media.
Apart from the Navier-Stokes equations, the evolution of temperature in a fluid is described by an additional equation. The form of this equation depends on the effects that are considered. In a very basic form, the advection-diffusion equation is sufficient to describe the temperature evolution. This equation explicitly depends on the fluid's velocity whose evolution is described by the Navier-Stokes equations. In this way, the advection-diffusion equation is coupled to the Navier-Stokes equations. A coupling of different manner appears if the fluid flow is also influenced by the temperature evolution, and not only the other way round. If one is interested in numerically simulating physical processes described by the full set of coupled equations, a method is necessary which considers these couplings. Hence, one cannot solve each equation separately. This work is concerned with the topics described above.
We organize it as follows, in chapter 1 we give a short historical background of lattice Boltzmann methods and derive the lattice Boltzmann method for fluid flows in detail. Afterwards, we show in a multi-scale expansion, that the numerical method approximates the incompressible Navier-Stokes equations. Hence, we verify that the lattice Boltzmann model can successfully be used to simulate fluid flows. The complete first chapter can bee seen as an detailed theoretical look on the main concept of the lattice

Boltzmann method. Nevertheless, the main concept alone is insufficient to apply the numerical method to real physical problems.
In chapter 2 we enhance the method determined in the foregoing chapter. We present different types of boundary conditions. Without boundary conditions an implementation of the lattice Boltzmann method, and thus the application to physical problems, is impossible. Moreover, we present a little modification of the main concept which allows us to simulate fluid flows under the influence of an acting force. This force needs not necessarily to be homogeneous. The focus of chapter 2 however lies on solving the advection-diffusion equation for the temperature coupled to the Navier-Stokes equations. Therefore, we deduce an energy conservation equation directly from the Boltzmann equation and transform it to the advection-diffusion equation. We propose a numerical method to approximate the solution of the advection-diffusion equation. The proposed method is closely related to the lattice Boltzmann method for fluid flows. Again in a multi-scale expansion we verify that method. We finish this chapter by describing buoyancy effects macroscopically and showing how these effects can be realized with the previously determined methods.
In the last chapter of the main part, chapter 3, we present some numerical tests to emphasize the capability of the presented methods to simulate problems described by the Navier-Stokes equations in conjunction with the advection-diffusion equation. We simulate a two- and a three-dimensional Poiseuille flow and compare our simulation with the analytical solution of it. Furthermore, we simulate a flow past a rectangular and a cuboid obstacle, respectively. These simulations show the capability of the lattice Boltzmann method for fluid flows. Afterwards, we take also the second method into account, thus we can approximately solve problems satisfying the Navier-Stokes equations and the advection-diffusion equation. We test the coupled method by simulating Rayleigh-Bénard convection. We perform the simulation of Rayleigh-Bénard convection in two as well as three dimension. The simulation of Rayleigh-Bénard convection considers especially buoyancy effects. Approximating solutions of the heat equation is also possible with our model and we give one example.
Finally, subsequent to the last chapter of the main part we give an outlook. There we talk about some nice features the determined methods can be used for and we mention some further enhancements which, in our opinion, are very interesting.

CHAPTER 1

Lattice Boltzmann Method for Fluid Flows

In this chapter we develop a numerical method capable of simulating the motion of a fluid flow. This method is known as the lattice Boltzmann method (LBM) and satisfies the incompressible Navier-Stokes equations.
The LBM is a relatively new numerical scheme. It has recently achieved considerable success in simulating fluid flows in porous media [23] and associated transport phenomena [10]. This method has been shown to be particularly useful in application involving interfacial dynamics. While traditional methods in Computational Fluid Dynamics (CFD) solve the Navier-Stokes equations directly [19, 36] (and related [13, 52]), the lattice Boltzmann method solves the Boltzmann equation from which the Navier-Stokes equations can be recovered. The Boltzmann equation describes phenomena of the fluid microscopically based on particle densities and collisions.

All calculations within this chapter concerning the Boltzmann equation and the lattice Boltzmann method are performed for the three dimensional case and are kept general as long as easily possible. At some points the calculations are done for a specific three dimensional model (D3Q19), but they can also be transferred for most models analogue.

In the subsequent section we briefly describe cellular automata (CA) and we introduce lattice gas automata (LGA) which are closely related to CA and can be seen as the forebears of the lattice Boltzmann method [42]. Afterwards, we present the Boltzmann equation and show that the Navier-Stokes equations are recovered. Then we develop the numerical scheme, the lattice Boltzmann method, based on the Boltzmann equation where we approximate the collision term by a single time relaxation term. The lattice Boltzmann method, or more precisely the lattice Bhatnagar-Gross-Krook (LBGK) method due to the approximation of the collision term, is achieved by discretizing the Boltzmann equation appropriately. Finally, we show by a multi-scale expansion that the numerical scheme satisfies the incompressible Navier-Stokes equations.

1.1. Historical Background and Basics

For a better understanding of the lattice Boltzmann method, we primarily begin this chapter with a short introduction to cellular automata and lattice gas gas automata.

Historically, the lattice Boltzmann method is based on lattice gas automata. Probably, the latter can be better understood with at least little knowledge of cellular automata.

1.1.1. Cellular Automata

A cellular automaton is a discrete model which was introduced by John von Neumann [66]. A formal description of a D-dimensional cellular automata can be made by introducing a set $\mathcal{C} \subset \mathbb{Z}^D$ describing the position of the cells $\boldsymbol{C}_i \in \mathcal{C},\ i = 1, \ldots, m_c$ [34]. The cells are arranged regularly and each cell holds a state. The state of cell $\boldsymbol{C}_i$ is denoted by $s_i \in \mathcal{S}$, with the finite set of possible states $\mathcal{S} \subset \mathbb{Z}$, which does not depend on the cell itself. At discrete time levels the states are updated simultaneously by prescribed deterministic rules. These local rules are given by a mapping $r : \mathcal{S}^{m_n} \to \mathcal{S}$, where m_n gives the number of elements in the neighborhood $\mathcal{N}$. For interior cells the elements of the neighborhood $\mathcal{N} = \{\boldsymbol{N}_1, \ldots, \boldsymbol{N}_{m_n}\} \subset \mathbb{Z}^D$ have to be interpreted as relative coordinates of neighboring cells, this means that $\boldsymbol{C}_i + \boldsymbol{N}_j \in \mathcal{C}$ for all $i \in \mathbb{Z}$ and $j = 1, \ldots, m_n$. Boundary cells are updated due to some appropriate update rules. We assume that $(0, \ldots, 0) \in \mathcal{N}$, i.e. the updated state of cell $\boldsymbol{C}_i$ depends at least on the current state of cell $\boldsymbol{C}_i$.

As an illustrating example, we consider a one-dimensional cellular automaton consisting of 400 cells with only two possible states at each cell. We assume the two possible states are $\mathcal{S} = \{0, 1\}$ and the updating rule depends only on the two nearest adjacent cells and the cell itself, i.e. $\mathcal{N} = \{-1, 0, 1\}$.
Thus, the cellular automaton is fully described by the updating rules, more precisely by the values $r_i \in \mathcal{S},\ i = 0, \ldots, 7$ on the right hand sides of (1.1). The state of each cell is updated by the following rule

$$s_i' = r(s_{i-1}, s_i, s_{i+1}), \qquad i = 2, \ldots, 399,$$

where s_i' is the updated state and s_{i-1}, s_{i+1} are the states of the left and right adjacent cell, respectively. States of cell C_1 and C_{400} are set to 0 and are not updated. Eight combinations of states determine the rule

$$\begin{aligned} r(0,0,0) &= r_0, \qquad r(0,0,1) = r_1, \\ r(0,1,0) &= r_2, \qquad r(0,1,1) = r_3, \\ r(1,0,0) &= r_4, \qquad r(1,0,1) = r_5, \\ r(1,1,0) &= r_6, \qquad r(1,1,1) = r_7. \end{aligned} \tag{1.1}$$

Since we allow two states there exist $2^8 = 256$ different updating rules. Figure 1.1 illustrates the evolution of the cellular automaton with specified values $r_{0,2,5,7} = 0$ and $r_{1,3,4,6} = 1$, also known as rule 90 after the notation of Wolfram [70].

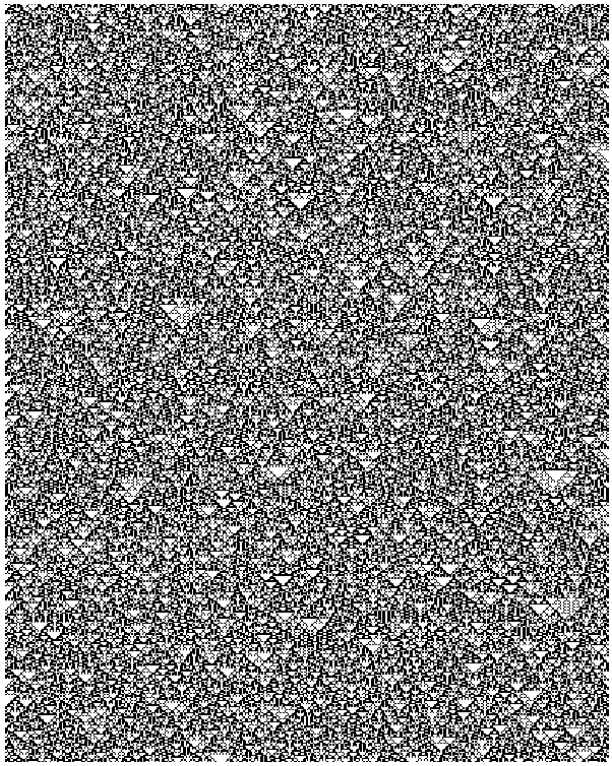

Figure 1.1.: Evolution of a one-dimensional, two-state, two-neighbor cellular automata. Initial states (top line) are chosen randomly with 50% probability to have state 1 (black square) and 50% probability to have state 0 (white square). Subsequent time levels are shown with progressing lines from top to bottom.

1.1.2. Lattice Gas Automata

Lattice gas automata are derived from classical cellular automata after some modifications [69]. These modifications simplify the construction and application of automata to given physical processes. For instance, unlike the first lattice gas automaton, introduced by Hardy, de Pazzis and Pomeau (HPP model) [25], today there exist lattice gas automata which lead to the Navier-Stokes equations in the macroscopic limit [71]. Hence, they are capable to simulate fluid flows successfully. Despite of their relatively simple nature, lattice gas automata can be applied in less simple themes such as for instance in the simulation of flows through porous media [9].

As the basic principle of the lattice Boltzmann method and lattice gas automata is the same, we discuss this principle here in some detail.
The first introduced lattice gas automaton (the HPP model) was proposed as a new however not working technique for the numerical study of the Navier-Stokes equations. Instead of a direct integration of partial differential equations (PDEs) LGA are based on the simulation of a very simple microscopic system. Here, particles are allowed to move on a regular lattice, and local collision rules are introduced on the nodes which

conserve the number of particles and momentum.

The following description will be done generally [69] but with a supporting accompanying example. The chosen example uses a triangular lattice (see figure 1.2) and was introduced by Frisch, Hasslacher and Pomeau (FHP model) in 1986 [20]. The FHP model was the first LGA which successfully yields the Navier-Stokes equations in the macroscopic limit. The major difference between the HPP and FHP model is the usage of a triangular lattice in the latter compared to a square lattice in the former. This leads to an specific isotropic tensor of rank four in FHP but not in HPP which is necessary to achieve the Navier-Stokes equations, see [69] for details.

The first step of a formal description of LGA lies in defining a regular lattice in space. Depending on the lattice a number of k lattice vectors $\boldsymbol{d}_i$, $i = 1, \ldots, k$, are introduced which connect nearest neighbors. For the FHP model they read

$$\boldsymbol{d}_i = \left(\cos\left(\frac{\pi}{3}i\right), \sin\left(\frac{\pi}{3}i\right)\right), \qquad i = 1, \ldots, 6,$$

and are shown in figure 1.3. Furthermore, all particles shall have the same mass m. Then, each lattice node consists of a set of k cells with binary state. The state of each cell is given by

$$n_i(\boldsymbol{x}, t) = \begin{cases} 0, & \text{cell } i \text{ is not occupied by a particle} \\ 1, & \text{cell } i \text{ is occupied by a particle} \end{cases}, \qquad i = 1, \ldots, k.$$

Here, t and $\boldsymbol{x}$ indicate time and the position of the corresponding node, respectively. Each cell may contain at most one particle. We combine all k state functions of the

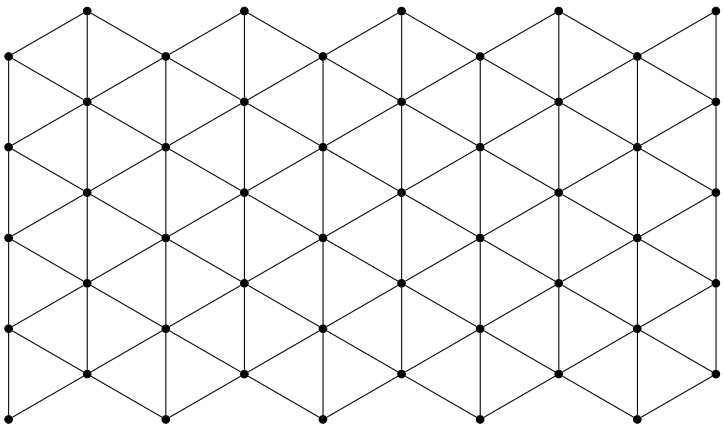

Figure 1.2.: Triangular lattice used in the FHP model.

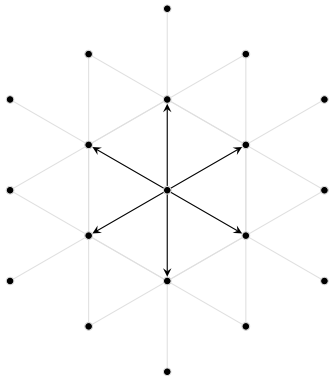

Figure 1.3.: Lattice vectors of the FHP model.

same node in

$$\boldsymbol{n}(\boldsymbol{x},t) = \begin{pmatrix} n_1(\boldsymbol{x},t) \\ n_2(\boldsymbol{x},t) \\ \vdots \\ n_k(\boldsymbol{x},t) \end{pmatrix}.$$

Like cellular automata, LGA are discrete time models, the states of nodes or cells are updated at the discrete time levels simultaneously, where the updating process consists of two parts. One part is referred to as collision and the other as streaming. Connecting each cell of a node to a corresponding lattice vector (see figure 1.4) helps determining collision rules as well as understanding both updating parts.
In the streaming part particles are transfered from node to node, more precisely the state of cell i at node with position $\boldsymbol{x}$ is transfered to the state of cell i at node with

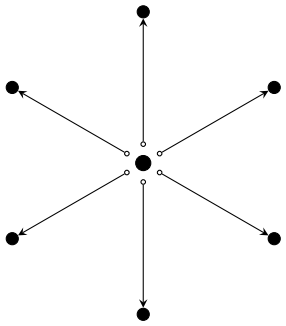

Figure 1.4.: Connection of cells (tiny empty circles) and lattice vectors in the case of FHP model.

position $\boldsymbol{x} + \boldsymbol{d}_i$, i.e.

$$n_i(\boldsymbol{x} + \boldsymbol{d}_i, t + \Delta t) = n_i(\boldsymbol{x}, t), \qquad i = 1, \ldots, k. \tag{1.2}$$

The time step Δt is set to 1, hence lattice vectors can also be interpreted as lattice velocities since $\boldsymbol{d}_i$ and $\frac{\boldsymbol{d}_i}{\Delta t}$ have the same numerical value.
The other part, collision, is best described by local rules which only depend on and alternate the state of the node, i.e. the state of cells at that node. The collision rules should be chosen such that they conserve the number of particles and momentum. Since their choice is influenced by the applied lattice, we cannot give the rules in general, hence we only give the rules of the original FHP model, see figure 1.5. In the first introduced FHP model only two and three particle collisions are considered. For the two particle head on collision there are two possible outcomes which conserve the number of particles and momentum and one has to take a choice randomly. Configurations not listed in figure 1.5 are not affected due to collision.
An implementation can be realized by first changing the states of cells at each node based on the collision rules, and afterwards applying the streaming process. The following equation contains both parts of this procedure, thus the complete evolution of LGA is given by

$$n_i(\boldsymbol{x} + \boldsymbol{d}_i, t + \Delta t) - n_i(\boldsymbol{x}, t) = \Psi_i\left(\boldsymbol{n}(\boldsymbol{x}, t)\right), \qquad i = 1, \ldots, k. \tag{1.3}$$

The left hand side describes the streaming part, compare (1.2), and the right hand side is a collision function. When expressing the states after applying the collision rules by $\tilde{\boldsymbol{n}}(\boldsymbol{x}, t)$ we can define the collision function by

$$\boldsymbol{\Psi}\left(\boldsymbol{n}(\boldsymbol{x}, t)\right) = \begin{pmatrix} \Psi_1\left(\boldsymbol{n}(\boldsymbol{x}, t)\right) \\ \vdots \\ \Psi_k\left(\boldsymbol{n}(\boldsymbol{x}, t)\right) \end{pmatrix} = \tilde{\boldsymbol{n}}(\boldsymbol{x}, t) - \boldsymbol{n}(\boldsymbol{x}, t),$$

where $\boldsymbol{n}(\boldsymbol{x}, t)$ denotes the states before collision.

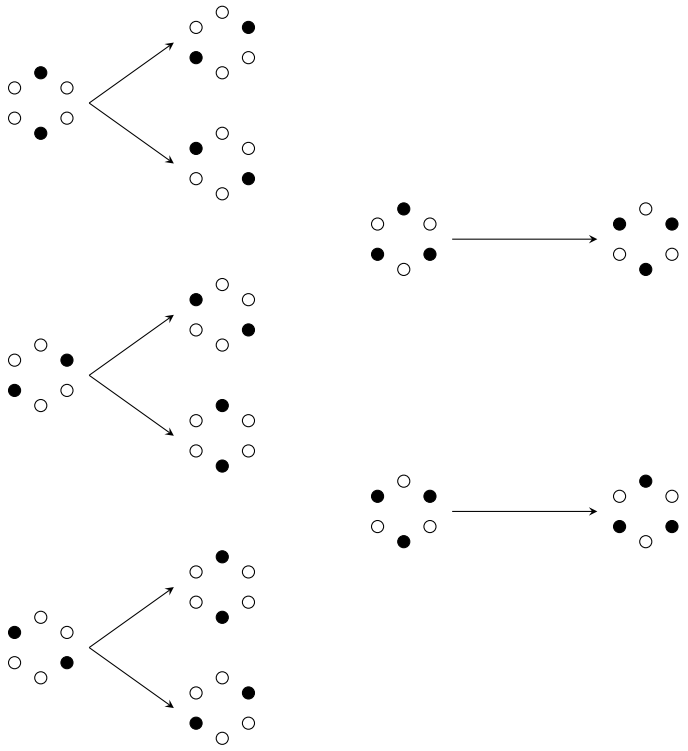

Figure 1.5.: Collision rules used in the FHP model. Empty circles indicate a state of 0, whereas solid circles are occupied cells of state 1. Left column contains two particle collisions, right column contains three particle collisions.

1.2. The Boltzmann Equation

The classical Boltzmann equation reads [61]

$$\frac{\partial f(\boldsymbol{x},\boldsymbol{v},t)}{\partial t} + \boldsymbol{v}\cdot\boldsymbol{\nabla} f(\boldsymbol{x},\boldsymbol{v},t) = Q(f,f), \tag{1.4}$$

defined for $\boldsymbol{v}\in\mathbb{R}^3$, $t>0$ and to avoid the treatment of boundaries we investigate the equation for $\boldsymbol{x}\in\mathbb{R}^3$ in the current chapter. The symbol $\boldsymbol{\nabla}$ expresses the partial differential operators with respect to space $\boldsymbol{x}$. The Boltzmann equation is an evolution equation in time t for the single particle distribution $f(\boldsymbol{x},\boldsymbol{v},t)$. The value $f(\boldsymbol{x},\boldsymbol{v},t)\,\mathrm{d}\boldsymbol{x}\,\mathrm{d}\boldsymbol{v}$ for all infinitesimal small $\mathrm{d}\boldsymbol{x}$ and $\mathrm{d}\boldsymbol{v}$ represents the number of particles which at time t have position $\boldsymbol{x}$ and velocity $\boldsymbol{v}$, multiplied by the constant particle mass m. In general the right hand side of (1.4) represents the collision term which is here expressed as a collision integral [69]

$$Q(f,f) = \int_{\mathbb{R}^3}\int_{\mathbb{S}^2} \sigma(\Omega)|\boldsymbol{v}-\boldsymbol{w}|\left[f(\boldsymbol{x},\boldsymbol{v}',t)f(\boldsymbol{x},\boldsymbol{w}',t) - f(\boldsymbol{x},\boldsymbol{v},t)f(\boldsymbol{x},\boldsymbol{w},t)\right]\,\mathrm{d}\Omega\,\mathrm{d}\boldsymbol{w}. \tag{1.5}$$

This collision integral is based on several assumptions [54]. One condition is that the particles interact only in two-particle collisions, this means we assume that interactions involving more then two particles can be neglected. For all two-particle collisions we assume that they appear locally in the sense that they take place at a single point $\boldsymbol{x}$. A similar condition holds for time t, it is assumed that the duration of a collision is negligible. Particles involved in a collision are assumed to be uncorrelated, and the collision itself is modeled as an elastic collision, meaning that kinetic energy and especially momentum are conserved. The velocities before collision are denoted by $\boldsymbol{v}$ and $\boldsymbol{w}$, and the velocities after collision by $\boldsymbol{v}'$ and $\boldsymbol{w}'$. Since the collision is elastic the following two equations have to be fulfilled (note that particles have same mass m):

$$\boldsymbol{v} + \boldsymbol{w} = \boldsymbol{v}' + \boldsymbol{w}' \quad \text{and} \quad |\boldsymbol{v}|^2 + |\boldsymbol{w}|^2 = |\boldsymbol{v}'|^2 + |\boldsymbol{w}'|^2.$$

The post-collision velocities $\boldsymbol{v}'$ and $\boldsymbol{w}'$ can be computed in dependence of the pre-collision velocities $\boldsymbol{v}$, $\boldsymbol{w}$ and the impact angle. In (1.5) $\sigma(\Omega)$ denotes the differential collision cross section and the inner integration is done over all possible solid angles Ω.

We define macroscopic quantities over integrals of the particle distribution $f(\boldsymbol{x}, \boldsymbol{v}, t)$. In detail, the mass density $\rho(\boldsymbol{x}, t)$ is given by

$$\rho(\boldsymbol{x}, t) = \int_{\mathbb{R}^3} f(\boldsymbol{x}, \boldsymbol{v}, t)\, \mathrm{d}\boldsymbol{v} \tag{1.6}$$

and the macroscopic velocity $\boldsymbol{u}(\boldsymbol{x}, t)$ is defined as

$$\rho(\boldsymbol{x}, t)\boldsymbol{u}(\boldsymbol{x}, t) = \int_{\mathbb{R}^3} \boldsymbol{v} f(\boldsymbol{x}, \boldsymbol{v}, t)\, \mathrm{d}\boldsymbol{v}. \tag{1.7}$$

With these definitions we are able to deduce the continuity equation and the conservation equation for momentum from the Boltzmann equation.
Furthermore, we define the temperature $T(\boldsymbol{x}, t)$ by

$$\rho(\boldsymbol{x}, t)\frac{3}{2}\frac{k_B T(\boldsymbol{x}, t)}{m} = \int_{\mathbb{R}^3} \frac{|\boldsymbol{v} - \boldsymbol{u}(\boldsymbol{x}, t)|^2}{2} f(\boldsymbol{x}, \boldsymbol{v}, t)\, \mathrm{d}\boldsymbol{v}, \tag{1.8}$$

with Boltzmann constant k_B and particle mass m. This equation will be used later but not in the derivation of the continuity equation and momentum equation.

1.2.1. Continuity Equation

We derive the continuity equation by integrating the Boltzmann equation over velocity space. The left hand side of the Boltzmann equation is denoted as $B(\boldsymbol{x}, \boldsymbol{v}, t)$ in the

following.

$$\begin{aligned}\int_{\mathbb{R}^3} B(\boldsymbol{x},\boldsymbol{v},t)\,\mathrm{d}\boldsymbol{v} &:= \int_{\mathbb{R}^3} \frac{\partial}{\partial t} f(\boldsymbol{x},\boldsymbol{v},t)\,\mathrm{d}\boldsymbol{v} + \int_{\mathbb{R}^3} \boldsymbol{v}\cdot\boldsymbol{\nabla} f(\boldsymbol{x},\boldsymbol{v},t)\,\mathrm{d}\boldsymbol{v} \\ &= \frac{\partial}{\partial t}\int_{\mathbb{R}^3} f(\boldsymbol{x},\boldsymbol{v},t)\,\mathrm{d}\boldsymbol{v} + \boldsymbol{\nabla}\cdot\int_{\mathbb{R}^3} \boldsymbol{v} f(\boldsymbol{x},\boldsymbol{v},t)\,\mathrm{d}\boldsymbol{v} \\ &= \frac{\partial}{\partial t}\rho(\boldsymbol{x},t) + \boldsymbol{\nabla}\cdot(\rho(\boldsymbol{x},t)\boldsymbol{u}(\boldsymbol{x},t)).\end{aligned}$$

For the right hand side it follows [5]

$$\int_{\mathbb{R}^3} Q(f,f)\,\mathrm{d}\boldsymbol{v} = 0, \tag{1.9}$$

which leads by considering both sides to the continuity equation

$$\frac{\partial}{\partial t}\rho(\boldsymbol{x},t) + \boldsymbol{\nabla}\cdot(\rho(\boldsymbol{x},t)\boldsymbol{u}(\boldsymbol{x},t)) = 0.$$

1.2.2. Momentum Equation

In order to deduce the momentum equation we introduce a general form of the dot-product.

Notation. *For a matrix valued function*

$$A(\boldsymbol{x}) = \begin{pmatrix} a_{1,1}(\boldsymbol{x}) & a_{1,2}(\boldsymbol{x}) & \dots & a_{1,n}(\boldsymbol{x}) \\ a_{2,1}(\boldsymbol{x}) & a_{2,2}(\boldsymbol{x}) & \dots & a_{2,n}(\boldsymbol{x}) \\ \vdots & \vdots & & \vdots \\ a_{m,1}(\boldsymbol{x}) & a_{m,2}(\boldsymbol{x}) & \dots & a_{m,n}(\boldsymbol{x}) \end{pmatrix} = \begin{pmatrix} \boldsymbol{a}_1(\boldsymbol{x})^T \\ \boldsymbol{a}_2(\boldsymbol{x})^T \\ \vdots \\ \boldsymbol{a}_m(\boldsymbol{x})^T \end{pmatrix}$$

and the nabla operator

$$\boldsymbol{\nabla} = \begin{pmatrix} \frac{\partial}{\partial x_1} \\ \frac{\partial}{\partial x_2} \\ \vdots \\ \frac{\partial}{\partial x_n} \end{pmatrix} \tag{1.10}$$

we compute the dot-product of the nabla operator and a matrix valued function as follows:

$$\boldsymbol{\nabla} \cdot A(\boldsymbol{x}) = \begin{pmatrix} \boldsymbol{\nabla} \cdot \boldsymbol{a}_1(\boldsymbol{x}) \\ \boldsymbol{\nabla} \cdot \boldsymbol{a}_2(\boldsymbol{x}) \\ \vdots \\ \boldsymbol{\nabla} \cdot \boldsymbol{a}_m(\boldsymbol{x}) \end{pmatrix}.$$

With help of this notation, we derive the momentum equation by first multiplying the Boltzmann equation with $\boldsymbol{v}$ and then integrating over velocity space. The arising integrals read [5]

$$\int_{\mathbb{R}^3} \boldsymbol{v} Q(f,f)\,\mathrm{d}\boldsymbol{v} = \boldsymbol{0} \tag{1.11}$$

and

$$\int_{\mathbb{R}^3} \boldsymbol{v} B(\boldsymbol{x},\boldsymbol{v},t)\,\mathrm{d}\boldsymbol{v} = \int_{\mathbb{R}^3} \frac{\partial}{\partial t}\boldsymbol{v} f(\boldsymbol{x},\boldsymbol{v},t)\,\mathrm{d}\boldsymbol{v} + \int_{\mathbb{R}^3} \boldsymbol{v}\left(\boldsymbol{v}\cdot\boldsymbol{\nabla} f(\boldsymbol{x},\boldsymbol{v},t)\right)\,\mathrm{d}\boldsymbol{v}. \tag{1.12}$$

The first integral on the right hand side of the latter equation is easy to compute

$$\int_{\mathbb{R}^3} \frac{\partial}{\partial t}\boldsymbol{v} f(\boldsymbol{x},\boldsymbol{v},t)\,\mathrm{d}\boldsymbol{v} = \frac{\partial}{\partial t}\int_{\mathbb{R}^3} \boldsymbol{v} f(\boldsymbol{x},\boldsymbol{v},t)\,\mathrm{d}\boldsymbol{v} = \frac{\partial}{\partial t}(\rho(\boldsymbol{x},t)\boldsymbol{u}(\boldsymbol{x},t)), \tag{1.13}$$

where one has just to use the definition of the macroscopic velocity $\boldsymbol{u}$. For the second integral on the right hand side of (1.12) we use the following calculation [18]:

$$\begin{aligned}
\int_{\mathbb{R}^3} \boldsymbol{v}\left[\boldsymbol{v}\cdot\boldsymbol{\nabla} f(\boldsymbol{x},\boldsymbol{v},t)\right]\,\mathrm{d}\boldsymbol{v} &= \boldsymbol{\nabla}\cdot\int_{\mathbb{R}^3} \boldsymbol{v}\boldsymbol{v}^T f(\boldsymbol{x},\boldsymbol{v},t)\,\mathrm{d}\boldsymbol{v} \\
&= \boldsymbol{\nabla}\cdot\int_{\mathbb{R}^3} (\boldsymbol{v}-\boldsymbol{u}(\boldsymbol{x},t)+\boldsymbol{u}(\boldsymbol{x},t)) \\
&\qquad\qquad (\boldsymbol{v}-\boldsymbol{u}(\boldsymbol{x},t)+\boldsymbol{u}(\boldsymbol{x},t))^T f(\boldsymbol{x},\boldsymbol{v},t)\,\mathrm{d}\boldsymbol{v} \\
&= \boldsymbol{\nabla}\cdot\int_{\mathbb{R}^3} (\boldsymbol{v}-\boldsymbol{u}(\boldsymbol{x},t))\,(\boldsymbol{v}-\boldsymbol{u}(\boldsymbol{x},t))^T f(\boldsymbol{x},\boldsymbol{v},t)\,\mathrm{d}\boldsymbol{v} \\
&\quad + \boldsymbol{\nabla}\cdot\int_{\mathbb{R}^3} \boldsymbol{u}(\boldsymbol{x},t)\boldsymbol{u}(\boldsymbol{x},t)^T f(\boldsymbol{x},\boldsymbol{v},t)\,\mathrm{d}\boldsymbol{v} \\
&\quad + \boldsymbol{\nabla}\cdot\int_{\mathbb{R}^3} (\boldsymbol{v}-\boldsymbol{u}(\boldsymbol{x},t))\,\boldsymbol{u}(\boldsymbol{x},t)^T f(\boldsymbol{x},\boldsymbol{v},t)\,\mathrm{d}\boldsymbol{v} \\
&\quad + \boldsymbol{\nabla}\cdot\int_{\mathbb{R}^3} \boldsymbol{u}(\boldsymbol{x},t)\,(\boldsymbol{v}-\boldsymbol{u}(\boldsymbol{x},t))^T f(\boldsymbol{x},\boldsymbol{v},t)\,\mathrm{d}\boldsymbol{v},
\end{aligned} \tag{1.14}$$

where the first step can be seen by a calculation in appendix A.1. The mixed integrals in (1.14) vanish due to

$$\begin{aligned}\int_{\mathbb{R}^3} (\boldsymbol{v}-\boldsymbol{u}(\boldsymbol{x},t))\,\boldsymbol{u}(\boldsymbol{x},t)^T f(\boldsymbol{x},\boldsymbol{v},t)\,\mathrm{d}\boldsymbol{v} &= \int_{\mathbb{R}^3} \boldsymbol{v}\boldsymbol{u}(\boldsymbol{x},t)^T f(\boldsymbol{x},\boldsymbol{v},t)\,\mathrm{d}\boldsymbol{v} \\ &\quad - \int_{\mathbb{R}^3} \boldsymbol{u}(\boldsymbol{x},t)\boldsymbol{u}(\boldsymbol{x},t)^T f(\boldsymbol{x},\boldsymbol{v},t)\,\mathrm{d}\boldsymbol{v} \\ &= \int_{\mathbb{R}^3} \boldsymbol{v} f(\boldsymbol{x},\boldsymbol{v},t)\,\mathrm{d}\boldsymbol{v}\ \boldsymbol{u}(\boldsymbol{x},t)^T \\ &\quad - \boldsymbol{u}(\boldsymbol{x},t)\boldsymbol{u}(\boldsymbol{x},t)^T \int_{\mathbb{R}^3} f(\boldsymbol{x},\boldsymbol{v},t)\,\mathrm{d}\boldsymbol{v} \\ &= \rho(\boldsymbol{x},t)\boldsymbol{u}(\boldsymbol{x},t)\boldsymbol{u}(\boldsymbol{x},t)^T - \boldsymbol{u}(\boldsymbol{x},t)\boldsymbol{u}(\boldsymbol{x},t)^T\rho(\boldsymbol{x},t) \\ &= 0\end{aligned}$$

and an analogue computation for $\int_{\mathbb{R}^3} \boldsymbol{u}(\boldsymbol{x},t)\,(\boldsymbol{v}-\boldsymbol{u}(\boldsymbol{x},t))^T\, f(\boldsymbol{x},\boldsymbol{v},t)\,\mathrm{d}\boldsymbol{v}$.
Thus, the equation (1.14) simplifies to

$$\begin{aligned}\int_{\mathbb{R}^3} \boldsymbol{v}\,[\boldsymbol{v}\cdot\boldsymbol{\nabla} f(\boldsymbol{x},\boldsymbol{v},t)]\,\mathrm{d}\boldsymbol{v} &= \boldsymbol{\nabla}\cdot\int_{\mathbb{R}^3} (\boldsymbol{v}-\boldsymbol{u}(\boldsymbol{x},t))\,(\boldsymbol{v}-\boldsymbol{u}(\boldsymbol{x},t))^T\, f(\boldsymbol{x},\boldsymbol{v},t)\,\mathrm{d}\boldsymbol{v} \\ &\quad + \boldsymbol{\nabla}\cdot\int_{\mathbb{R}^3} \boldsymbol{u}(\boldsymbol{x},t)\boldsymbol{u}(\boldsymbol{x},t)^T f(\boldsymbol{x},\boldsymbol{v},t)\,\mathrm{d}\boldsymbol{v} \\ &= \boldsymbol{\nabla}\cdot\int_{\mathbb{R}^3} (\boldsymbol{v}-\boldsymbol{u}(\boldsymbol{x},t))\,(\boldsymbol{v}-\boldsymbol{u}(\boldsymbol{x},t))^T\, f(\boldsymbol{x},\boldsymbol{v},t)\,\mathrm{d}\boldsymbol{v} \\ &\quad + \boldsymbol{\nabla}\cdot\left(\rho(\boldsymbol{x},t)\boldsymbol{u}(\boldsymbol{x},t)\boldsymbol{u}(\boldsymbol{x},t)^T\right)\end{aligned}$$

and combining the latter equation with (1.11), (1.13) yields

$$\begin{aligned}&\frac{\partial}{\partial t}(\rho(\boldsymbol{x},t)\boldsymbol{u}(\boldsymbol{x},t)) + \boldsymbol{\nabla}\cdot\left(\rho(\boldsymbol{x},t)\boldsymbol{u}(\boldsymbol{x},t)\boldsymbol{u}(\boldsymbol{x},t)^T\right) \\ &\qquad = -\boldsymbol{\nabla}\cdot\int_{\mathbb{R}^3} (\boldsymbol{v}-\boldsymbol{u}(\boldsymbol{x},t))\,(\boldsymbol{v}-\boldsymbol{u}(\boldsymbol{x},t))^T\, f(\boldsymbol{x},\boldsymbol{v},t)\,\mathrm{d}\boldsymbol{v}.\end{aligned}$$

The integral represents the momentum flux tensor, whose entry at position (i,j) satisfies [30]

$$\int_{\mathbb{R}^3} \left(v^i - u^i(\boldsymbol{x},t)\right)\left(v^j - u^j(\boldsymbol{x},t)\right) f(\boldsymbol{x},\boldsymbol{v},t)\,\mathrm{d}\boldsymbol{v} = p(\boldsymbol{x},t)\delta_{ij} - \sigma_{i,j}(\boldsymbol{x},t),$$

with $p(\boldsymbol{x},t)$ denoting the pressure. On the right hand side, $p(\boldsymbol{x},t)\delta_{ij}$ is the portion of the equilibrium and therefore $\sigma_{i,j}(\boldsymbol{x},t)$ is referred to a correction term which expresses the dynamic portion in the momentum flux tensor. It holds for the correction tensor

$$\sigma(\boldsymbol{x},t) = \rho(\boldsymbol{x},t)\nu\left[\boldsymbol{\nabla}\boldsymbol{u}(\boldsymbol{x},t) + (\boldsymbol{\nabla}\boldsymbol{u}(\boldsymbol{x},t))^T\right],$$

with kinematic viscosity ν. In vector notation, the momentum flux tensor exhibits the form

$$\begin{aligned}\int_{\mathbb{R}^3} (\boldsymbol{v}-\boldsymbol{u}(\boldsymbol{x},t))\,(\boldsymbol{v}-\boldsymbol{u}(\boldsymbol{x},t))^T f(\boldsymbol{x},\boldsymbol{v},t)\,\mathrm{d}\boldsymbol{v} \\ = p(\boldsymbol{x},t)I - \rho(\boldsymbol{x},t)\nu\left[\boldsymbol{\nabla}\boldsymbol{u}(\boldsymbol{x},t) + (\boldsymbol{\nabla}\boldsymbol{u}(\boldsymbol{x},t))^T\right],\end{aligned} \tag{1.15}$$

with identity matrix I. Eventually, it follows the momentum conservation equation

$$\begin{aligned}\frac{\partial}{\partial t}(\rho(\boldsymbol{x},t)\boldsymbol{u}(\boldsymbol{x},t)) + \boldsymbol{\nabla}\cdot\left(\rho(\boldsymbol{x},t)\boldsymbol{u}(\boldsymbol{x},t)\boldsymbol{u}(\boldsymbol{x},t)^T\right) \\ = -\boldsymbol{\nabla}p(\boldsymbol{x},t) + \boldsymbol{\nabla}\cdot\left(\rho(\boldsymbol{x},t)\nu\left[\boldsymbol{\nabla}\boldsymbol{u}(\boldsymbol{x},t) + (\boldsymbol{\nabla}\boldsymbol{u}(\boldsymbol{x},t))^T\right]\right).\end{aligned}$$

1.3. BGK Approximation

The collision integral (1.5) possesses a rather complicated form. To achieve an efficient numerical scheme integrating the Boltzmann equation (1.4) a less difficult form of the collision term would gratefully be taken.
In the following, we motivate the approximation introduced by Bhatnagar, Gross and Krook [3] which today is frequently used when dealing with lattice Boltzmann methods, these schemes are often called LBGK-methods. In these schemes the complicated collision integral is replaced by a single time relaxation term. This term is chosen in such a way that it emulates specific properties of the original collision integral.
In the previous section we have already used (cf. (1.9) and (1.11)) some properties of the collision integral. We have seen that those properties were necessary to derive the conservation laws. It can be shown [5], that there exist five elementary invariants which read

$$\psi_1 = 1, \quad (\psi_2,\psi_3,\psi_4) = \boldsymbol{v} \quad \text{and} \quad \psi_5 = |\boldsymbol{v}|^2 \tag{1.16}$$

and lead to vanishing integrals

$$\int_{\mathbb{R}^3} Q(f,f)\,\mathrm{d}\boldsymbol{v} = 0, \quad \int_{\mathbb{R}^3} \boldsymbol{v}Q(f,f)\,\mathrm{d}\boldsymbol{v} = 0 \quad \text{and} \quad \int_{\mathbb{R}^3} |\boldsymbol{v}|^2 Q(f,f)\,\mathrm{d}\boldsymbol{v} = 0.$$

It even holds the following equivalence

$$\int_{\mathbb{R}^3} Q(f,f)\varphi(\boldsymbol{v})\,\mathrm{d}\boldsymbol{v} = 0 \qquad \Leftrightarrow \qquad \varphi(\boldsymbol{v}) = \sum_{i=1}^{5} s_i\psi_i = \alpha + \boldsymbol{\beta}\cdot\boldsymbol{v} + \gamma|\boldsymbol{v}|^2, \tag{1.17}$$

with real scalars $\alpha, \gamma, s_i \in \mathbb{R}$ $(i = 1, \ldots, 5)$ and a real vector $\boldsymbol{\beta} \in \mathbb{R}^3$ which can be chosen arbitrary for the backward direction of the equivalence. Furthermore, there exist positive functions $f(\boldsymbol{x}, \boldsymbol{v}, t)$ which lead to vanishing collision integrals and it holds the implication

$$Q(f,f) = 0 \qquad \Rightarrow \qquad f(\boldsymbol{x},\boldsymbol{v},t) = \exp\left(a + \boldsymbol{\delta}\cdot\boldsymbol{v} + b|\boldsymbol{v}|^2\right),$$

with $a \in \mathbb{R}$, $0 > b \in \mathbb{R}$ and $\boldsymbol{\delta} \in \mathbb{R}^3$. For our further investigation, an important function satisfying the latter feature is the Maxwell distribution

$$f^M(\boldsymbol{x},\boldsymbol{v},t) := \rho(\boldsymbol{x},t)\left(\frac{m}{2\pi k_B T(\boldsymbol{x},t)}\right)^{3/2} \exp\left(-\frac{m}{2k_B T(\boldsymbol{x},t)}|\boldsymbol{v} - \boldsymbol{u}(\boldsymbol{x},t)|^2\right), \tag{1.18}$$

with Boltzmann constant k_B, particle mass m and temperature $T(\boldsymbol{x}, t)$ [61]. Therefore, especially it holds [5]

$$Q(f^M, f^M) = 0. \tag{1.19}$$

The Maxwell distribution is also relevant in the famous H-Theorem which we will state subsequent to the following lemma. This lemma is intended as a preparation for the proof of the H-Theorem.

Lemma 1.
Let φ be an arbitrary function of the velocity $\boldsymbol{v}$. If φ satisfies the condition

$$\varphi(\boldsymbol{v}) + \varphi(\boldsymbol{w}) - \varphi(\boldsymbol{v}') - \varphi(\boldsymbol{w}') = 0,$$

for all pre-collision velocities $\boldsymbol{v}$ and $\boldsymbol{w}$, and post-collision velocities $\boldsymbol{v}'$ and $\boldsymbol{w}'$, then it holds

$$\varphi(\boldsymbol{v}) = \alpha + \boldsymbol{\beta}\cdot\boldsymbol{v} + \gamma|\boldsymbol{v}|^2,$$

with $\alpha \in \mathbb{R}$, $\beta \in \mathbb{R}^3$ and $\gamma \in \mathbb{R}$.

Proof. We only have to show that φ satisfies the following equation

$$\int_{\mathbb{R}^3} Q(f,f)\varphi(\boldsymbol{v})\,\mathrm{d}\boldsymbol{v} = 0,$$

because then (1.17) implies the claimed shape for the function φ.

For simplicity we use the shortcuts

$$f_{\boldsymbol{v}} = f(\boldsymbol{x}, \boldsymbol{v}, t), \quad f_{\boldsymbol{w}} = f(\boldsymbol{x}, \boldsymbol{w}, t), \quad f_{\boldsymbol{v}'} = f(\boldsymbol{x}, \boldsymbol{v}', t), \quad f_{\boldsymbol{w}'} = f(\boldsymbol{x}, \boldsymbol{w}', t).$$

In the following computation we use that the collision integral is invariant under exchanges of velocities. An analogue procedure is described more detailed also in the proof of the subsequent theorem below.

$$\begin{aligned}
\int_{\mathbb{R}^3} Q(f,f)\varphi(\boldsymbol{v})\,\mathrm{d}\boldsymbol{v} &= \int_{\mathbb{R}^3}\int_{\mathbb{R}^3}\int_{\mathbb{S}^2} \sigma(\Omega)|\boldsymbol{v}-\boldsymbol{w}|\left(f_{\boldsymbol{v}'}f_{\boldsymbol{w}'} - f_{\boldsymbol{v}}f_{\boldsymbol{w}}\right)\varphi(\boldsymbol{v})\,\mathrm{d}\Omega\,\mathrm{d}\boldsymbol{w}\,\mathrm{d}\boldsymbol{v} \\
&= \frac{1}{2}\int_{\mathbb{R}^3}\int_{\mathbb{R}^3}\int_{\mathbb{S}^2} \sigma(\Omega)|\boldsymbol{v}-\boldsymbol{w}|\left(f_{\boldsymbol{v}'}f_{\boldsymbol{w}'} - f_{\boldsymbol{v}}f_{\boldsymbol{w}}\right)\left(\varphi(\boldsymbol{v})+\varphi(\boldsymbol{w})\right)\mathrm{d}\Omega\,\mathrm{d}\boldsymbol{w}\,\mathrm{d}\boldsymbol{v} \\
&= \frac{1}{4}\int_{\mathbb{R}^3}\int_{\mathbb{R}^3}\int_{\mathbb{S}^2} \sigma(\Omega)|\boldsymbol{v}-\boldsymbol{w}|\left(f_{\boldsymbol{v}'}f_{\boldsymbol{w}'} - f_{\boldsymbol{v}}f_{\boldsymbol{w}}\right) \\
&\qquad\qquad \left(\varphi(\boldsymbol{v})+\varphi(\boldsymbol{w})-\varphi(\boldsymbol{v}')-\varphi(\boldsymbol{w}')\right)\mathrm{d}\Omega\,\mathrm{d}\boldsymbol{w}\,\mathrm{d}\boldsymbol{v}.
\end{aligned}$$

By using the assumed condition it follows

$$\int_{\mathbb{R}^3} Q(f,f)\varphi(\boldsymbol{v})\,\mathrm{d}\boldsymbol{v} = 0.$$

□

Theorem 1 (H-Theorem)**.**
For any positive function $f(\boldsymbol{x}, \boldsymbol{v}, t)$ with finite zeroth to second moments satisfying the Boltzmann equation (1.4) the function

$$H(\boldsymbol{x}, t) := \int_{\mathbb{R}^3} f(\boldsymbol{x}, \boldsymbol{v}, t)\ln\left(f(\boldsymbol{x}, \boldsymbol{v}, t)\right)\,\mathrm{d}\boldsymbol{v}$$

is

a) bounded from below for all $\boldsymbol{x}$ and t,

b) non-increasing in time, i.e.

$$\frac{\partial H(\boldsymbol{x}, t)}{\partial t} \leq 0, \quad \text{for all } \boldsymbol{x} \in \mathbb{R}^3,$$

and moreover it holds that the equality is only attained if $f(\boldsymbol{x}, \boldsymbol{v}, t)$ is a Maxwellian distribution (1.18) independent of $\boldsymbol{x}$.

The function $H(\boldsymbol{x}, t)$ is related to the local entropy by $S(\boldsymbol{x}, t) = -k_B H(\boldsymbol{x}, t)$, with the Boltzmann constant k_B. The H-theorem states that the entropy is maximized by Maxwellian distributions which are the equilibrium distributions in the continuous case.

Outline of a proof.
For part a) a hint from [6] was used. Another argumentation for the boundedness can be found in [15]. Part b) is close to the proof in [69].

a) As one can easily show the function $g(s) = -\ln(s)+(s-1)$ is minimized for $s = 1$. Since it holds $g(1) = 0$ we get the general inequality $-\ln(s) + (s-1) \geq 0$, valid for positive $s \in \mathbb{R}^+$. By substituting $s = \frac{y}{z}$ it follows

$$z\ln(z) - z\ln(y) + y - z \geq 0, \tag{1.20}$$

which is valid for all positive real numbers $y, z \in \mathbb{R}^+$.
For fixed $x \in \mathbb{R}^3$ and $t \in \mathbb{R}$ the function $f(\boldsymbol{x}, \boldsymbol{v}, t)$ implies a density, velocity and temperature by (1.6), (1.7) and (1.8), respectively. Hence, for all $x \in \mathbb{R}^3$ and $t \in \mathbb{R}$ we can define a Maxwellian distribution $M(\boldsymbol{v})$ by

$$M(\boldsymbol{v}) = \rho\left(\frac{m}{2\pi k_B T}\right)^{3/2} \exp\left(-\frac{m}{2k_B T}|\boldsymbol{v}-\boldsymbol{u}|^2\right),$$

where $\rho, \boldsymbol{u}$ and T are given by $f(\boldsymbol{x}, \boldsymbol{v}, t)$. From inequality (1.20) we derive the integral inequality

$$\begin{aligned}\int_{\mathbb{R}^3} f(\boldsymbol{x},\boldsymbol{v},t)\ln\left(f(\boldsymbol{x},\boldsymbol{v},t)\right)\,\mathrm{d}\boldsymbol{v} \geq \int_{\mathbb{R}^3} f(\boldsymbol{x},\boldsymbol{v},t)\ln\left(M(\boldsymbol{v})\right)\,\mathrm{d}\boldsymbol{v} \\ + \int_{\mathbb{R}^3} f(\boldsymbol{x},\boldsymbol{v},t)\,\mathrm{d}\boldsymbol{v} - \int_{\mathbb{R}^3} M(\boldsymbol{v})\,\mathrm{d}\boldsymbol{v}.\end{aligned} \tag{1.21}$$

The integrals in the second line of (1.21) cancel out, since they are both equal to ρ, due to construction of $M(\boldsymbol{v})$. The first integral on the right hand side of (1.21) can be simplified as follows

$$\begin{aligned}\int_{\mathbb{R}^3} f(\boldsymbol{x},\boldsymbol{v},t)\ln\left(M(\boldsymbol{v})\right)\,\mathrm{d}\boldsymbol{v} = \ln\left[\rho\left(\frac{m}{2\pi k_B T}\right)^{3/2}\right]\int_{\mathbb{R}^3} f(\boldsymbol{x},\boldsymbol{v},t)\,\mathrm{d}\boldsymbol{v} \\ - \frac{m}{k_B T}\int_{\mathbb{R}^3} f(\boldsymbol{x},\boldsymbol{v},t)\frac{|\boldsymbol{v}-\boldsymbol{u}|^2}{2}\,\mathrm{d}\boldsymbol{v}.\end{aligned}$$

Especially, it follows that the right hand side in the latter equation is bounded from below, hence we have shown the proposition

$$H(\boldsymbol{x},t) = \int_{\mathbb{R}^3} f(\boldsymbol{x},\boldsymbol{v},t)\ln\left(f(\boldsymbol{x},\boldsymbol{v},t)\right)\,\mathrm{d}\boldsymbol{v} > -\infty.$$

b) Let $\boldsymbol{x} \in \mathbb{R}^3$ be arbitrary but fixed. Differentiating the introduced function $H(\boldsymbol{x}, t)$

yields

$$\frac{\partial H(\boldsymbol{x},t)}{\partial t} = \int\limits_{\mathbb{R}^3} \frac{\partial f(\boldsymbol{x},\boldsymbol{v},t)}{\partial t} \left[1 + \ln\left(f(\boldsymbol{x},\boldsymbol{v},t)\right)\right] \mathrm{d}\boldsymbol{v}.$$

Since $f(\boldsymbol{x},\boldsymbol{v},t)$ is satisfying the Boltzmann equation (1.4) the latter equation can be written as

$$\begin{aligned}\frac{\partial H(\boldsymbol{x},t)}{\partial t} = &\int\limits_{\mathbb{R}^3} Q(f,f) \left[1 + \ln\left(f(\boldsymbol{x},\boldsymbol{v},t)\right)\right] \mathrm{d}\boldsymbol{v} \\ &- \int\limits_{\mathbb{R}^3} \left(\boldsymbol{v}\cdot\boldsymbol{\nabla} f(\boldsymbol{x},\boldsymbol{v},t)\right) \left[1 + \ln\left(f(\boldsymbol{x},\boldsymbol{v},t)\right)\right] \mathrm{d}\boldsymbol{v}\end{aligned}$$

and without discussion we assume that the second term on the right hand side vanishes [69]. For simplicity we use again the shortcuts

$$f_{\boldsymbol{v}} = f(\boldsymbol{x},\boldsymbol{v},t), \quad f_{\boldsymbol{w}} = f(\boldsymbol{x},\boldsymbol{w},t), \quad f_{\boldsymbol{v}'} = f(\boldsymbol{x},\boldsymbol{v}',t), \quad f_{\boldsymbol{w}'} = f(\boldsymbol{x},\boldsymbol{w}',t),$$

and thus we can write now

$$\frac{\partial H(\boldsymbol{x},t)}{\partial t} = \int\limits_{\mathbb{R}^3}\int\limits_{\mathbb{R}^3}\int\limits_{\mathbb{S}^2} \sigma(\Omega)|\boldsymbol{v}-\boldsymbol{w}| \left(f_{\boldsymbol{v}'}f_{\boldsymbol{w}'} - f_{\boldsymbol{v}}f_{\boldsymbol{w}}\right) \left[1 + \ln\left(f_{\boldsymbol{v}}\right)\right] \mathrm{d}\Omega\,\mathrm{d}\boldsymbol{w}\,\mathrm{d}\boldsymbol{v}. \quad (1.22)$$

This integral is invariant under exchange of $\boldsymbol{v}$ and $\boldsymbol{w}$ because $\sigma(\Omega)$ is invariant under such exchange:

$$\frac{\partial H(\boldsymbol{x},t)}{\partial t} = \int\limits_{\mathbb{R}^3}\int\limits_{\mathbb{R}^3}\int\limits_{\mathbb{S}^2} \sigma(\Omega)|\boldsymbol{w}-\boldsymbol{v}| \left(f_{\boldsymbol{v}'}f_{\boldsymbol{w}'} - f_{\boldsymbol{w}}f_{\boldsymbol{v}}\right) \left[1 + \ln\left(f_{\boldsymbol{w}}\right)\right] \mathrm{d}\Omega\,\mathrm{d}\boldsymbol{w}\,\mathrm{d}\boldsymbol{v}. \quad (1.23)$$

Adding (1.22) and (1.23) by taking half and half each we get

$$\frac{\partial H(\boldsymbol{x},t)}{\partial t} = \frac{1}{2}\int\limits_{\mathbb{R}^3}\int\limits_{\mathbb{R}^3}\int\limits_{\mathbb{S}^2} \sigma(\Omega)|\boldsymbol{v}-\boldsymbol{w}| \left(f_{\boldsymbol{v}'}f_{\boldsymbol{w}'} - f_{\boldsymbol{v}}f_{\boldsymbol{w}}\right) \left[2 + \ln\left(f_{\boldsymbol{v}}f_{\boldsymbol{w}}\right)\right] \mathrm{d}\Omega\,\mathrm{d}\boldsymbol{w}\,\mathrm{d}\boldsymbol{v}, \quad (1.24)$$

which is now invariant under exchange of $\{\boldsymbol{v},\boldsymbol{w}\}$ and $\{\boldsymbol{v}',\boldsymbol{w}'\}$ because for each collision there exists an inverse collision with the same cross section. Hence, we obtain

$$\frac{\partial H(\boldsymbol{x},t)}{\partial t} = \frac{1}{2}\int\limits_{\mathbb{R}^3}\int\limits_{\mathbb{R}^3}\int\limits_{\mathbb{S}^2} \sigma'(\Omega)|\boldsymbol{v}'-\boldsymbol{w}'| \left(f_{\boldsymbol{v}}f_{\boldsymbol{w}} - f_{\boldsymbol{v}'}f_{\boldsymbol{w}'}\right) \left[2 + \ln\left(f_{\boldsymbol{v}'}f_{\boldsymbol{w}'}\right)\right] \mathrm{d}\Omega\,\mathrm{d}\boldsymbol{w}'\,\mathrm{d}\boldsymbol{v}',$$

which is equivalent to

$$\frac{\partial H(\boldsymbol{x},t)}{\partial t} = \frac{1}{2}\int\limits_{\mathbb{R}^3}\int\limits_{\mathbb{R}^3}\int\limits_{\mathbb{S}^2} \sigma(\Omega)|\boldsymbol{v}-\boldsymbol{w}|\left(f_{\boldsymbol{v}}f_{\boldsymbol{w}} - f_{\boldsymbol{v}'}f_{\boldsymbol{w}'}\right)\left[2+\ln\left(f_{\boldsymbol{v}'}f_{\boldsymbol{w}'}\right)\right]\,\mathrm{d}\Omega\,\mathrm{d}\boldsymbol{w}\,\mathrm{d}\boldsymbol{v}, \tag{1.25}$$

since $\mathrm{d}\boldsymbol{v}\,\mathrm{d}\boldsymbol{w} = \mathrm{d}\boldsymbol{v}'\,\mathrm{d}\boldsymbol{w}'$, $|\boldsymbol{v}-\boldsymbol{w}| = |\boldsymbol{v}'-\boldsymbol{w}'|$ and $\sigma(\Omega) = \sigma'(\Omega)$. Now adding (1.24) and (1.25) again by taking half and half each we get

$$\frac{\partial H(\boldsymbol{x},t)}{\partial t} = \frac{1}{4}\int\limits_{\mathbb{R}^3}\int\limits_{\mathbb{R}^3}\int\limits_{\mathbb{S}^2} \sigma(\Omega)|\boldsymbol{v}-\boldsymbol{w}|\left(f_{\boldsymbol{v}'}f_{\boldsymbol{w}'} - f_{\boldsymbol{v}}f_{\boldsymbol{w}}\right)\left[\ln(f_{\boldsymbol{v}}f_{\boldsymbol{w}}) - \ln(f_{\boldsymbol{v}'}f_{\boldsymbol{w}'})\right]\,\mathrm{d}\Omega\,\mathrm{d}\boldsymbol{w}\,\mathrm{d}\boldsymbol{v}. \tag{1.26}$$

From the inequality

$$(b-a)(\ln(a)-\ln(b)) < 0, \qquad a>0,\ b>0,\ a\neq b,$$

it follows that the integrand is never positive and we can conclude

$$\frac{\partial H(\boldsymbol{x},t)}{\partial t} \leq 0,$$

where the equality is attained if and only if

$$f_{\boldsymbol{v}'}f_{\boldsymbol{w}'} - f_{\boldsymbol{v}}f_{\boldsymbol{w}} = 0 \tag{1.27}$$

for all $\boldsymbol{v}', \boldsymbol{w}'$ that result from $\boldsymbol{v}, \boldsymbol{w}$ by collision. Moreover, equation (1.27) implies

$$\frac{\partial f(\boldsymbol{x},\boldsymbol{v},t)}{\partial t} = 0,$$

for all $\boldsymbol{v} \in \mathbb{R}^3$ which can be seen by

$$\begin{aligned}\frac{\partial H(\boldsymbol{x},t)}{\partial t} &= \int\limits_{\mathbb{R}^3} \frac{\partial f(\boldsymbol{x},\boldsymbol{v},t)}{\partial t}\left[1+\ln\left(f_{\boldsymbol{v}}\right)\right]\,\mathrm{d}\boldsymbol{v} \\ &= \int\limits_{\mathbb{R}^3}\left[\int\limits_{\mathbb{R}^3}\int\limits_{\mathbb{S}^2} \sigma(\Omega)|\boldsymbol{v}-\boldsymbol{w}|\left(f_{\boldsymbol{v}'}f_{\boldsymbol{w}'} - f_{\boldsymbol{v}}f_{\boldsymbol{w}}\right)\,\mathrm{d}\Omega\,\mathrm{d}\boldsymbol{w}\right]\left[1+\ln\left(f_{\boldsymbol{v}}\right)\right]\,\mathrm{d}\boldsymbol{v}.\end{aligned}$$

Note that (1.27) also implies

$$\ln(f_{\boldsymbol{v}}) + \ln(f_{\boldsymbol{w}}) - \ln(f_{\boldsymbol{v}'}) - \ln(f_{\boldsymbol{w}'}) = 0,$$

and from Lemma 1 one can then conclude that if the integral (1.26) vanishes, then

$\ln(f_{\boldsymbol{v}})$ is an integration invariant and therefore of the form (1.17), hence

$$\ln(f_{\boldsymbol{v}}) = \ln(f(\boldsymbol{x},\boldsymbol{v},t)) = \alpha(\boldsymbol{x},t) + \boldsymbol{\beta}(\boldsymbol{x},t)\cdot\boldsymbol{v} + \gamma(\boldsymbol{x},t)|\boldsymbol{v}|^2.$$

This can be transformed to

$$f(\boldsymbol{x},\boldsymbol{v},t) = \exp\left(\alpha(\boldsymbol{x},t) + \boldsymbol{\beta}(\boldsymbol{x},t)\cdot\boldsymbol{v} + \gamma(\boldsymbol{x},t)|\boldsymbol{v}|^2\right)$$

and with the substitution $\gamma(\boldsymbol{x},t) \to -\frac{1}{2}\hat{\gamma}(\boldsymbol{x},t)$ we can write it as

$$f(\boldsymbol{x},\boldsymbol{v},t) = \delta(\boldsymbol{x},t)\exp\left(-\frac{1}{2}\hat{\gamma}(\boldsymbol{x},t)\left|\boldsymbol{v} - \frac{\boldsymbol{\beta}(\boldsymbol{x},t)}{\hat{\gamma}(\boldsymbol{x},t)}\right|^2\right),$$

with $\delta(\boldsymbol{x},t) = \exp\left(\alpha(\boldsymbol{x},t) + \frac{|\boldsymbol{\beta}(\boldsymbol{x},t)|^2}{2\hat{\gamma}(\boldsymbol{x},t)}\right)$.
The unknowns $\delta(\boldsymbol{x},t)$, $\hat{\gamma}(\boldsymbol{x},t)$ and $\boldsymbol{\beta}(\boldsymbol{x},t)$ can be determined with use of the macroscopic quantities. Since $f(\boldsymbol{x},\boldsymbol{v},t)$ satisfies the Boltzmann equation the following integral equations have to be fulfilled:

$$\int_{\mathbb{R}^3} \delta(\boldsymbol{x},t)\exp\left(-\frac{1}{2}\hat{\gamma}(\boldsymbol{x},t)\left|\boldsymbol{v} - \frac{\boldsymbol{\beta}(\boldsymbol{x},t)}{\hat{\gamma}(\boldsymbol{x},t)}\right|^2\right)\,\mathrm{d}\boldsymbol{v} = \rho(\boldsymbol{x},t),$$

$$\int_{\mathbb{R}^3} \boldsymbol{v}\delta(\boldsymbol{x},t)\exp\left(-\frac{1}{2}\hat{\gamma}(\boldsymbol{x},t)\left|\boldsymbol{v} - \frac{\boldsymbol{\beta}(\boldsymbol{x},t)}{\hat{\gamma}(\boldsymbol{x},t)}\right|^2\right)\,\mathrm{d}\boldsymbol{v} = \rho(\boldsymbol{x},t)\boldsymbol{u}(\boldsymbol{x},t),$$

$$\int_{\mathbb{R}^3} \frac{|\boldsymbol{v}-\boldsymbol{u}(\boldsymbol{x},t)|^2}{2}\delta(\boldsymbol{x},t)\exp\left(-\frac{1}{2}\hat{\gamma}(\boldsymbol{x},t)\left|\boldsymbol{v} - \frac{\boldsymbol{\beta}(\boldsymbol{x},t)}{\hat{\gamma}(\boldsymbol{x},t)}\right|^2\right)\,\mathrm{d}\boldsymbol{v} = \rho(\boldsymbol{x},t)\frac{3}{2}\frac{k_BT(\boldsymbol{x},t)}{m}.$$

It follows

$$\begin{aligned}
\delta(\boldsymbol{x},t) &= \rho(\boldsymbol{x},t)(2\pi)^{-3/2}(\hat{\gamma}(\boldsymbol{x},t))^{3/2},\\
\hat{\gamma}(\boldsymbol{x},t) &= \frac{m}{k_BT(\boldsymbol{x},t)},\\
\boldsymbol{\beta}(\boldsymbol{x},t) &= \hat{\gamma}(\boldsymbol{x},t)\boldsymbol{u}(\boldsymbol{x},t),
\end{aligned}$$

which leads to a Maxwellian distribution

$$f(\boldsymbol{x},\boldsymbol{v},t) = \rho(\boldsymbol{x},t)\left(\frac{m}{2\pi k_BT(\boldsymbol{x},t)}\right)^{3/2}\exp\left(-\frac{m}{2k_BT(\boldsymbol{x},t)}|\boldsymbol{v}-\boldsymbol{u}(\boldsymbol{x},t)|^2\right).$$

A further restriction for the unknowns comes from the above implication that the

derivative with respect to time should equal zero. For all $\boldsymbol{v} \in \mathbb{R}^3$:

$$\frac{\partial f(\boldsymbol{x},\boldsymbol{v},t)}{\partial t} = -\boldsymbol{v}\cdot\boldsymbol{\nabla}\left[\delta(\boldsymbol{x},t)\exp\left(-\frac{1}{2}\hat{\gamma}(\boldsymbol{x},t)\left|\boldsymbol{v}-\frac{\boldsymbol{\beta}(\boldsymbol{x},t)}{\hat{\gamma}(\boldsymbol{x},t)}\right|^2\right)\right] = 0,$$

note the validity of (1.19). This restriction leads to the condition that the function $f(\boldsymbol{x},\boldsymbol{v},t)$ may not depend on $\boldsymbol{x}$, hence also the unknowns are independent of $\boldsymbol{x}$. One can even further argue that in a closed system all unknowns also have to be independent of time t, since the macroscopic quantities are conserved. This shows that $\frac{\partial H(\boldsymbol{x},t)}{\partial t}$ vanishes only if the function $f(\boldsymbol{x},\boldsymbol{v},t)$ is a Maxwellian (1.18) with each density, velocity and temperature spatially constant.

□

Recapitulating the already known properties of the collision integral state five integration invariants (cf. (1.17)) and a vanishing collision term (cf. (1.19)) for a Maxwellian distribution. From the previous theorem we derive the last desired property. For all space points $\boldsymbol{x}$ the H-theorem shows a tendency of the distribution function $f(\boldsymbol{x},\boldsymbol{v},t)$, more precisely of the collision integral $Q(f,f)$, towards a Maxwellian distribution.

Emulating the mentioned properties of the collision integral motivates the choice of the so called BGK approximation $\Omega(f)$ for the collision term which was already introduced in 1954. It is a single time relaxation term, expressed by

$$\Omega(f) := -\frac{1}{\tau_c}\left[f(\boldsymbol{x},\boldsymbol{v},t) - f^{(eq)}(\boldsymbol{x},\boldsymbol{v},t)\right], \tag{1.28}$$

where τ_c is the relaxation time and $f^{(eq)}(\boldsymbol{x},\boldsymbol{v},t)$ denotes the equilibrium state. The local equilibrium state used in the BGK approximation depends on spatial position $\boldsymbol{x}$ and time t, the reason for this becomes evident when considering the property of integration invariants:

$$\int_{\mathbb{R}^3}\psi_k\Omega(f)\,\mathrm{d}\boldsymbol{v} = -\frac{1}{\tau_c}\left[\int_{\mathbb{R}^3}\psi_k f(\boldsymbol{x},\boldsymbol{v},t)\,\mathrm{d}\boldsymbol{v} - \int_{\mathbb{R}^3}\psi_k f^{(eq)}(\boldsymbol{x},\boldsymbol{v},t)\,\mathrm{d}\boldsymbol{v}\right] = 0,$$

for $k = 1,\ldots,5$ and the ψ_k given by (1.16) [69]. This means at any position $\boldsymbol{x}$ and time t the equilibrium distribution function $f^{(eq)}(\boldsymbol{x},\boldsymbol{v},t)$ has to have the same density, velocity and temperature as implied by $f(\boldsymbol{x},\boldsymbol{v},t)$. The latter values are not uniform in space and time, hence a uniform and steady equilibrium distribution cannot be chosen. This means the local equilibrium distribution $f^{(eq)}(\boldsymbol{x},\boldsymbol{v},t)$ is a Maxwellian distribution where the density, velocity and temperature are implied by $f(\boldsymbol{x},\boldsymbol{v},t)$ via (1.6), (1.7) and (1.8), respectively.

1.4. Discretizing Boltzmann Equation

Starting with the continuous Boltzmann equation with BGK approximation

$$\frac{\partial f(\boldsymbol{x},\boldsymbol{v},t)}{\partial t} + \boldsymbol{v}\cdot\boldsymbol{\nabla} f(\boldsymbol{x},\boldsymbol{v},t) = -\frac{1}{\tau_c}\left[f(\boldsymbol{x},\boldsymbol{v},t) - f^{(eq)}(\boldsymbol{x},\boldsymbol{v},t)\right] \tag{1.29}$$

the BGK lattice Boltzmann equation, also called the lattice BGK (LBGK) equation, can be derived, see also [28]. The derivation is done by a suitable discretization of space, velocity space and time, then a finite difference scheme is applied [69].
We aim to achieve a numerical method which is correct up to second order in macroscopic velocity $\boldsymbol{u}$.

1.4.1. Lattice BGK Equation

In a first step a (velocity) discrete Boltzmann equation is derived, where the continuous velocity space is discretized. Instead of $\boldsymbol{v}\in\mathbb{R}^3$ a finite set of possible velocities $\boldsymbol{v}_i$ is introduced

$$\mathcal{V} = \left\{ \boldsymbol{v}_i = \begin{pmatrix} v_i^1 \\ v_i^2 \\ v_i^3 \end{pmatrix} \in \mathbb{R}^3 \,:\, i = 0,\dots,n_v \right\}. \tag{1.30}$$

How some suitable $\mathcal{V}$ can be constructed is discussed in the subsequent section. Then the discrete Boltzmann equation reads

$$\frac{\partial f_i(\boldsymbol{x},t)}{\partial t} + \boldsymbol{v}_i\cdot\boldsymbol{\nabla} f_i(\boldsymbol{x},t) = -\frac{1}{\tau_c}\left[f_i(\boldsymbol{x},t) - f_i^{(eq)}(\boldsymbol{x},t)\right],\ i = 0,\dots,n_v, \tag{1.31}$$

with a new distribution function $f(\boldsymbol{x},\boldsymbol{v}_i,t)\to f_i(\boldsymbol{x},t)$ and besides a discrete equilibrium distribution function is introduced $f^{(eq)}(\boldsymbol{x},\boldsymbol{v}_i,t)\to f_i^{(eq)}(\boldsymbol{x},t)$. We will handle this discrete equilibrium distribution later on in this section. For fixed $\boldsymbol{x}$ and t we call each $f_i(\boldsymbol{x},t)$ a population of the distribution.
A nondimensionalization of (1.31) is achieved by introducing scaling quantities, more precisely a reference velocity U, a reference density n_r, the characteristic length scale L and the time between particle collisions t_c. In the substituted variables

$$\boldsymbol{c}_i = \begin{pmatrix} c_i^1 \\ c_i^2 \\ c_i^3 \end{pmatrix} = \frac{1}{U}\boldsymbol{v}_i, \quad \hat{\boldsymbol{x}} = \frac{1}{L}\boldsymbol{x}, \quad \hat{t} = t\frac{U}{L}, \quad \hat{\tau}_c = \frac{\tau_c}{t_c}, \tag{1.32}$$

with according operator and right hand side

$$\hat{\boldsymbol{\nabla}} = L\boldsymbol{\nabla}, \quad F_i(\hat{\boldsymbol{x}},\hat{t}) = \frac{f_i(\boldsymbol{x},t)}{n_r}, \quad F_i^{(eq)}(\hat{\boldsymbol{x}},\hat{t}) = \frac{f_i^{(eq)}(\boldsymbol{x},t)}{n_r},$$

the nondimensionalized discrete Boltzmann equation is given by

$$\frac{\partial F_i(\hat{\boldsymbol{x}},\hat{t})}{\partial \hat{t}} + \boldsymbol{c}_i \cdot \hat{\boldsymbol{\nabla}} F_i(\hat{\boldsymbol{x}},\hat{t}) = -\frac{1}{\varepsilon \hat{\tau}_c}\left[F_i(\hat{\boldsymbol{x}},\hat{t}) - F_i^{(eq)}(\hat{\boldsymbol{x}},\hat{t})\right],\ i = 0,\ldots,n_v, \tag{1.33}$$

using the scaling parameter

$$\varepsilon = t_c \frac{U}{L}. \tag{1.34}$$

In order to use a finite difference scheme for (1.33), a spatial discretization and a discretization in time is necessary. We denote the step size in time as Δt and also scale it to achieve a nondimensionalized quantity. In the further derivation we see that $\Delta t = t_c$ should be used, since this choice simplifies the lattice BGK equation. Thus it holds

$$\Delta \hat{t} = \Delta t \frac{U}{L} \quad \text{and} \quad \Delta t = t_c. \tag{1.35}$$

A characteristic of the discretization used in lattice Boltzmann methods is a connection of the underlying discretizations of time, space and velocity space. For the (nondimensionalized) spatial discretization we demand that for all velocities $\boldsymbol{c}_i$ there exist in the discretized space a $\Delta_i \hat{\boldsymbol{x}} = (\Delta_i \hat{x}_1, \Delta_i \hat{x}_2, \Delta_i \hat{x}_3)^T$ such that

$$\Delta_i \hat{\boldsymbol{x}} = \boldsymbol{c}_i \Delta \hat{t} \tag{1.36}$$

is fulfilled. This means, if $\hat{\boldsymbol{x}}$ is a point of the spatial discretization, then also $\hat{\boldsymbol{x}} + \boldsymbol{c}_i \Delta \hat{t}$ is one. In the subsequent section we deal with some popular discretizations for lattice Boltzmann methods.

The derivative with respect to time in (1.33) is approximated with an Euler scheme

$$\frac{\partial F_i(\hat{\boldsymbol{x}},\hat{t})}{\partial \hat{t}} \approx \frac{F_i(\hat{\boldsymbol{x}},\hat{t}+\Delta\hat{t}) - F_i(\hat{\boldsymbol{x}},\hat{t})}{\Delta \hat{t}}, \tag{1.37}$$

similarly each component of the gradient is approximated. It is necessary for our purpose to evaluate the approximation of that gradient at the new time point $\hat{t} + \Delta\hat{t}$, since the unknown in the finally resulting scheme comes from this part. With the abbreviations

$$\vec{\Delta}_i^1 \hat{\boldsymbol{x}} = \begin{pmatrix} \Delta_i \hat{x}_1 \\ 0 \\ 0 \end{pmatrix}, \quad \vec{\Delta}_i^2 \hat{\boldsymbol{x}} = \begin{pmatrix} 0 \\ \Delta_i \hat{x}_2 \\ 0 \end{pmatrix}, \quad \vec{\Delta}_i^3 \hat{\boldsymbol{x}} = \begin{pmatrix} 0 \\ 0 \\ \Delta_i \hat{x}_3 \end{pmatrix} \tag{1.38}$$

these approximations read

$$\hat{\boldsymbol{\nabla}} F_i(\hat{\boldsymbol{x}}, \hat{t} + \Delta\hat{t}) \approx \begin{pmatrix} \frac{F_i(\hat{\boldsymbol{x}} + \vec{\Delta}_i^1 \hat{\boldsymbol{x}}, \hat{t} + \Delta\hat{t}) - F_i(\hat{\boldsymbol{x}}, \hat{t} + \Delta\hat{t})}{\Delta_i \hat{x}_1} \\ \frac{F_i(\hat{\boldsymbol{x}} + \vec{\Delta}_i^2 \hat{\boldsymbol{x}}, \hat{t} + \Delta\hat{t}) - F_i(\hat{\boldsymbol{x}}, \hat{t} + \Delta\hat{t})}{\Delta_i \hat{x}_2} \\ \frac{F_i(\hat{\boldsymbol{x}} + \vec{\Delta}_i^3 \hat{\boldsymbol{x}}, \hat{t} + \Delta\hat{t}) - F_i(\hat{\boldsymbol{x}}, \hat{t} + \Delta\hat{t})}{\Delta_i \hat{x}_3} \end{pmatrix}. \tag{1.39}$$

Hence, provided the function $F_i(\hat{\boldsymbol{x}}, \hat{t} + \Delta\hat{t})$ is total differentiable with respect to $\hat{\boldsymbol{x}}$, and considering the second term of the left hand side in (1.33) one obtains with use of (1.36),

$$\begin{aligned} \boldsymbol{c}_i \cdot \hat{\boldsymbol{\nabla}} F_i(\hat{\boldsymbol{x}}, \hat{t} + \Delta\hat{t}) = c_i^1 &\frac{F_i(\hat{\boldsymbol{x}} + \vec{\Delta}_i^1 \hat{\boldsymbol{x}}, \hat{t} + \Delta\hat{t}) - F_i(\hat{\boldsymbol{x}}, \hat{t} + \Delta\hat{t})}{\Delta_i \hat{x}_1} \\ &+ c_i^2 \frac{F_i(\hat{\boldsymbol{x}} + \vec{\Delta}_i^2 \hat{\boldsymbol{x}}, \hat{t} + \Delta\hat{t}) - F_i(\hat{\boldsymbol{x}}, \hat{t} + \Delta\hat{t})}{\Delta_i \hat{x}_2} \\ &+ c_i^3 \frac{F_i(\hat{\boldsymbol{x}} + \vec{\Delta}_i^3 \hat{\boldsymbol{x}}, \hat{t} + \Delta\hat{t}) - F_i(\hat{\boldsymbol{x}}, \hat{t} + \Delta\hat{t})}{\Delta_i \hat{x}_3} + \mathcal{O}(|\Delta_i \hat{\boldsymbol{x}}|) \\ = &\frac{F_i(\hat{\boldsymbol{x}} + \vec{c}_i^1 \Delta\hat{t}, \hat{t} + \Delta\hat{t}) - F_i(\hat{\boldsymbol{x}}, \hat{t} + \Delta\hat{t})}{\Delta\hat{t}} \\ &+ \frac{F_i(\hat{\boldsymbol{x}} + \vec{c}_i^2 \Delta\hat{t}, \hat{t} + \Delta\hat{t}) - F_i(\hat{\boldsymbol{x}}, \hat{t} + \Delta\hat{t})}{\Delta\hat{t}} \\ &+ \frac{F_i(\hat{\boldsymbol{x}} + \vec{c}_i^3 \Delta\hat{t}, \hat{t} + \Delta\hat{t}) - F_i(\hat{\boldsymbol{x}}, \hat{t} + \Delta\hat{t})}{\Delta\hat{t}} + \mathcal{O}(\Delta\hat{t}) \\ \approx &\frac{F_i(\hat{\boldsymbol{x}} + \boldsymbol{c}_i \Delta\hat{t}, \hat{t} + \Delta\hat{t}) - F_i(\hat{\boldsymbol{x}}, \hat{t} + \Delta\hat{t})}{\Delta\hat{t}} + \mathcal{O}(\Delta\hat{t}) \end{aligned} \tag{1.40}$$

with $\vec{c}_i^1, \vec{c}_i^2$ and $\vec{c}_i^3$ defined analogue to (1.38) and using $\mathcal{O}(|\Delta_i \hat{\boldsymbol{x}}|) = \mathcal{O}(\Delta\hat{t})$. Thus, the error made in the last step, the first approximation, is of the same order as the approximations (1.39).

Alternatively, one can obtain the approximation (1.40) for $\boldsymbol{c}_i \cdot \hat{\boldsymbol{\nabla}} F_i(\hat{\boldsymbol{x}}, \hat{t} + \Delta\hat{t})$ more intuitively by approximating directly the directional derivative. The directional derivative $\nabla_{\boldsymbol{a}} F_i(\hat{\boldsymbol{x}}, \hat{t} + \Delta\hat{t})$ along a normalized vector $\boldsymbol{a}$ can be written as

$$\nabla_{\boldsymbol{a}} F_i(\hat{\boldsymbol{x}}, \hat{t} + \Delta\hat{t}) = \boldsymbol{a} \cdot \nabla F_i(\hat{\boldsymbol{x}}, \hat{t} + \Delta\hat{t}).$$

Thus,

$$\begin{aligned}
\boldsymbol{c}_i \cdot \hat{\boldsymbol{\nabla}} F_i(\hat{\boldsymbol{x}}, \hat{t} + \Delta\hat{t}) &= |\boldsymbol{c}_i| \left(\frac{\boldsymbol{c}_i}{|\boldsymbol{c}_i|} \cdot \hat{\boldsymbol{\nabla}} F_i(\hat{\boldsymbol{x}}, \hat{t} + \Delta\hat{t}) \right) \\
&= |\boldsymbol{c}_i| \nabla_{|\boldsymbol{c}_i|^{-1}\boldsymbol{c}_i} F_i(\hat{\boldsymbol{x}}, \hat{t} + \Delta\hat{t}) \\
&= |\boldsymbol{c}_i| \lim_{h \to 0} \frac{F_i(\hat{\boldsymbol{x}} + \frac{\boldsymbol{c}_i}{|\boldsymbol{c}_i|} h, \hat{t} + \Delta\hat{t}) - F_i(\hat{\boldsymbol{x}}, \hat{t} + \Delta\hat{t})}{h} \\
&\approx |\boldsymbol{c}_i| \frac{F_i(\hat{\boldsymbol{x}} + \frac{\boldsymbol{c}_i}{|\boldsymbol{c}_i|} |\Delta_i \hat{\boldsymbol{x}}|, \hat{t} + \Delta\hat{t}) - F_i(\hat{\boldsymbol{x}}, \hat{t} + \Delta\hat{t})}{|\Delta_i \hat{\boldsymbol{x}}|} \\
&= \frac{F_i(\hat{\boldsymbol{x}} + \boldsymbol{c}_i \Delta\hat{t}, \hat{t} + \Delta\hat{t}) - F_i(\hat{\boldsymbol{x}}, \hat{t} + \Delta\hat{t})}{\Delta\hat{t}},
\end{aligned}$$

again (1.36) was used.

Plugging in the finite differences (1.37) and (1.40) in (1.33) yields for all $i = 0, \ldots, n_v$ (reverse order)

$$\begin{aligned}
-\frac{1}{\varepsilon\hat{\tau}_c} \left[F_i(\hat{\boldsymbol{x}}, \hat{t}) - F_i^{(eq)}(\hat{\boldsymbol{x}}, \hat{t}) \right] &= \frac{F_i(\hat{\boldsymbol{x}}, \hat{t} + \Delta\hat{t}) - F_i(\hat{\boldsymbol{x}}, \hat{t})}{\Delta\hat{t}} \\
&\quad + \frac{F_i(\hat{\boldsymbol{x}} + \boldsymbol{c}_i \Delta\hat{t}, \hat{t} + \Delta\hat{t}) - F_i(\hat{\boldsymbol{x}}, \hat{t} + \Delta\hat{t})}{\Delta\hat{t}} \\
&= \frac{F_i(\hat{\boldsymbol{x}} + \boldsymbol{c}_i \Delta\hat{t}, \hat{t} + \Delta\hat{t}) - F_i(\hat{\boldsymbol{x}}, \hat{t})}{\Delta\hat{t}}.
\end{aligned} \tag{1.41}$$

Noticing that due to (1.34) and (1.35) we have

$$\frac{\Delta\hat{t}}{\hat{\tau}_c \varepsilon} = \frac{\Delta t \frac{U}{L}}{\hat{\tau}_c t_c \frac{U}{L}} = \frac{1}{\hat{\tau}_c}.$$

We multiply the outcome of (1.33), i.e. (1.41), by $\Delta\hat{t}$ to eventually obtain the desired lattice BGK equation, it reads

$$F_i(\hat{\boldsymbol{x}} + \boldsymbol{c}_i \Delta\hat{t}, \hat{t} + \Delta\hat{t}) - F_i(\hat{\boldsymbol{x}}, \hat{t}) = -\frac{1}{\hat{\tau}_c} \left[F_i(\hat{\boldsymbol{x}}, \hat{t}) - F_i^{(eq)}(\hat{\boldsymbol{x}}, \hat{t}) \right]. \tag{1.42}$$

Comparing (1.3) and (1.42) directly shows the close relation between lattice gas automata and the lattice Boltzmann method.

The special discretization in lattice Boltzmann methods, i.e. the relation (1.36), causes the distributions to move in one time step exactly from a lattice point till another lattice point.

1.4.2. Influence of Discretization

The discretization of the velocity space has an immediate effect on the calculation of the macroscopic density (1.6) and velocity (1.7). An integration is no longer required,

instead a summation over all possible velocities is sufficient. We achieve an adapted density

$$\hat{\rho}(\hat{\boldsymbol{x}}, \hat{t}) = \sum_{i=0}^{n_v} F_i(\hat{\boldsymbol{x}}, \hat{t}) \tag{1.43}$$

and velocity

$$\hat{\rho}(\hat{\boldsymbol{x}}, \hat{t})\hat{\boldsymbol{u}}(\hat{\boldsymbol{x}}, \hat{t}) = \sum_{i=0}^{n_v} \boldsymbol{c}_i F_i(\hat{\boldsymbol{x}}, \hat{t}). \tag{1.44}$$

Another influence from the discretization of the velocity space is given for the equilibrium distribution in the collision term. We have introduced a discrete equilibrium distribution in (1.31). We choose this discrete distribution such that the desired properties (cf. the previous section 1.3) are kept valid. Especially, this means we demand

$$\rho(\boldsymbol{x}, t) = \sum_{i=0}^{n_v} f_i^{(eq)}(\boldsymbol{x}, t), \qquad \rho(\boldsymbol{x}, t)\boldsymbol{u}(\boldsymbol{x}, t) = \sum_{i=0}^{n_v} \boldsymbol{v} f_i^{(eq)}(\boldsymbol{x}, t). \tag{1.45}$$

At least two popular methods exist how discrete distributions can be computed [33, 45, 69]. The (discrete) equilibrium distributions are not unique, what we will also see in the subsequent section.
The method we choose uses an ansatz function whose shape is derived from a Taylor expansion of the continuous equilibrium distribution [45]. Omitting all arguments, then a Taylor expansion of the Maxwellian distribution in $\boldsymbol{u}$ around zero up to second order reads:

$$\begin{aligned} f^{(eq)} &= \rho \left(\frac{m}{2\pi k_B T}\right)^{3/2} \exp\left(-\frac{m}{2k_B T}|\boldsymbol{v}-\boldsymbol{u}|^2\right) \\ &= \rho \left(\frac{m}{2\pi k_B T}\right)^{3/2} \exp\left(-\frac{m}{2k_B T}|\boldsymbol{v}|^2\right) \exp\left(\frac{m}{k_B T}(\boldsymbol{v}\cdot\boldsymbol{u}) - \frac{m}{2k_B T}|\boldsymbol{u}|^2\right) \\ &\approx \rho \left(\frac{m}{2\pi k_B T}\right)^{3/2} \exp\left(-\frac{m}{2k_B T}|\boldsymbol{v}|^2\right) \\ &\qquad \left[1 + \frac{m}{k_B T}(\boldsymbol{v}\cdot\boldsymbol{u}) + \frac{1}{2}\left(\frac{m}{k_B T}\right)^2 (\boldsymbol{v}\cdot\boldsymbol{u})^2 - \frac{m}{2k_B T}|\boldsymbol{u}|^2\right]. \end{aligned} \tag{1.46}$$

For the discrete equilibrium distribution, for all $i = 0, \ldots, n_v$, functions of the shape

$$f_i^{(eq)}(\boldsymbol{x}, t) = \tilde{A}_i(\boldsymbol{x}, t) + \tilde{B}_i(\boldsymbol{x}, t)(\boldsymbol{v}_i \cdot \boldsymbol{u}(\boldsymbol{x}, t)) + \tilde{C}_i(\boldsymbol{x}, t)(\boldsymbol{v}_i \cdot \boldsymbol{u}(\boldsymbol{x}, t))^2 + \tilde{D}_i(\boldsymbol{x}, t)|\boldsymbol{u}(\boldsymbol{x}, t)|^2$$

are taken. And associated nondimensionalized distribution functions are then given by

$$F_i^{(eq)}(\hat{\boldsymbol{x}},\hat{t}) = \hat{A}_i(\hat{\boldsymbol{x}},\hat{t}) + \hat{B}_i(\hat{\boldsymbol{x}},\hat{t})(\boldsymbol{c}_i\cdot\hat{\boldsymbol{u}}(\hat{\boldsymbol{x}},\hat{t})) + \hat{C}_i(\hat{\boldsymbol{x}},\hat{t})(\boldsymbol{c}_i\cdot\hat{\boldsymbol{u}}(\hat{\boldsymbol{x}},\hat{t}))^2 + \hat{D}_i(\hat{\boldsymbol{x}},\hat{t})|\hat{\boldsymbol{u}}(\hat{\boldsymbol{x}},\hat{t})|^2. \tag{1.47}$$

The coefficient functions $\tilde{A}_i(\boldsymbol{x},t)$, $\tilde{B}_i(\boldsymbol{x},t)$, $\tilde{C}_i(\boldsymbol{x},t)$, $\tilde{D}_i(\boldsymbol{x},t)$ and those of (1.47) $\hat{A}_i(\hat{\boldsymbol{x}},\hat{t})$, $\hat{B}_i(\hat{\boldsymbol{x}},\hat{t})$, $\hat{C}_i(\hat{\boldsymbol{x}},\hat{t})$, $\hat{D}_i(\hat{\boldsymbol{x}},\hat{t})$ are functions depending also on the density $\rho(\boldsymbol{x},t)$ and $\hat{\rho}(\hat{\boldsymbol{x}},\hat{t})$, respectively. Their explicit magnitude depends strongly on the applied discretization. In the subsequent section we will calculate them for a specific discretization.

Another possibility to compute the discrete equilibrium distribution is based on the H-theorem (Theorem 1). They can also be computed by maximizing the local entropy under given constraints [33].

1.5. Discretization Models

In this section we present some common choices for the discretization used in lattice Boltzmann methods. For a specific choice, known as D3Q19, we calculate the discrete equilibrium distribution function. For the other presented discretizations we only give the magnitude of the corresponding coefficient functions.
The discretizations are described by nondimensionalized lattice velocities which is sufficient, since there is a close connection in the discretization, see section 1.4 for details. Classically, the nondimensionalization is done such a way that the smallest velocity is normalized.

There is a wide-spread notation which goes back to Qian et al. [51], it reads DxQy, where x denotes the (spatial) dimension and y the number of lattice velocities. The latter corresponds to $n_v + 1$ in (1.30). For all presented discretization models we set $\boldsymbol{c}_0 = 0$, this velocity is related to a rest state.

1.5.1. Models of Dimension 1

When considering a one dimensional space, the simplest discretization is the division in intervals of same length where then the set of lattice points consists of the interval boundaries. The D1Q3 model as well as the D1Q5 model are based on such a discretization. In addition to the zero velocity c_0 we have in the D1Q3 model the velocities $c_1 = 1$ and $c_2 = -1$. For each direction there appear only single velocity vectors. By contrast, the D1Q5 model is a so called multi-speed model, where velocity vectors of different

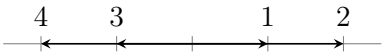

Figure 1.6.: Lattice velocities in one dimensional space.

length appear for same directions. The full set of velocities read here

$$c_0 = 0, \qquad c_1 = 1, \qquad c_2 = -1, \qquad c_3 = 2, \qquad c_4 = -2.$$

Figure 1.6 illustrates these both one dimensional models.

1.5.2. Models of Dimension 2

At the beginning of this section we gave a short introduction to lattice gas automata. There we had as an example the FHP model, and we have mentioned the HPP model which are both two dimensional. The FHP model uses a triangular lattice (see also figure 1.2) and the HPP a square lattice. The former can also be successfully used when dealing with lattice Boltzmann methods for the simulation of fluid flows. The associated discretization of FHP is referred to as D2Q7 with corresponding velocities

$$\boldsymbol{c}_i = \left(\cos\left(\frac{2\pi i}{6}\right), \sin\left(\frac{2\pi i}{6}\right) \right), \qquad i = 1, \dots 6,$$

figure 1.7 (a) depicts this model. The HPP model uses a four velocity discretization, adding a rest state we can state the D2Q5 model with lattice velocities

$$\boldsymbol{c}_1 = (1, 0), \qquad \boldsymbol{c}_2 = (0, 1), \qquad \boldsymbol{c}_3 = (-1, 0), \qquad \boldsymbol{c}_4 = (0, -0),$$

but note that the HPP model failed to yield the Navier-Stokes equations, because of insufficient symmetry of the lattice. A very common discretization in two dimensions is the D2Q9 model, used e.g. in [37]. That model consists of each four velocity vectors of

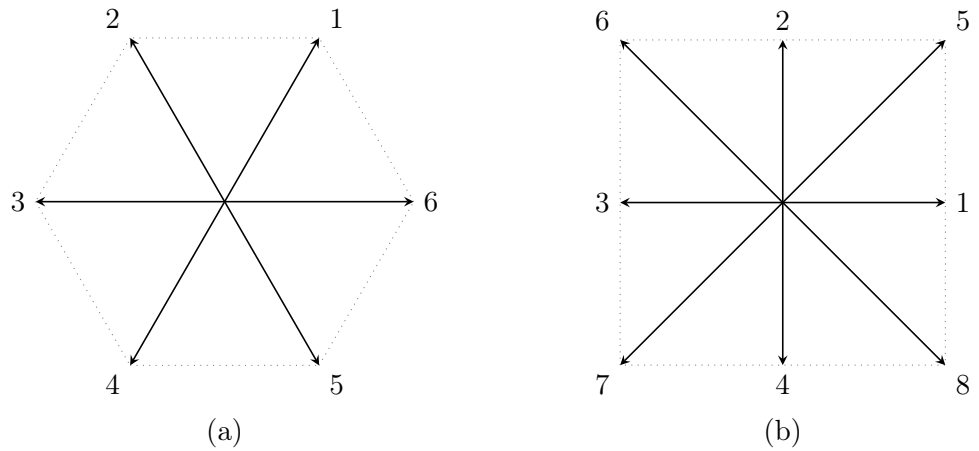

Figure 1.7.: Lattice velocities for a triangular (a) and square (b) lattice in two dimensions.

length 1 and $\sqrt{2}$, they read

$$\begin{aligned} \boldsymbol{c}_1 &= (1,0), & \boldsymbol{c}_2 &= (0,1), & \boldsymbol{c}_3 &= (-1,0), & \boldsymbol{c}_4 &= (0,-1), \\ \boldsymbol{c}_5 &= (1,1), & \boldsymbol{c}_6 &= (-1,1), & \boldsymbol{c}_7 &= (-1,-1), & \boldsymbol{c}_8 &= (1,-1), \end{aligned}$$

see figure 1.7 (b) for a visualization. Several extensions of the D2Q9 model exist. As only one example the multi-speed D2Q13 model exhibits the additional velocity vectors

$$\boldsymbol{c}_9 = (2,0), \qquad \boldsymbol{c}_{10} = (0,2), \qquad \boldsymbol{c}_{11} = (-2,0), \qquad \boldsymbol{c}_{12} = (0,-2).$$

1.5.3. Models of Dimension 3

In three dimensions the analogue to the square lattice in two dimensions is a cubic lattice. Connecting nearest neighbors we achieve six lattice velocities of length 1, twelve velocity vectors of length $\sqrt{2}$ and eight of length $\sqrt{3}$, see figure 1.8 (a), (b) and (c), respectively. Different combinations of these lattice velocities yield to well-known three dimensional models at a time [68]. We get the D3Q15 model by taking the velocity vectors of length 1 and $\sqrt{3}$, hence

$$\begin{aligned} \boldsymbol{c}_1 &= (1,0,0), & \boldsymbol{c}_2 &= (0,1,0), & \boldsymbol{c}_3 &= (-1,0,0), & \boldsymbol{c}_4 &= (0,-1,0), \\ \boldsymbol{c}_5 &= (0,0,1), & \boldsymbol{c}_6 &= (0,0,-1), & & & & \\ \boldsymbol{c}_7 &= (1,-1,1), & \boldsymbol{c}_8 &= (1,1,1), & \boldsymbol{c}_9 &= (-1,1,1), & \boldsymbol{c}_{10} &= (-1,-1,1), \\ \boldsymbol{c}_{11} &= (1,-1,-1), & \boldsymbol{c}_{12} &= (1,1,-1), & \boldsymbol{c}_{13} &= (-1,1,-1), & \boldsymbol{c}_{14} &= (-1,-1,-1). \end{aligned}$$

Extending this model by the twelve $\sqrt{2}$-velocity vectors we obtain the D3Q27 model, that is

$$\begin{aligned} \boldsymbol{c}_{15} &= (1,1,0), & \boldsymbol{c}_{16} &= (-1,1,0), & \boldsymbol{c}_{17} &= (-1,-1,0), & \boldsymbol{c}_{18} &= (1,-1,0), \\ \boldsymbol{c}_{19} &= (1,0,1), & \boldsymbol{c}_{20} &= (-1,0,1), & \boldsymbol{c}_{21} &= (-1,0,-1), & \boldsymbol{c}_{22} &= (1,0,-1), \\ \boldsymbol{c}_{23} &= (0,1,1), & \boldsymbol{c}_{24} &= (0,-1,1), & \boldsymbol{c}_{25} &= (0,-1,-1), & \boldsymbol{c}_{26} &= (0,1,-1). \end{aligned}$$

The already mentioned D3Q19 model is constructed with lattice velocities of length 1 and $\sqrt{2}$. For this model we compute the discrete equilibrium distribution function in the following.
The triangular and square lattice in two dimensions, as well as the cubic lattice in the three dimensional space are space filling discretizations. But also advantageous non-space filling discretization models were proposed, see for more information [47].

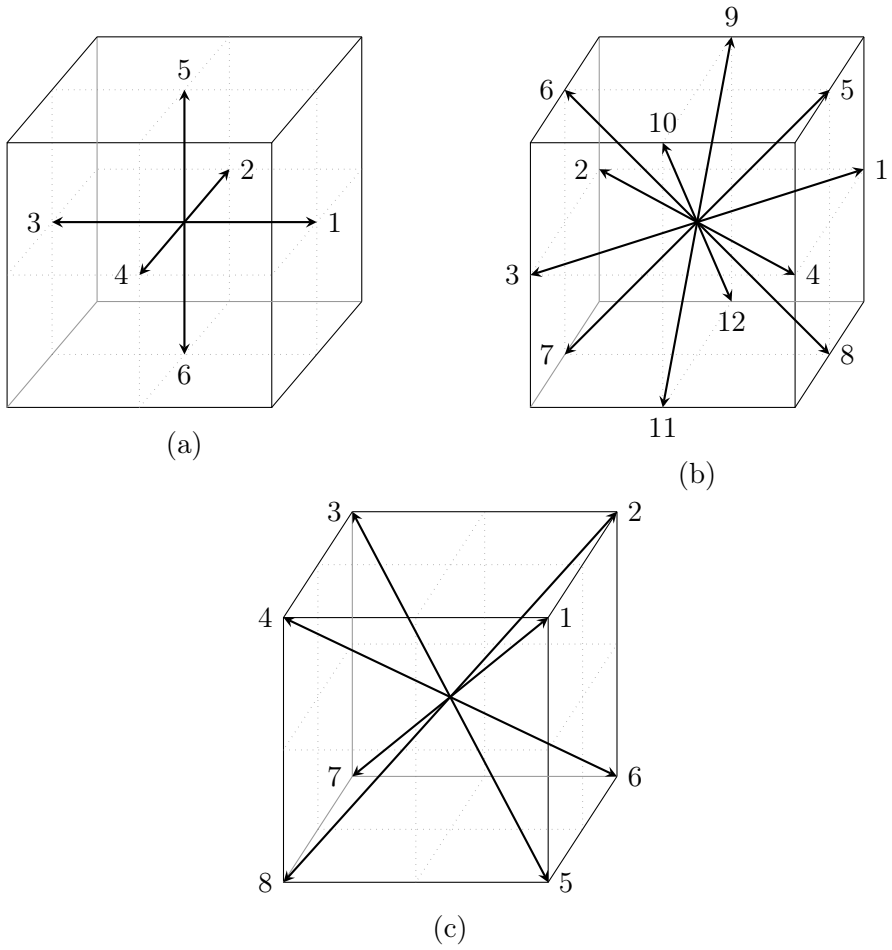

Figure 1.8.: Lattice velocities for cubic lattice in three dimensions.

1.5.4. Discrete Equilibrium Distribution in D3Q19

In this subsection we compute the discrete equilibrium distribution function in the D3Q19 model, analogue to [69]. This means we compute the coefficient functions in (1.47) for all $i = 0, \ldots, 18$. A reasonable choice for the coefficients ensures the non-negativity for all $F_i^{(eq)}$, later on in the calculation the demand of non-negativity will be

used. The full set of lattice velocities in D3Q19 read as follows:

$$\begin{aligned}
&\boldsymbol{c}_0 = (0,0,0),\\
&\boldsymbol{c}_1 = (1,0,0), \quad \boldsymbol{c}_2 = (0,1,0), \quad \boldsymbol{c}_3 = (-1,0,0), \quad \boldsymbol{c}_4 = (0,-1,0),\\
&\boldsymbol{c}_5 = (0,0,1), \quad \boldsymbol{c}_6 = (0,0,-1),\\
&\boldsymbol{c}_7 = (1,1,0), \quad \boldsymbol{c}_8 = (-1,1,0), \quad \boldsymbol{c}_9 = (-1,-1,0), \quad \boldsymbol{c}_{10} = (1,-1,0),\\
&\boldsymbol{c}_{11} = (1,0,1), \quad \boldsymbol{c}_{12} = (-1,0,1), \quad \boldsymbol{c}_{13} = (-1,0,-1), \quad \boldsymbol{c}_{14} = (1,0,-1),\\
&\boldsymbol{c}_{15} = (0,1,1), \quad \boldsymbol{c}_{16} = (0,-1,1), \quad \boldsymbol{c}_{17} = (0,-1,-1), \quad \boldsymbol{c}_{18} = (0,1,-1).
\end{aligned} \tag{1.48}$$

The coefficient functions should depend only on the mass density. We assume that for fixed $\hat{\boldsymbol{x}}$ and $\hat{t}$, $\hat{A}_i(\hat{\boldsymbol{x}},\hat{t})$ and $\hat{A}_j(\hat{\boldsymbol{x}},\hat{t})$ given in (1.47) differ only if $|\boldsymbol{c}_i|$ and $|\boldsymbol{c}_j|$ have different values, for $i,j = 0,\dots,18$. Same for the $\hat{B}_i(\hat{\boldsymbol{x}},\hat{t})$, $\hat{C}_i(\hat{\boldsymbol{x}},\hat{t})$ and $\hat{D}_i(\hat{\boldsymbol{x}},\hat{t})$, $i = 0,\dots,18$. Therefore we can rewrite the coefficients in (1.47) by

$$\begin{aligned}
&A_0 \equiv A_0(\hat{\boldsymbol{x}},\hat{t}) := \hat{A}_0(\hat{\boldsymbol{x}},\hat{t}), && B_0 \equiv B_0(\hat{\boldsymbol{x}},\hat{t}) := \hat{B}_0(\hat{\boldsymbol{x}},\hat{t}),\\
&C_0 \equiv C_0(\hat{\boldsymbol{x}},\hat{t}) := \hat{C}_0(\hat{\boldsymbol{x}},\hat{t}), && D_0 \equiv D_0(\hat{\boldsymbol{x}},\hat{t}) := \hat{D}_0(\hat{\boldsymbol{x}},\hat{t}),\\
&A_1 \equiv A_1(\hat{\boldsymbol{x}},\hat{t}) := \hat{A}_i(\hat{\boldsymbol{x}},\hat{t}), && B_1 \equiv B_1(\hat{\boldsymbol{x}},\hat{t}) := \hat{B}_i(\hat{\boldsymbol{x}},\hat{t}), && i = 1,\dots 6,\\
&C_1 \equiv C_1(\hat{\boldsymbol{x}},\hat{t}) := \hat{C}_i(\hat{\boldsymbol{x}},\hat{t}), && D_1 \equiv D_1(\hat{\boldsymbol{x}},\hat{t}) := \hat{D}_i(\hat{\boldsymbol{x}},\hat{t}), && i = 1,\dots 6,\\
&A_2 \equiv A_2(\hat{\boldsymbol{x}},\hat{t}) := \hat{A}_i(\hat{\boldsymbol{x}},\hat{t}), && B_2 \equiv B_2(\hat{\boldsymbol{x}},\hat{t}) := \hat{B}_i(\hat{\boldsymbol{x}},\hat{t}), && i = 7,\dots 18,\\
&C_2 \equiv C_2(\hat{\boldsymbol{x}},\hat{t}) := \hat{C}_i(\hat{\boldsymbol{x}},\hat{t}), && D_2 \equiv D_2(\hat{\boldsymbol{x}},\hat{t}) := \hat{D}_i(\hat{\boldsymbol{x}},\hat{t}), && i = 7,\dots 18,
\end{aligned}$$

which yields a reduced system of equations with 10 free parameters

$$F_i^{(eq)}(\hat{\boldsymbol{x}},\hat{t}) = \begin{cases} A_0 + D_0|\hat{\boldsymbol{u}}(\hat{\boldsymbol{x}},\hat{t})|^2, & i = 0\\ A_1 + B_1(\boldsymbol{c}_i\cdot\hat{\boldsymbol{u}}(\hat{\boldsymbol{x}},\hat{t})) + C_1(\boldsymbol{c}_i\cdot\hat{\boldsymbol{u}}(\hat{\boldsymbol{x}},\hat{t}))^2 + D_1|\hat{\boldsymbol{u}}(\hat{\boldsymbol{x}},\hat{t})|^2, & i = 1,\dots,6\\ A_2 + B_2(\boldsymbol{c}_i\cdot\hat{\boldsymbol{u}}(\hat{\boldsymbol{x}},\hat{t})) + C_2(\boldsymbol{c}_i\cdot\hat{\boldsymbol{u}}(\hat{\boldsymbol{x}},\hat{t}))^2 + D_2|\hat{\boldsymbol{u}}(\hat{\boldsymbol{x}},\hat{t})|^2, & i = 7,\dots,18 \end{cases} \tag{1.49}$$

where B_0 and C_0 do not appear, because $\boldsymbol{c}_0\cdot\hat{\boldsymbol{u}}(\hat{\boldsymbol{x}},\hat{t}) = 0$ and hence they do not have a contribution. The parameters are actually still coefficient functions, depending on spatial position, time and density. In the computation we fix $\hat{\boldsymbol{x}}$ and $\hat{t}$, that is why we omit the function arguments here and in the following computation. We obtain from a nondimensionalized version of (1.45) the following general constraints

$$\begin{aligned}
\hat{\rho} &= \sum_{i=0}^{n_v} F_i^{(eq)},\\
\hat{\rho}\hat{\boldsymbol{u}} &= \sum_{i=0}^{n_v} \boldsymbol{c}_i F_i^{(eq)},
\end{aligned} \tag{1.50}$$

which imply, when using the lattice velocities (1.48) explicitly, two equations for the free parameters ($n_v = 18$):

$$\begin{aligned}
\hat{\rho} &= F_0^{(eq)} + \sum_{i=1}^{6} F_i^{(eq)} + \sum_{i=7}^{18} F_i^{(eq)} \\
&= \left[A_0 + D_0|\hat{\boldsymbol{u}}|^2\right] + \Bigg[6A_1 + B_1 \underbrace{\sum_{i=1}^{6}(\boldsymbol{c}_i \cdot \boldsymbol{u})}_{=0} + C_1 \underbrace{\sum_{i=1}^{6}(\boldsymbol{c}_i \cdot \boldsymbol{u})^2}_{=2|\hat{\boldsymbol{u}}|^2} + 6D_1|\hat{\boldsymbol{u}}|^2\Bigg] \\
&\quad + \Bigg[12A_2 + B_2 \underbrace{\sum_{i=7}^{18}(\boldsymbol{c}_i \cdot \boldsymbol{u})}_{=0} + C_2 \underbrace{\sum_{i=7}^{18}(\boldsymbol{c}_i \cdot \boldsymbol{u})^2}_{=8|\hat{\boldsymbol{u}}|^2} + 12D_2|\hat{\boldsymbol{u}}|^2\Bigg] \\
&= A_0 + 6A_1 + 12A_2 + \left(2C_1 + 8C_2 + D_0 + 6D_1 + 12D_2\right)|\hat{\boldsymbol{u}}|^2,
\end{aligned}$$

$$\hat{\rho}\hat{\boldsymbol{u}} = (2B_1 + 8B_2)\hat{\boldsymbol{u}}$$

This can be decomposed into three constraints

$$\begin{aligned}
\hat{\rho} &= A_0 + 6A_1 + 12A_2, \\
0 &= 2C_1 + 8C_2 + D_0 + 6D_1 + 12D_2, \\
\hat{\rho} &= 2B_1 + 8B_2,
\end{aligned} \tag{1.51}$$

and we have only three equations for ten unknowns. Clearly, the solution is not unique. Additional constraints can be imposed, thus we demand constraints [69] which transform the (zeroth order) momentum flux tensor

$$\left(P_{\alpha,\beta}\right)_{\alpha,\beta=1,2,3} = \sum_{i=0}^{18} c_i^{\alpha} c_i^{\beta} F_i^{(eq)}$$

into the form

$$P = \hat{\rho}\hat{\boldsymbol{u}}\hat{\boldsymbol{u}}^T + pI, \tag{1.52}$$

which reads here

$$P = \begin{pmatrix} \hat{\rho}\hat{u}^1\hat{u}^1 + p & \hat{\rho}\hat{u}^1\hat{u}^2 & \hat{\rho}\hat{u}^1\hat{u}^3 \\ \hat{\rho}\hat{u}^1\hat{u}^2 & \hat{\rho}\hat{u}^2\hat{u}^2 + p & \hat{\rho}\hat{u}^2\hat{u}^3 \\ \hat{\rho}\hat{u}^1\hat{u}^3 & \hat{\rho}\hat{u}^2\hat{u}^3 & \hat{\rho}\hat{u}^3\hat{u}^3 + p \end{pmatrix},$$

with pressure p, identity matrix I and c_i^j, $\hat{u}^j$ denoting the jth component of $\boldsymbol{c}_i$ and $\hat{\boldsymbol{u}}$, respectively. Taking again the lattice velocities (1.48) into account the entries in the

tensor can be computed, we obtain

$$P_{k,k} = (2A_1 + 8A_2) + (2C_1 + 4C_2)\left(\hat{u}^k\right)^2 + (4C_2 + 2D_1 + 8D_2)|\hat{\boldsymbol{u}}|^2, \qquad k = 1,2,3,$$
$$P_{j,k} = 8C_2\hat{u}^j\hat{u}^k, \qquad j,k = 1,2,3, \quad j \neq k.$$

Here, we can deduce the constraints to achieve the momentum flux tensor in the desired form, we get

$$\begin{aligned} \hat{\rho} &= 2C_1 + 4C_2, \\ 0 &= 4C_2 + 2D_1 + 8D_2, \\ \hat{\rho} &= 8C_2, \end{aligned} \tag{1.53}$$

and the pressure p is then given by the portion which is independent of the velocity $\hat{\boldsymbol{u}}$, i.e. in this model by $p = 2A_1 + 8A_2$. From the first and third equation of (1.53) we can conclude

$$C_1 = \frac{1}{4}\hat{\rho} \quad \text{and} \quad C_2 = \frac{1}{8}\hat{\rho},$$

and hence the second equation of (1.51) and (1.53) each can be rewritten. The not yet determined unknowns A_0, A_1, A_2, B_1, B_2, D_0, D_1 and D_2 are restricted by only four equations

$$\begin{aligned} \hat{\rho} &= A_0 + 6A_1 + 12A_2, \\ -\frac{3}{2}\hat{\rho} &= D_0 + 6D_1 + 12D_2, \\ \hat{\rho} &= 2B_1 + 8B_2, \\ -\frac{1}{2}\hat{\rho} &= 2D_1 + 8D_2. \end{aligned} \tag{1.54}$$

The constraints we imposed to transform the momentum flux tensor do not lead to a unique equilibrium distribution. Some further arbitrary constraints can be imposed, we adapt the idea of linear relations from [69] to the given discretization model here:

$$\begin{aligned} A_0 &= 3rA_1, \\ A_1 &= rA_2, \\ B_1 &= rB_2, \\ D_0 &= 3rD_1. \end{aligned}$$

for an additional free parameter $r \in \mathbb{R}$. The third equation of (1.54) simplifies

$$\hat{\rho} = B_2(2r + 8) \qquad \Rightarrow \qquad B_2 = \frac{\hat{\rho}}{2(r+4)},$$

	weights for				
	$\|\boldsymbol{c}_i\| = 0$	$\|\boldsymbol{c}_i\| = 1$	$\|\boldsymbol{c}_i\| = \sqrt{2}$	$\|\boldsymbol{c}_i\| = \sqrt{3}$	$\|\boldsymbol{c}_i\| = 2$
D1Q3	$\frac{2}{3}$	$\frac{1}{6}$	-	-	-
D1Q5	$\frac{1}{2}$	$\frac{1}{6}$	-	-	$\frac{1}{12}$
D2Q5	$\frac{1}{3}$	$\frac{1}{6}$	-	-	-
D2Q7	$\frac{1}{2}$	$\frac{1}{12}$	-	-	-
D2Q9	$\frac{4}{9}$	$\frac{1}{9}$	$\frac{1}{36}$	-	-
D3Q15	$\frac{2}{9}$	$\frac{1}{9}$	-	$\frac{1}{72}$	-
D3Q19	$\frac{1}{3}$	$\frac{1}{18}$	$\frac{1}{36}$	-	-
D3Q27	$\frac{8}{27}$	$\frac{2}{27}$	$\frac{1}{54}$	$\frac{1}{216}$	-

Table 1.1.: Weights for equilibrium distribution function for several models.

and from the first equation of (1.54) we get

$$\hat{\rho} = 3A_2(r^2 + 2r + 4) \qquad \Rightarrow \quad A_2 = \frac{\hat{\rho}}{3(r^2 + 2r + 4)}.$$

When we equate the right hand side of the second equation of (1.54) with three times the right hand side of the forth equation we obtain

$$D_1(3r + 6) + 12D_2 = 6D_1 + 24D_2 \qquad \Leftrightarrow \qquad rD_1 - 4D_2 = 0.$$

With the additional condition $D_1 = rD_2$ we can resolve the latter equation, this yields $(r^2 - 4)D_2 = 0$ and we can conclude $r = \pm 2$. The solution $r = -2$ yields negative equilibrium distributions, hence we take $r = 2$. This implies

$$\begin{aligned} A_2 = \frac{1}{36}\hat{\rho} \quad &\Rightarrow \quad A_1 = \frac{2}{36}\hat{\rho} \quad \Rightarrow \quad A_0 = \frac{12}{36}\hat{\rho}, \\ B_2 = \frac{1}{12}\hat{\rho} \quad &\Rightarrow \quad B_1 = \frac{2}{12}\hat{\rho}. \end{aligned}$$

And finally the magnitudes of D_0, D_1 and D_2 can be obtained by the forth equation of (1.54)

$$-\frac{1}{2}\hat{\rho} = 2D_1 + 8D_2 = 12D_2 \quad \Rightarrow \quad D_2 = -\frac{1}{24}\hat{\rho},$$

which implies $D_1 = -\frac{2}{24}\hat{\rho}$ and $D_0 = -\frac{12}{24}\hat{\rho}$. Since all free parameters in (1.49) are now computed, we can state the discrete equilibrium distribution for the D3Q19 model:

$$
\begin{aligned}
F_0^{(eq)}(\hat{\boldsymbol{x}},\hat{t}) &= \hat{\rho}(\hat{\boldsymbol{x}},\hat{t})\left[\frac{1}{3} - \frac{1}{2}|\hat{\boldsymbol{u}}(\hat{\boldsymbol{x}},\hat{t})|^2\right],\\
F_i^{(eq)}(\hat{\boldsymbol{x}},\hat{t}) &= \hat{\rho}(\hat{\boldsymbol{x}},\hat{t})\left[\frac{1}{18} + \frac{1}{6}(\boldsymbol{c}_i\cdot\hat{\boldsymbol{u}}(\hat{\boldsymbol{x}},\hat{t})) + \frac{1}{4}(\boldsymbol{c}_i\cdot\hat{\boldsymbol{u}}(\hat{\boldsymbol{x}},\hat{t}))^2 - \frac{1}{12}|\hat{\boldsymbol{u}}(\hat{\boldsymbol{x}},\hat{t})|^2\right],\\
F_j^{(eq)}(\hat{\boldsymbol{x}},\hat{t}) &= \hat{\rho}(\hat{\boldsymbol{x}},\hat{t})\left[\frac{1}{36} + \frac{1}{12}(\boldsymbol{c}_j\cdot\hat{\boldsymbol{u}}(\hat{\boldsymbol{x}},\hat{t})) + \frac{1}{8}(\boldsymbol{c}_j\cdot\hat{\boldsymbol{u}}(\hat{\boldsymbol{x}},\hat{t}))^2 - \frac{1}{24}|\hat{\boldsymbol{u}}(\hat{\boldsymbol{x}},\hat{t})|^2\right],
\end{aligned}
$$

for $i = 1,\dots,6$ and $j = 7,\dots,18$. Writing these equation as

$$
\begin{aligned}
F_0^{(eq)}(\hat{\boldsymbol{x}},\hat{t}) &= \omega_0\hat{\rho}(\hat{\boldsymbol{x}},\hat{t})\left[1 - \frac{3}{2}|\hat{\boldsymbol{u}}(\hat{\boldsymbol{x}},\hat{t})|^2\right]\\
F_i^{(eq)}(\hat{\boldsymbol{x}},\hat{t}) &= \omega_i\hat{\rho}(\hat{\boldsymbol{x}},\hat{t})\left[1 + 3(\boldsymbol{c}_i\cdot\hat{\boldsymbol{u}}(\hat{\boldsymbol{x}},\hat{t})) + \frac{9}{2}(\boldsymbol{c}_i\cdot\hat{\boldsymbol{u}}(\hat{\boldsymbol{x}},\hat{t}))^2 - \frac{3}{2}|\hat{\boldsymbol{u}}(\hat{\boldsymbol{x}},\hat{t})|^2\right]
\end{aligned}
\tag{1.55}
$$

for $i = 1,\dots,18$, with

$$
\omega_0 = \frac{1}{3},\ \omega_j = \frac{1}{18},\ \omega_k = \frac{1}{36}, \qquad j = 1,\dots,6, \quad k = 7,\dots,18, \tag{1.56}
$$

is more suitable for an implementation. This result coincides with the Taylor expansion of the continuous equilibrium distribution (1.46) in the sense that the coefficient of the $|\boldsymbol{u}|^2$ term within the square bracket is -0.5 times the coefficient of the $\boldsymbol{v}\cdot\boldsymbol{u}$ term. Same for the coefficient of the $(\boldsymbol{v}\cdot\boldsymbol{u})^2$ term which is 0.5 times the coefficient of the $\boldsymbol{v}\cdot\boldsymbol{u}$ term squared. The pressure in this D3Q19 model is given by

$$
p(\hat{\boldsymbol{x}},\hat{t}) = 2A_1 + 8A_2 = \frac{1}{3}\hat{\rho}(\hat{\boldsymbol{x}},\hat{t}). \tag{1.57}
$$

The derivation of discrete equilibrium distributions for other models is analogue to our calculation presented here. For the other models stated in the current section possible equilibrium distributions are given in table 1.1 which correspond to equilibrium distribution functions in the shape of (1.55) [44, 46, 59, 61]. In table 1.1 only the weights ω_i are given.

1.6. Chapman-Enskog Expansion

In section 1.2 we have shown that the continuous Boltzmann equation (1.4) covers macroscopic equations. The computational simulation is based on the lattice BGK equation (1.42), a discretized version of the Boltzmann equation (1.4) with an approximating term (1.28) for the collision integral. In order to show that the lattice BGK equation also satisfies some meaningful macroscopic equations, we use a Chapman-Enskog expansion. For more details and the background of the Chapman-Enskog expansion see for instance

[7, 54, 61, 69].

1.6.1. Terms of First and Second Order

The procedure used in the current and subsequent subsection was inspired by [10, 27, 32]. Beginning the calculation, we employ a Taylor expansion of the left hand side of (1.42) and obtain for all $i = 0, \dots, n_v$ up to order $\Delta\hat{t}^2$:

$$F_i(\hat{\boldsymbol{x}} + \boldsymbol{c}_i\Delta\hat{t}, \hat{t} + \Delta\hat{t}) = \Delta\hat{t}\left(\frac{\partial}{\partial\hat{t}} + \boldsymbol{c}_i \cdot \boldsymbol{\nabla}\right) F_i(\hat{\boldsymbol{x}}, \hat{t}) + \frac{1}{2}\Delta\hat{t}^2\left(\frac{\partial}{\partial\hat{t}} + \boldsymbol{c}_i \cdot \boldsymbol{\nabla}\right)^2 F_i(\hat{\boldsymbol{x}}, \hat{t}).$$

The Knudsen number is a dimensionless number defined as the ratio of the particle mean free path to the characteristic length scale. Since t_c gives the time between collisions, and L is the characteristic length scale, the parameter ε defined in (1.32) can be considered as the Knudsen number. Due to (1.35) the nondimensionalized time step $\Delta\hat{t}$ equals the parameter ε.
The complete lattice BGK equation after a Taylor expansion of the left hand side up to second order then reads

$$\varepsilon\left(\frac{\partial}{\partial\hat{t}} + \boldsymbol{c}_i \cdot \boldsymbol{\nabla}\right) F_i(\hat{\boldsymbol{x}}, \hat{t}) + \frac{1}{2}\varepsilon^2\left(\frac{\partial}{\partial\hat{t}} + \boldsymbol{c}_i \cdot \boldsymbol{\nabla}\right)^2 F_i(\hat{\boldsymbol{x}}, \hat{t}) = -\frac{1}{\hat{\tau}_c}\left[F_i(\hat{\boldsymbol{x}}, \hat{t}) - F_i^{(eq)}(\hat{\boldsymbol{x}}, \hat{t})\right]. \tag{1.58}$$

We expand the distributions $F_i(\hat{\boldsymbol{x}}, \hat{t})$ around the equilibrium distribution, we get

$$F_i(\hat{\boldsymbol{x}}, \hat{t}) = F_i^{(0)}(\hat{\boldsymbol{x}}, \hat{t}) + \varepsilon F_i^{(1)}(\hat{\boldsymbol{x}}, \hat{t}) + \varepsilon^2 F_i^{(2)}(\hat{\boldsymbol{x}}, \hat{t}) + \mathcal{O}(\varepsilon^3), \tag{1.59}$$

where the zeroth order $F_i^{(0)}(\hat{\boldsymbol{x}}, \hat{t})$ represents the equilibrium distribution $F_i^{(eq)}(\hat{\boldsymbol{x}}, \hat{t})$. The definitions of the macroscopic density (1.43) and velocity (1.44) as well as the demanded constraints (1.50) in the construction of the equilibrium distributions yield

$$\begin{aligned} \hat{\rho}(\hat{\boldsymbol{x}}, \hat{t}) &= \sum_{i=0}^{n_v} F_i(\hat{\boldsymbol{x}}, \hat{t}) = \sum_{i=0}^{n_v} F_i^{(0)}(\hat{\boldsymbol{x}}, \hat{t}), \\ \hat{\rho}(\hat{\boldsymbol{x}}, \hat{t})\hat{\boldsymbol{u}}(\hat{\boldsymbol{x}}, \hat{t}) &= \sum_{i=0}^{n_v} \boldsymbol{c}_i F_i(\hat{\boldsymbol{x}}, \hat{t}) = \sum_{i=0}^{n_v} \boldsymbol{c}_i F_i^{(0)}(\hat{\boldsymbol{x}}, \hat{t}). \end{aligned} \tag{1.60}$$

Hence, we can conclude

$$\begin{aligned} \sum_{i=0}^{n_v} F_i^{(1)}(\hat{\boldsymbol{x}}, \hat{t}) &= \sum_{i=0}^{n_v} F_i^{(2)}(\hat{\boldsymbol{x}}, \hat{t}) = 0, \\ \sum_{i=0}^{n_v} \boldsymbol{c}_i F_i^{(1)}(\hat{\boldsymbol{x}}, \hat{t}) &= \sum_{i=0}^{n_v} \boldsymbol{c}_i F_i^{(2)}(\hat{\boldsymbol{x}}, \hat{t}) = 0. \end{aligned} \tag{1.61}$$

In a similar manner as the distribution $F_i(\hat{\boldsymbol{x}}, \hat{t})$ we expand the differential operator with respect to time by

$$\frac{\partial}{\partial \hat{t}} = \frac{\partial^{(1)}}{\partial \hat{t}} + \varepsilon \frac{\partial^{(2)}}{\partial \hat{t}} + \mathcal{O}(\varepsilon^2), \tag{1.62}$$

whereas the spatial differential operator obeys

$$\boldsymbol{\nabla} = \boldsymbol{\nabla}^{(1)}. \tag{1.63}$$

We substitute (1.59), (1.62) and (1.63) in (1.58) and split terms with respect to orders of ε. The terms of order ε read

$$\varepsilon \left(\frac{\partial^{(1)}}{\partial \hat{t}} + \boldsymbol{c}_i \cdot \boldsymbol{\nabla}^{(1)} \right) F_i^{(0)}(\hat{\boldsymbol{x}}, \hat{t}) = -\frac{1}{\hat{\tau}_c} \varepsilon F_i^{(1)}(\hat{\boldsymbol{x}}, \hat{t}). \tag{1.64}$$

Taking a further derivative this equation implies the following relation between $F_i^{(0)}(\hat{\boldsymbol{x}}, \hat{t})$ and $F_i^{(1)}(\hat{\boldsymbol{x}}, \hat{t})$

$$\frac{1}{2} \left(\frac{\partial^{(1)}}{\partial \hat{t}} + \boldsymbol{c}_i \cdot \boldsymbol{\nabla}^{(1)} \right)^2 F_i^{(0)}(\hat{\boldsymbol{x}}, \hat{t}) = -\frac{1}{2\hat{\tau}_c} \left(\frac{\partial^{(1)}}{\partial \hat{t}} + \boldsymbol{c}_i \cdot \boldsymbol{\nabla}^{(1)} \right) F_i^{(1)}(\hat{\boldsymbol{x}}, \hat{t}). \tag{1.65}$$

The terms of order ε^2 are given by

$$\varepsilon^2 \left[\left(\frac{\partial^{(1)}}{\partial \hat{t}} + \boldsymbol{c}_i \cdot \boldsymbol{\nabla}^{(1)} \right) F_i^{(1)}(\hat{\boldsymbol{x}}, \hat{t}) + \frac{\partial^{(2)}}{\partial \hat{t}} F_i^{(0)}(\hat{\boldsymbol{x}}, \hat{t}) \right.$$
$$\left. + \frac{1}{2} \left(\frac{\partial^{(1)}}{\partial \hat{t}} + \boldsymbol{c}_i \cdot \boldsymbol{\nabla}^{(1)} \right)^2 F_i^{(0)}(\hat{\boldsymbol{x}}, \hat{t}) \right] = -\frac{1}{\hat{\tau}_c} \varepsilon^2 F_i^{(2)}(\hat{\boldsymbol{x}}, \hat{t}),$$

which can be simplified by using (1.65) to

$$\varepsilon^2 \left[\left(1 - \frac{1}{2\hat{\tau}_c} \right) \left(\frac{\partial^{(1)}}{\partial \hat{t}} + \boldsymbol{c}_i \cdot \boldsymbol{\nabla}^{(1)} \right) F_i^{(1)}(\hat{\boldsymbol{x}}, \hat{t}) + \frac{\partial^{(2)}}{\partial \hat{t}} F_i^{(0)}(\hat{\boldsymbol{x}}, \hat{t}) \right] = -\frac{1}{\hat{\tau}_c} \varepsilon^2 F_i^{(2)}(\hat{\boldsymbol{x}}, \hat{t}). \tag{1.66}$$

In the continuous case the macroscopic equations were obtained by an integration of the Boltzmann equation, more precisely the continuity equation was achieved in this manner. For the momentum equation the first moment of the Boltzmann equation was computed, i.e. an integration of the Boltzmann equation multiplied with $\boldsymbol{v}$ led to that equation. Now considering the discretized equation we take the summation over all possible velocities instead. The first order terms are achieved by equation (1.64),

meaning

$$\sum_{i=0}^{n_v} \varepsilon \left(\frac{\partial^{(1)}}{\partial \hat{t}} + \boldsymbol{c}_i \cdot \boldsymbol{\nabla}^{(1)} \right) F_i^{(0)}(\hat{\boldsymbol{x}}, \hat{t}) = \sum_{i=0}^{n_v} \left(-\frac{1}{\hat{\tau}_c} \right) \varepsilon F_i^{(1)}(\hat{\boldsymbol{x}}, \hat{t}).$$

Division by ε and using (1.60) and (1.61) for the left and right hand side, respectively, yields

$$\frac{\partial^{(1)}}{\partial \hat{t}} \hat{\rho}(\hat{\boldsymbol{x}}, \hat{t}) + \boldsymbol{\nabla}^{(1)} \cdot \left(\hat{\rho}(\hat{\boldsymbol{x}}, \hat{t}) \hat{\boldsymbol{u}}(\hat{\boldsymbol{x}}, \hat{t}) \right) = 0. \tag{1.67}$$

Analogue to the continuous case, summing (1.64) after multiplying with $\boldsymbol{c}_i$ gives for the momentum

$$\frac{\partial^{(1)}}{\partial \hat{t}} \left(\hat{\rho}(\hat{\boldsymbol{x}}, \hat{t}) \hat{\boldsymbol{u}}(\hat{\boldsymbol{x}}, \hat{t}) \right) + \boldsymbol{\nabla}^{(1)} \cdot P^{(0)}(\hat{\boldsymbol{x}}, \hat{t}) = 0, \tag{1.68}$$

with

$$P^{(0)}(\hat{\boldsymbol{x}}, \hat{t}) = \sum_{i=0}^{n_v} \boldsymbol{c}_i \boldsymbol{c}_i^T F_i^{(0)}(\hat{\boldsymbol{x}}, \hat{t})$$

where the equation was divided by ε and the conditions (1.60) and (1.61) were used. The expansion (1.59) implies an expansion for the momentum flux tensor

$$P(\hat{\boldsymbol{x}}, \hat{t}) = P^{(0)}(\hat{\boldsymbol{x}}, \hat{t}) + \varepsilon P^{(1)}(\hat{\boldsymbol{x}}, \hat{t}) + \varepsilon^2 P^{(2)}(\hat{\boldsymbol{x}}, \hat{t}) + \mathcal{O}(\varepsilon^3),$$

with

$$P(\hat{\boldsymbol{x}}, \hat{t}) = \sum_{i=0}^{n_v} \boldsymbol{c}_i \boldsymbol{c}_i^T F(\hat{\boldsymbol{x}}, \hat{t}).$$

In the construction of the equilibrium distribution (see section 1.5) we prescribed the form of the zeroth order momentum flux tensor $P^{(0)}(\hat{\boldsymbol{x}}, \hat{t})$, cf. (1.52), hence equation (1.68) changes to

$$\frac{\partial^{(1)}}{\partial \hat{t}} \left(\hat{\rho}(\hat{\boldsymbol{x}}, \hat{t}) \hat{\boldsymbol{u}}(\hat{\boldsymbol{x}}, \hat{t}) \right) + \boldsymbol{\nabla}^{(1)} \cdot \left(\hat{\rho}(\hat{\boldsymbol{x}}, \hat{t}) \hat{\boldsymbol{u}}(\hat{\boldsymbol{x}}, \hat{t}) \hat{\boldsymbol{u}}(\hat{\boldsymbol{x}}, \hat{t})^T \right) = -\boldsymbol{\nabla}^{(1)} p(\hat{\boldsymbol{x}}, \hat{t}). \tag{1.69}$$

Clearly, this step is only valid, if the momentum flux tensor is given in the form (1.52), that condition to the equilibrium distribution is satisfied by the models presented in the previous section.

For the second order terms (1.66), a simple summation yields

$$\varepsilon^2 \sum_{i=0}^{n_v} \left[\left(1 - \frac{1}{2\hat{\tau}_c} \right) \left(\frac{\partial^{(1)}}{\partial \hat{t}} + \boldsymbol{c}_i \cdot \boldsymbol{\nabla}^{(1)} \right) F_i^{(1)}(\hat{\boldsymbol{x}}, \hat{t}) + \frac{\partial^{(2)}}{\partial \hat{t}} F_i^{(0)}(\hat{\boldsymbol{x}}, \hat{t}) \right] = -\frac{\varepsilon^2}{\hat{\tau}_c} \sum_{i=0}^{n_v} F_i^{(2)}(\hat{\boldsymbol{x}}, \hat{t}),$$

which reduces by using (1.60), (1.61) and division by ε^2 to

$$\frac{\partial^{(2)}}{\partial \hat{t}} \hat{\rho}(\hat{\boldsymbol{x}}, \hat{t}) = 0. \tag{1.70}$$

Summation of (1.66) after multiplying with $\boldsymbol{c}_i$ gives the terms of the momentum equation of second order. It follows after division by ε^2

$$\left(1 - \frac{1}{2\hat{\tau}_c}\right) \left[\frac{\partial^{(1)}}{\partial \hat{t}} \sum_{i=0}^{n_v} \boldsymbol{c}_i F_i^{(1)}(\hat{\boldsymbol{x}}, \hat{t}) + \boldsymbol{\nabla}^{(1)} \cdot P^{(1)}(\hat{\boldsymbol{x}}, \hat{t})\right] + \frac{\partial^{(2)}}{\partial \hat{t}} \sum_{i=0}^{n_v} \boldsymbol{c}_i F_i^{(0)}(\hat{\boldsymbol{x}}, \hat{t}) = 0$$

with the first order momentum flux tensor

$$P^{(1)}(\hat{\boldsymbol{x}}, \hat{t}) = \sum_{i=0}^{n_v} \boldsymbol{c}_i \boldsymbol{c}_i^T F_i^{(1)}(\hat{\boldsymbol{x}}, \hat{t}).$$

Note that (1.61) was already used for the right hand side, applying (1.60) and (1.61) also for the left hand side simplifies this equation to

$$\boldsymbol{\nabla}^{(1)} \cdot \left[\left(1 - \frac{1}{2\hat{\tau}_c}\right) P^{(1)}(\hat{\boldsymbol{x}}, \hat{t})\right] + \frac{\partial^{(2)}}{\partial \hat{t}} \left(\hat{\rho}(\hat{\boldsymbol{x}}, \hat{t}) \hat{\boldsymbol{u}}(\hat{\boldsymbol{x}}, \hat{t})\right) = 0. \tag{1.71}$$

1.6.2. Computation of $P^{(1)}(\hat{\boldsymbol{x}}, \hat{t})$

Unlike $P^{(0)}(\hat{\boldsymbol{x}}, \hat{t})$ we do not know $P^{(1)}(\hat{\boldsymbol{x}}, \hat{t})$ from previous calculations, hence we have to compute it. From equation (1.64) we get the relation

$$F_i^{(1)}(\hat{\boldsymbol{x}}, \hat{t}) = -\hat{\tau}_c \left(\frac{\partial^{(1)}}{\partial \hat{t}} + \boldsymbol{c}_i \cdot \boldsymbol{\nabla}^{(1)}\right) F_i^{(0)}(\hat{\boldsymbol{x}}, \hat{t}),$$

which can be used in the computation of $P^{(1)}(\hat{\boldsymbol{x}}, \hat{t})$. It follows

$$\begin{aligned} P^{(1)}(\hat{\boldsymbol{x}}, \hat{t}) &= -\hat{\tau}_c \left[\frac{\partial^{(1)}}{\partial \hat{t}} \sum_{i=0}^{n_v} \boldsymbol{c}_i \boldsymbol{c}_i^T F_i^{(0)}(\hat{\boldsymbol{x}}, \hat{t}) + \sum_{i=0}^{n_v} \boldsymbol{c}_i \boldsymbol{c}_i^T \left(\boldsymbol{c}_i \cdot \boldsymbol{\nabla}^{(1)}\right) F_i^{(0)}(\hat{\boldsymbol{x}}, \hat{t})\right] \\ &= -\hat{\tau}_c \left[\frac{\partial^{(1)}}{\partial \hat{t}} P^{(0)}(\hat{\boldsymbol{x}}, \hat{t}) + \underbrace{\sum_{i=0}^{n_v} \boldsymbol{c}_i \boldsymbol{c}_i^T \left(\boldsymbol{c}_i \cdot \boldsymbol{\nabla}^{(1)}\right) F_i^{(0)}(\hat{\boldsymbol{x}}, \hat{t})}_{=: R^{(1)}(\hat{\boldsymbol{x}}, \hat{t})}\right]. \end{aligned} \tag{1.72}$$

The entries of the matrix $R^{(1)}(\hat{\boldsymbol{x}}, \hat{t})$ are given by

$$R_{\alpha,\beta}^{(1)} = \sum_{i=0}^{n_v} \boldsymbol{c}_i^\alpha \boldsymbol{c}_i^\beta \left(\sum_{j=1}^{3} \boldsymbol{c}_i^j \frac{\partial^{(1)}}{\partial \hat{x}_j}\right) F_i^{(0)}(\hat{\boldsymbol{x}}, \hat{t}) = \sum_{j=1}^{3} \frac{\partial^{(1)}}{\partial \hat{x}_j} \sum_{i=0}^{n_v} \boldsymbol{c}_i^\alpha \boldsymbol{c}_i^\beta \boldsymbol{c}_i^j F_i^{(0)}(\hat{\boldsymbol{x}}, \hat{t}), \tag{1.73}$$

with $\alpha, \beta = 1, 2, 3$ running through the dimension of space. The matrix $R^{(1)}(\hat{\boldsymbol{x}}, \hat{t})$ cannot be stated in general, the equilibrium distribution $F_i^{(0)}$ as well as the lattice velocities $\boldsymbol{c}_i$ have to be taken into account. Hence we consider the D3Q19 model again. Using the explicit form (1.55) of the equilibrium distribution in this model and the lattice velocities (1.48), it follows when omitting all function arguments

$$\begin{aligned}
F_1^{(0)} - F_3^{(0)} &= \tfrac{1}{3}\hat{\rho}\hat{u}_1, & F_2^{(0)} - F_4^{(0)} &= \tfrac{1}{3}\hat{\rho}\hat{u}_2,\\
F_5^{(0)} - F_6^{(0)} &= \tfrac{1}{3}\hat{\rho}\hat{u}_3, & F_7^{(0)} - F_9^{(0)} &= \tfrac{1}{6}\hat{\rho}(\hat{u}_1 + \hat{u}_2),\\
F_{10}^{(0)} - F_8^{(0)} &= \tfrac{1}{6}\hat{\rho}(\hat{u}_1 - \hat{u}_2), & F_{11}^{(0)} - F_{13}^{(0)} &= \tfrac{1}{6}\hat{\rho}(\hat{u}_1 + \hat{u}_3),\\
F_{14}^{(0)} - F_{12}^{(0)} &= \tfrac{1}{6}\hat{\rho}(\hat{u}_1 - \hat{u}_3), & F_{15}^{(0)} - F_{17}^{(0)} &= \tfrac{1}{6}\hat{\rho}(\hat{u}_2 + \hat{u}_3),\\
F_{18}^{(0)} - F_{16}^{(0)} &= \tfrac{1}{6}\hat{\rho}(\hat{u}_2 - \hat{u}_3).
\end{aligned}$$

With help of the latter equations and the values given in table 1.2 we can calculate the inner sums of (1.73). A general expression for these sums is obtained by [23]

$$\sum_{i=0}^{18} \boldsymbol{c}_i^\alpha \boldsymbol{c}_i^\beta \boldsymbol{c}_i^j F_i^{(0)}(\hat{\boldsymbol{x}}, \hat{t}) = \frac{1}{3}\hat{\rho}(\hat{\boldsymbol{x}}, \hat{t}) \left[\delta_{\alpha\beta}\hat{u}^j(\hat{\boldsymbol{x}}, \hat{t}) + \delta_{\alpha j}\hat{u}^\beta(\hat{\boldsymbol{x}}, \hat{t}) + \delta_{\beta j}\hat{u}^\alpha(\hat{\boldsymbol{x}}, \hat{t})\right], \tag{1.74}$$

with $\alpha, \beta, j = 1, 2, 3$ and Kronecker delta $\delta_{ij} = \begin{cases} 1, & \text{if } i = j \\ 0, & \text{if } i \neq j \end{cases}$. With aid of the latter expression it follows for the matrix (1.73) in case of the D3Q19 model and all other models which satisfy (1.74) (with n_v instead of 18)

$$\begin{aligned}
R_{\alpha,\beta}^{(1)} &= \sum_{j=1}^{3} \frac{\partial^{(1)}}{\partial \hat{x}_j} \left(\frac{1}{3}\hat{\rho}(\hat{\boldsymbol{x}}, \hat{t}) \left[\delta_{\alpha\beta}\hat{u}^j(\hat{\boldsymbol{x}}, \hat{t}) + \delta_{\alpha j}\hat{u}^\beta(\hat{\boldsymbol{x}}, \hat{t}) + \delta_{\beta j}\hat{u}^\alpha(\hat{\boldsymbol{x}}, \hat{t})\right]\right)\\
&= \frac{1}{3}\left(\sum_{j=1}^{3} \frac{\partial^{(1)}}{\partial \hat{x}_j}\big(\hat{\rho}(\hat{\boldsymbol{x}}, \hat{t})\hat{u}^j(\hat{\boldsymbol{x}}, \hat{t})\delta_{\alpha\beta}\big) + \frac{\partial^{(1)}}{\partial \hat{x}_\alpha}\left(\hat{\rho}(\hat{\boldsymbol{x}}, \hat{t})\hat{u}^\beta(\hat{\boldsymbol{x}}, \hat{t})\right) + \frac{\partial^{(1)}}{\partial \hat{x}_\beta}\left(\hat{\rho}(\hat{\boldsymbol{x}}, \hat{t})\hat{u}^\alpha(\hat{\boldsymbol{x}}, \hat{t})\right)\right)\\
&= \frac{1}{3}\left(\delta_{\alpha\beta}\left(\boldsymbol{\nabla}^{(1)} \cdot \big(\hat{\rho}(\hat{\boldsymbol{x}}, \hat{t})\hat{\boldsymbol{u}}(\hat{\boldsymbol{x}}, \hat{t})\big)\right) + \frac{\partial^{(1)}}{\partial \hat{x}_\alpha}\left(\hat{\rho}(\hat{\boldsymbol{x}}, \hat{t})\hat{u}^\beta(\hat{\boldsymbol{x}}, \hat{t})\right) + \frac{\partial^{(1)}}{\partial \hat{x}_\beta}\big(\hat{\rho}(\hat{\boldsymbol{x}}, \hat{t})\hat{u}^\alpha(\hat{\boldsymbol{x}}, \hat{t})\big)\right).
\end{aligned}$$

For the further calculation of the right hand side of (1.72) we use the representation (cf. (1.52))

$$P_{\alpha,\beta}^{(0)}(\hat{\boldsymbol{x}}, \hat{t}) = \hat{\rho}(\hat{\boldsymbol{x}}, \hat{t})\hat{u}^\alpha(\hat{\boldsymbol{x}}, \hat{t})\hat{u}^\beta(\hat{\boldsymbol{x}}, \hat{t}) + p(\hat{\boldsymbol{x}}, \hat{t})\delta_{\alpha\beta},$$

			i																	
j	α	β	0	1	2	3	4	5	6	7	8	9	10	11	12	13	14	15	16	17	18
1	1	1		1		-1				1	-1	-1	1	1	-1	-1	1				
	1	2								1	1	-1	-1								
	1	3												1	1	-1	-1				
	2	2								1	-1	-1	1								
	2	3																			
	3	3												1	-1	-1	1				
2	1	1								1	1	-1	-1								
	1	2								1	-1	-1	1								
	1	3																			
	2	2			1		-1			1	1	-1	-1					1	-1	-1	1
	2	3																1	1	-1	-1
	3	3																1	-1	-1	1
3	1	1												1	1	-1	-1				
	1	2																			
	1	3												1	-1	-1	1				
	2	2																1	1	-1	-1
	2	3																1	-1	-1	1
	3	3						1	-1					1	1	-1	-1	1	1	-1	-1

Table 1.2.: Result of the product $\boldsymbol{c}_i^\alpha \boldsymbol{c}_i^\beta \boldsymbol{c}_i^j$ for D3Q19 model. Lattice velocities are given in (1.48) and empty spaces indicate a result of zero.

and (1.67) for the first addend in the latter equation. Thus, we obtain with the pressure density relation (1.57)

$$\begin{aligned} P^{(1)}_{\alpha,\beta}(\hat{\boldsymbol{x}},\hat{t}) =& -\hat{\tau}_c\Bigg[\frac{\partial^{(1)}}{\partial\hat{t}}\left(\hat{\rho}(\hat{\boldsymbol{x}},\hat{t})\hat{u}^\alpha(\hat{\boldsymbol{x}},\hat{t})\hat{u}^\beta(\hat{\boldsymbol{x}},\hat{t})\right) + \frac{\partial^{(1)}}{\partial\hat{t}}p(\hat{\boldsymbol{x}},\hat{t})\delta_{\alpha\beta} - \frac{1}{3}\delta_{\alpha\beta}\frac{\partial^{(1)}}{\partial\hat{t}}\hat{\rho}(\hat{\boldsymbol{x}},\hat{t}) \\ &+ \frac{1}{3}\frac{\partial^{(1)}}{\partial\hat{x}_\alpha}\left(\hat{\rho}(\hat{\boldsymbol{x}},\hat{t})\hat{u}^\beta(\hat{\boldsymbol{x}},\hat{t})\right) + \frac{1}{3}\frac{\partial^{(1)}}{\partial\hat{x}_\beta}\left(\hat{\rho}(\hat{\boldsymbol{x}},\hat{t})\hat{u}^\alpha(\hat{\boldsymbol{x}},\hat{t})\right)\Bigg] \\ =& -\hat{\tau}_c\Bigg[\frac{\partial^{(1)}}{\partial\hat{t}}\left(\hat{\rho}(\hat{\boldsymbol{x}},\hat{t})\hat{u}^\alpha(\hat{\boldsymbol{x}},\hat{t})\hat{u}^\beta(\hat{\boldsymbol{x}},\hat{t})\right) + \frac{1}{3}\frac{\partial^{(1)}}{\partial\hat{x}_\alpha}\left(\hat{\rho}(\hat{\boldsymbol{x}},\hat{t})\hat{u}^\beta(\hat{\boldsymbol{x}},\hat{t})\right) \\ &+ \frac{1}{3}\frac{\partial^{(1)}}{\partial\hat{x}_\beta}\left(\hat{\rho}(\hat{\boldsymbol{x}},\hat{t})\hat{u}^\alpha(\hat{\boldsymbol{x}},\hat{t})\right)\Bigg], \end{aligned} \tag{1.75}$$

which can also be written in vector notation by

$$\begin{aligned} P^{(1)}(\hat{\boldsymbol{x}},\hat{t}) =& -\hat{\tau}_c\Bigg[\frac{\partial^{(1)}}{\partial\hat{t}}\left(\hat{\rho}(\hat{\boldsymbol{x}},\hat{t})\hat{\boldsymbol{u}}(\hat{\boldsymbol{x}},\hat{t})\hat{\boldsymbol{u}}(\hat{\boldsymbol{x}},\hat{t})^T\right) + \frac{1}{3}\boldsymbol{\nabla}^{(1)}\left[\hat{\rho}(\hat{\boldsymbol{x}},\hat{t})\hat{\boldsymbol{u}}(\hat{\boldsymbol{x}},\hat{t})^T\right] \\ &+ \frac{1}{3}\left(\boldsymbol{\nabla}^{(1)}\left[\hat{\rho}(\hat{\boldsymbol{x}},\hat{t})\hat{\boldsymbol{u}}(\hat{\boldsymbol{x}},\hat{t})^T\right]\right)^T\Bigg]. \end{aligned}$$

In the latter expression the time derivative exhibits the form

$$\frac{\partial^{(1)}}{\partial \hat{t}}\left(\hat{\rho}(\hat{\boldsymbol{x}},\hat{t})\hat{u}^{\alpha}(\hat{\boldsymbol{x}},\hat{t})\hat{u}^{\beta}(\hat{\boldsymbol{x}},\hat{t})\right) = -\hat{u}^{\alpha}(\hat{\boldsymbol{x}},\hat{t})\frac{\partial^{(1)}}{\partial \hat{x}_{\beta}}p(\hat{\boldsymbol{x}},\hat{t}) - \hat{u}^{\beta}(\hat{\boldsymbol{x}},\hat{t})\frac{\partial^{(1)}}{\partial \hat{x}_{\alpha}}p(\hat{\boldsymbol{x}},\hat{t}) \tag{1.76}$$

$$-\sum_{j=1}^{3}\frac{\partial^{(1)}}{\partial \hat{x}_j}\left(\hat{\rho}(\hat{\boldsymbol{x}},\hat{t})\hat{u}^{\alpha}(\hat{\boldsymbol{x}},\hat{t})\hat{u}^{\beta}(\hat{\boldsymbol{x}},\hat{t})\hat{u}^{j}(\hat{\boldsymbol{x}},\hat{t})\right), \tag{1.77}$$

which is computed in detail in appendix A.2. Substituting the right hand side of the latter equation in (1.75) and using product rule for the spatial derivative the outcome then reads

$$\begin{aligned}
P^{(1)}_{\alpha,\beta}(\hat{\boldsymbol{x}},\hat{t}) = -\hat{\tau}_c\Bigg[& -\hat{u}^{\alpha}(\hat{\boldsymbol{x}},\hat{t})\frac{\partial^{(1)}}{\partial \hat{x}_{\beta}}p(\hat{\boldsymbol{x}},\hat{t}) - \hat{u}^{\beta}(\hat{\boldsymbol{x}},\hat{t})\frac{\partial^{(1)}}{\partial \hat{x}_{\alpha}}p(\hat{\boldsymbol{x}},\hat{t}) \\
& + \frac{1}{3}\Bigg(\hat{u}^{\beta}(\hat{\boldsymbol{x}},\hat{t})\frac{\partial^{(1)}}{\partial \hat{x}_{\alpha}}\hat{\rho}(\hat{\boldsymbol{x}},\hat{t}) + \hat{\rho}(\hat{\boldsymbol{x}},\hat{t})\frac{\partial^{(1)}}{\partial \hat{x}_{\alpha}}\hat{u}^{\beta}(\hat{\boldsymbol{x}},\hat{t}) \\
& \qquad + \hat{u}^{\alpha}(\hat{\boldsymbol{x}},\hat{t})\frac{\partial^{(1)}}{\partial \hat{x}_{\beta}}\hat{\rho}(\hat{\boldsymbol{x}},\hat{t}) + \hat{\rho}(\hat{\boldsymbol{x}},\hat{t})\frac{\partial^{(1)}}{\partial \hat{x}_{\beta}}\hat{u}^{\alpha}(\hat{\boldsymbol{x}},\hat{t})\Bigg) \\
& - \sum_{j=1}^{3}\frac{\partial^{(1)}}{\partial \hat{x}_j}\left(\hat{\rho}(\hat{\boldsymbol{x}},\hat{t})\hat{u}^{\alpha}(\hat{\boldsymbol{x}},\hat{t})\hat{u}^{\beta}(\hat{\boldsymbol{x}},\hat{t})\hat{u}^{j}(\hat{\boldsymbol{x}},\hat{t})\right)\Bigg] \\
= -\hat{\tau}_c\Bigg[& \frac{\hat{\rho}(\hat{\boldsymbol{x}},\hat{t})}{3}\left(\frac{\partial^{(1)}}{\partial \hat{x}_{\alpha}}\hat{u}^{\beta}(\hat{\boldsymbol{x}},\hat{t}) + \frac{\partial^{(1)}}{\partial \hat{x}_{\beta}}\hat{u}^{\alpha}(\hat{\boldsymbol{x}},\hat{t})\right) \\
& - \sum_{j=1}^{3}\frac{\partial^{(1)}}{\partial \hat{x}_j}\left(\hat{\rho}(\hat{\boldsymbol{x}},\hat{t})\hat{u}^{\alpha}(\hat{\boldsymbol{x}},\hat{t})\hat{u}^{\beta}(\hat{\boldsymbol{x}},\hat{t})\hat{u}^{j}(\hat{\boldsymbol{x}},\hat{t})\right)\Bigg],
\end{aligned}$$

where the pressure density relation (1.57) was used. Note that the second step was not a general one, since the pressure is in general not given by (1.57).
When using a discrete equilibrium distribution in the type of (1.55), the $\mathcal{O}(|\hat{\boldsymbol{u}}|^3)$ term in the latter equation should be neglected to be consistent with the approximation of the equilibrium distribution which itself is an approximation of order $\mathcal{O}(|\hat{\boldsymbol{u}}|^2)$ (cf. (1.46)). Thus we achieve in vector notation

$$P^{(1)}(\hat{\boldsymbol{x}},\hat{t}) = -\frac{\hat{\tau}_c}{3}\hat{\rho}(\hat{\boldsymbol{x}},\hat{t})\left[\boldsymbol{\nabla}^{(1)}\hat{\boldsymbol{u}}(\hat{\boldsymbol{x}},\hat{t}) + \left(\boldsymbol{\nabla}^{(1)}\hat{\boldsymbol{u}}(\hat{\boldsymbol{x}},\hat{t})\right)^{T}\right].$$

1.6.3. Results up to Second Order

From previous calculations we already know the first order approximations (1.67) and (1.69) of the continuity equation and momentum equation, respectively. The second order approximation for the continuity equation is also known and given above by (1.70).

Eventually, with the final equation from the previous subsection the second order approximation (1.71) for the momentum equation reads

$$\frac{\partial^{(2)}}{\partial \hat{t}} \left(\hat{\rho}(\hat{\boldsymbol{x}}, \hat{t}) \hat{\boldsymbol{u}}(\hat{\boldsymbol{x}}, \hat{t}) \right) = \frac{2\hat{\tau}_c - 1}{6} \boldsymbol{\nabla}^{(1)} \cdot \left[\hat{\rho}(\hat{\boldsymbol{x}}, \hat{t}) \boldsymbol{\nabla}^{(1)} \hat{\boldsymbol{u}}(\hat{\boldsymbol{x}}, \hat{t}) + \hat{\rho}(\hat{\boldsymbol{x}}, \hat{t}) \Big(\boldsymbol{\nabla}^{(1)} \hat{\boldsymbol{u}}(\hat{\boldsymbol{x}}, \hat{t}) \Big)^T \right]. \tag{1.78}$$

Adding (1.67) and (1.70) leads to an approximation up to second order of the continuity equation

$$\frac{\partial}{\partial \hat{t}} \hat{\rho}(\hat{\boldsymbol{x}}, \hat{t}) + \boldsymbol{\nabla} \cdot \left(\hat{\rho}(\hat{\boldsymbol{x}}, \hat{t}) \hat{\boldsymbol{u}}(\hat{\boldsymbol{x}}, \hat{t}) \right) = 0. \tag{1.79}$$

Similarly, by addition of the first and second order approximations (1.69) and (1.78) the resulting term is an approximation up to second order of the momentum equation, it reads

$$\begin{aligned} &\frac{\partial}{\partial \hat{t}} \left(\hat{\rho}(\hat{\boldsymbol{x}}, \hat{t}) \hat{\boldsymbol{u}}(\hat{\boldsymbol{x}}, \hat{t}) \right) + \boldsymbol{\nabla} \cdot \left(\hat{\rho}(\hat{\boldsymbol{x}}, \hat{t}) \hat{\boldsymbol{u}}(\hat{\boldsymbol{x}}, \hat{t}) \hat{\boldsymbol{u}}(\hat{\boldsymbol{x}}, \hat{t})^T \right) \\ &\qquad = -\boldsymbol{\nabla} p(\hat{\boldsymbol{x}}, \hat{t}) + \nu \boldsymbol{\nabla} \cdot \left[\hat{\rho}(\hat{\boldsymbol{x}}, \hat{t}) \boldsymbol{\nabla} \hat{\boldsymbol{u}}(\hat{\boldsymbol{x}}, \hat{t}) + \hat{\rho}(\hat{\boldsymbol{x}}, \hat{t}) \big(\boldsymbol{\nabla} \hat{\boldsymbol{u}}(\hat{\boldsymbol{x}}, \hat{t}) \big)^T \right], \end{aligned} \tag{1.80}$$

with $\nu = \frac{2\hat{\tau}_c - 1}{6}$, being the kinematic viscosity, as we will see in the subsequent subsection.

1.6.4. Incompressible Navier Stokes Equation

Summarizing the computation above, the main results are (1.79) and (1.80). The question arising is how these two equations can be interpreted. A further calculation will answer this. We show below that the equations can be interpreted as the incompressible Navier-Stokes equations. Recalling the following equations [65]:
For an incompressible fluid the Navier-Stokes equations read

$$\begin{aligned} \frac{\partial \vec{u}}{\partial t} + \left(\vec{u} \cdot \vec{\nabla} \right) \vec{u} &= -\vec{\nabla} \hat{p} + \hat{\nu} \Delta \vec{u}, \\ \vec{\nabla} \cdot \vec{u} &= 0, \end{aligned} \tag{1.81}$$

with velocity $\vec{u}$, kinematic viscosity $\hat{\nu}$ and $\hat{p}$ equal to the ratio of scalar pressure p and density ρ.

We assume that changes in $\hat{\rho}(\hat{\boldsymbol{x}}, \hat{t})$ are negligible, what is valid if changes in the density are small enough. In the following the density is treated as being a constant, thus equation (1.79) changes to

$$\boldsymbol{\nabla} \cdot \hat{\boldsymbol{u}}(\hat{\boldsymbol{x}}, \hat{t}) = 0, \tag{1.82}$$

conditioning the macroscopic velocity to be divergence free. The approximating momen-

tum equation (1.80) also changes, we obtain the following

$$\hat{\rho}(\hat{\boldsymbol{x}},\hat{t})\left(\frac{\partial}{\partial\hat{t}}\hat{\boldsymbol{u}}(\hat{\boldsymbol{x}},\hat{t})+\boldsymbol{\nabla}\cdot\left(\hat{\boldsymbol{u}}(\hat{\boldsymbol{x}},\hat{t})\hat{\boldsymbol{u}}(\hat{\boldsymbol{x}},\hat{t})^T\right)\right)$$
$$=-\boldsymbol{\nabla}p(\hat{\boldsymbol{x}},\hat{t})+\nu\hat{\rho}(\hat{\boldsymbol{x}},\hat{t})\boldsymbol{\nabla}\cdot\left[\boldsymbol{\nabla}\hat{\boldsymbol{u}}(\hat{\boldsymbol{x}},\hat{t})+\left(\boldsymbol{\nabla}\hat{\boldsymbol{u}}(\hat{\boldsymbol{x}},\hat{t})\right)^T\right].$$

Using (1.82) we can simplify on the left hand side as follows

$$\begin{aligned}\boldsymbol{\nabla}\cdot\left(\hat{\boldsymbol{u}}(\hat{\boldsymbol{x}},\hat{t})\hat{\boldsymbol{u}}(\hat{\boldsymbol{x}},\hat{t})^T\right)&=\hat{\boldsymbol{u}}(\hat{\boldsymbol{x}},\hat{t})\cdot\boldsymbol{\nabla}\hat{\boldsymbol{u}}(\hat{\boldsymbol{x}},\hat{t})+\hat{\boldsymbol{u}}(\hat{\boldsymbol{x}},\hat{t})\left(\boldsymbol{\nabla}\cdot\hat{\boldsymbol{u}}(\hat{\boldsymbol{x}},\hat{t})\right)\\&=\hat{\boldsymbol{u}}(\hat{\boldsymbol{x}},\hat{t})\cdot\boldsymbol{\nabla}\hat{\boldsymbol{u}}(\hat{\boldsymbol{x}},\hat{t}).\end{aligned}$$

Also the right hand side of equation (1.82) can be simplified

$$\begin{aligned}\boldsymbol{\nabla}\cdot\left[\boldsymbol{\nabla}\hat{\boldsymbol{u}}(\hat{\boldsymbol{x}},\hat{t})+\left(\boldsymbol{\nabla}\hat{\boldsymbol{u}}(\hat{\boldsymbol{x}},\hat{t})\right)^T\right]&=\boldsymbol{\nabla}\cdot\boldsymbol{\nabla}\hat{\boldsymbol{u}}(\hat{\boldsymbol{x}},\hat{t})+\boldsymbol{\nabla}\cdot\left(\boldsymbol{\nabla}\hat{\boldsymbol{u}}(\hat{\boldsymbol{x}},\hat{t})\right)^T\\&=\boldsymbol{\nabla}\left(\boldsymbol{\nabla}\cdot\hat{\boldsymbol{u}}(\hat{\boldsymbol{x}},\hat{t})\right)+\Delta\hat{\boldsymbol{u}}(\hat{\boldsymbol{x}},\hat{t})\\&=\Delta\hat{\boldsymbol{u}}(\hat{\boldsymbol{x}},\hat{t}),\end{aligned}$$

with Laplacian Δ which is applied to each component of $\hat{\boldsymbol{u}}(\hat{\boldsymbol{x}},\hat{t})$. Using both simplifications and division by $\hat{\rho}(\hat{\boldsymbol{x}},\hat{t})$, we achieve

$$\frac{\partial}{\partial\hat{t}}\hat{\boldsymbol{u}}(\hat{\boldsymbol{x}},\hat{t})+\hat{\boldsymbol{u}}(\hat{\boldsymbol{x}},\hat{t})\cdot\boldsymbol{\nabla}\hat{\boldsymbol{u}}(\hat{\boldsymbol{x}},\hat{t})=-\boldsymbol{\nabla}\tilde{p}(\hat{\boldsymbol{x}},\hat{t})+\nu\Delta\boldsymbol{u}(\hat{\boldsymbol{x}},\hat{t}),\tag{1.83}$$

with $\tilde{p}(\hat{\boldsymbol{x}},\hat{t})=\frac{p(\hat{\boldsymbol{x}},\hat{t})}{\hat{\rho}(\hat{\boldsymbol{x}},\hat{t})}$. Note that the gradient of the pressure was not neglected, although it is related to the density. By not neglecting it, we observe that equations (1.82) and (1.83) are exactly the same as the incompressible Navier-Stokes equations (1.81).

1.7. Summary and Algorithm

We finish the current chapter by summarizing the chapter so far and recapitulating the most important equations and results from the foregoing sections. Afterwards, we present an algorithm for the lattice BGK method in pseudo code.

Starting from lattice gas automata, the basis of lattice Boltzmann methods, where explained: Single particles collide and hop on a regular lattice, where the collisions are described by local rules. If the lattice exhibits a sufficient symmetry one can successfully simulate fluid flows with lattice gas automata, for instance with the FHP model. A counterexample is the HPP model, which fails to yield the Navier-Stokes equations. Since, in general, a fluid consists of a huge number of molecules and lattice gas automata consider only single particles an average over many simulations with different initial conditions has to be build in order to gain physically meaningful results. The statistical noise emerging by this averaging is eliminated in lattice Boltzmann methods. Here, instead of single particles a stochastic distribution moves and "collides" on a lattice.

We derived the lattice Boltzmann method from the Boltzmann equation ((1.4))

$$\frac{\partial f(\boldsymbol{x},\boldsymbol{v},t)}{\partial t} + \boldsymbol{v}\cdot\boldsymbol{\nabla} f(\boldsymbol{x},\boldsymbol{v},t) = Q(f,f)$$

by a suitable discretization. We showed that solving the Boltzmann equation is an appropriate approach for the simulation of fluid flows, since Navier-Stokes equations are recovered from the Boltzmann equation. Important for recovering the Navier-Stokes equations were the definitions of macroscopic quantities ((1.6) and (1.7))

$$\rho(\boldsymbol{x},t) = \int\limits_{\mathbb{R}^3} f(\boldsymbol{x},\boldsymbol{v},t)\,\mathrm{d}\boldsymbol{v},$$
$$\rho(\boldsymbol{x},t)\boldsymbol{u}(\boldsymbol{x},t) = \int\limits_{\mathbb{R}^3} \boldsymbol{v} f(\boldsymbol{x},\boldsymbol{v},t)\,\mathrm{d}\boldsymbol{v}.$$

The associated discretized equations ((1.43) and (1.44)) were

$$\hat{\rho}(\hat{\boldsymbol{x}},\hat{t}) = \sum_{i=0}^{n_v} F_i(\hat{\boldsymbol{x}},\hat{t}),$$
$$\hat{\rho}(\hat{\boldsymbol{x}},\hat{t})\hat{\boldsymbol{u}}(\hat{\boldsymbol{x}},\hat{t}) = \sum_{i=0}^{n_v} \boldsymbol{c}_i F_i(\hat{\boldsymbol{x}},\hat{t}).$$

In section 1.3 we motivated an approximation of the complicated collision integral $Q(f,f)$ by a single relaxation term. In addition with the discretized left hand side of the Boltzmann equation this led to the lattice BGK equation ((1.42))

$$F_i(\hat{\boldsymbol{x}}+\boldsymbol{c}_i\Delta\hat{t},\hat{t}+\Delta\hat{t}) - F_i(\hat{\boldsymbol{x}},\hat{t}) = -\frac{1}{\hat{\tau}_c}\left[F_i(\hat{\boldsymbol{x}},\hat{t}) - F_i^{(eq)}(\hat{\boldsymbol{x}},\hat{t})\right].$$

The equilibrium distribution $F_i^{(eq)}(\hat{\boldsymbol{x}},\hat{t})$ used in the lattice BGK equation was derived for the D3Q19 model in section 1.5. The presented procedure can be applied to other discretization models as well. The discrete equilibrium distribution arose from a Taylor expansion of the continuous equilibrium distribution in the macroscopic velocity up to second order. Hence, the presented lattice BGK methods are not suitable for the simulation of fluids with high velocities. The deduced discrete equilibrium distribution was ((1.55))

$$F_0^{(eq)}(\hat{\boldsymbol{x}},\hat{t}) = \omega_0\hat{\rho}(\hat{\boldsymbol{x}},\hat{t})\left[1-\frac{3}{2}|\hat{\boldsymbol{u}}(\hat{\boldsymbol{x}},\hat{t})|^2\right],$$
$$F_i^{(eq)}(\hat{\boldsymbol{x}},\hat{t}) = \omega_i\hat{\rho}(\hat{\boldsymbol{x}},\hat{t})\left[1+3(\boldsymbol{c}_i\cdot\hat{\boldsymbol{u}}(\hat{\boldsymbol{x}},\hat{t})) + \frac{9}{2}(\boldsymbol{c}_i\cdot\hat{\boldsymbol{u}}(\hat{\boldsymbol{x}},\hat{t}))^2 - \frac{3}{2}|\hat{\boldsymbol{u}}(\hat{\boldsymbol{x}},\hat{t})|^2\right],$$

with weights ω_i given for several models in table 1.1.
In section 1.6 we attested that the lattice BGK method is capable to approximate phys-

ically meaningful equations. This verification was done by using a Chapman-Enskog expansion. We saw that if changes in the macroscopic density are small then LBGK methods approximate the incompressible Navier-Stokes equations. Hence, lattice Boltzmann methods with BGK approximation can be used to simulate fluid flows in the incompressible limit. Comparison of the incompressible Navier-Stokes equations and the result of the Chapman-Enskog expansion implied that the kinematic viscosity in the numerical scheme ((1.80) and (1.83)) is given by

$$\nu = \frac{2\hat{\tau}_c - 1}{6}.$$

This means the relaxation parameter $\hat{\tau}_c$ can be chosen to tune the viscosity. An relaxation parameter $\hat{\tau}_c \in (\frac{1}{2}, \infty)$ leads to a positive viscosity.

Finally, we state the results above in a pseudo code algorithm. As an representative for lattice BGK methods we choose the discretization model D3Q19. The algorithm illustrates the principal idea, nevertheless it is impossible to implement it, because the lines *foreach lattice point* $\hat{x}$ *do* refer to an infinite number of lattice points. For an implementation it is necessary to restrict the fluid to a bounded domain, meaning investigating the Boltzmann equation for $\boldsymbol{x} \in \mathcal{X} \subset \mathbb{R}^3$ instead of $\boldsymbol{x} \in \mathbb{R}^3$, where $\mathcal{X}$ satisfies the condition

$$\|\boldsymbol{y} - \boldsymbol{z}\|_2 < M, \quad \text{with } M \in \mathbb{R} \text{ and for all } \boldsymbol{y}, \boldsymbol{z} \in \mathcal{X}.$$

The following chapter deals, among others, with this and resulting topics.

Algorithm: Sketch: Simple LBGK D3Q19

Initialization:

Set time horizon T_{end} for simulation
Define lattice velocities:

$c_0 = [0;0;0]$, $c_1 = [1;0;0]$
$c_2 = [0;1;0]$, $c_3 = [-1;0;0]$
$c_4 = [0;-1;0]$, $c_5 = [0;0;1]$
$c_6 = [0;0;-1]$, $c_7 = [1;1;0]$
$c_8 = [-1;1;0]$, $c_9 = [-1;-1;0]$
$c_{10} = [1;-1;0]$, $c_{11} = [1;0;1]$
$c_{12} = [-1;0;1]$, $c_{13} = [-1;0;-1]$
$c_{14} = [1;0;-1]$, $c_{15} = [0;1;1]$
$c_{16} = [0;-1;1]$, $c_{17} = [0;-1;-1]$
$c_{18} = [0;1;-1]$

Set $\hat{t} = 0$
Choose relaxation parameter $\hat{\tau}_c$
Determine time step $\Delta\hat{t}$
Set initial values:

foreach *lattice point* $\hat{\boldsymbol{x}}$ **do**
  for *i=0* **to** *18* **do**
    Set initial values $F_i(\hat{\boldsymbol{x}}, 0)$
  end
end

Time Evolution:

while $\hat{t} < T_{end}$ **do**
  Collision:
  foreach *lattice point* $\hat{\boldsymbol{x}}$ **do**
    Compute density: $\hat{\rho} = \sum_{i=0}^{18} F_i(\hat{\boldsymbol{x}}, \hat{t})$
    Compute velocity: $\hat{u} = \frac{1}{\hat{\rho}} \sum_{i=0}^{18} c_i F_i(\hat{\boldsymbol{x}}, \hat{t})$
    Compute equilibrium distribution:
    $F_0^{(eq)} = \frac{1}{3}\hat{\rho}[1 - \frac{3}{2}|\hat{u}|^2]$
    for *i=1* **to** *6* **do**
      $F_i^{(eq)} = \frac{1}{18}\hat{\rho}\left[1 + 3(c_i \cdot \hat{u}) + \frac{9}{2}(c_i \cdot \hat{u})^2 - \frac{3}{2}|\hat{u}|^2\right]$
    end
    for *i=7* **to** *18* **do**
      $F_i^{(eq)} = \frac{1}{36}\hat{\rho}\left[1 + 3(c_i \cdot \hat{u}) + \frac{9}{2}(c_i \cdot \hat{u})^2 - \frac{3}{2}|\hat{u}|^2\right]$
    end
    for *i=0* **to** *18* **do**
      $F_i(\hat{\boldsymbol{x}}, \hat{t}) = F_i(\hat{\boldsymbol{x}}, \hat{t}) - \frac{1}{\hat{\tau}_c}\left[F_i(\hat{\boldsymbol{x}}, \hat{t}) - F_i^{(eq)}\right]$
    end
  end
  Streaming:
  foreach *lattice point* $\hat{\boldsymbol{x}}$ **do**
    for *i=0* **to** *18* **do**
      $F_i(\hat{\boldsymbol{x}} + \boldsymbol{c}_i\Delta\hat{t}, \hat{t} + \Delta\hat{t}) = F_i(\hat{\boldsymbol{x}}, \hat{t})$
    end
  end
  Update:
  $\hat{t} = \hat{t} + \Delta\hat{t}$
end

CHAPTER 2

Enhancements of the Lattice Boltzmann Method

The previous chapter introduced the lattice Boltzmann method[1], nevertheless the focus of the presented model was exclusively on streaming and collision. However, the simplest lattice Boltzmann models that can be implemented are based on the concepts presented in the preceding chapter, we enhance the method in this chapter and thus enlarge the means of its application.

There is a wide range of problems where lattice Boltzmann methods can be applied, it contains, only as examples, magnetohydrodynamical problems [8] or multi-component flows in porous media [39]. Roughly speaking, if one considers a specific problem one also needs a specific Boltzmann method which results after an appropriate investigation. Hence, we do not present enhancements of the basic lattice Boltzmann method here, in such a way that we are capable of applying it to plenty of physical problems.

A true strengths of lattice Boltzmann methods lies in their ability to simulate both single-component (SC) and multi-component (MC) multiphase (MP) fluid flows. Each component refers to a chemical constituent of the fluid which has its own properties like viscosity or density. The phases refer in a sense to the states of matter, such that for example a single-component, say H_2O, multiphase system would involve the liquid and vapor phases of water. With multi-component models it is possible to simulate both miscible and immiscible fluids, such as in [22, 31, 64]. An overview and introduction to some both SC-MP and MC-MP models is given in [63].

Despite SC-MP models opens the approach of interesting problems involving for instance phase separation [64], capillary rise [53], adsorption and capillary condensation [62] we restrict the investigation in this chapter to singlephase (SP) models. These are single fluid models that represent the behavior of a single gas or liquid phase for example.

As already mentioned at the end of the preceding chapter an implementation of a method demands the restriction to a finite number of lattice points, meaning to simulate the behavior of the fluid in a bounded domain. Consequently, we get boundaries and we have to describe how the fluid behaves on the boundary. The first section deals with boundary conditions, where we give an introduction to the most common ones. In the then subsequent section, we demonstrate how one can easily add external forces to

[1] More precisely the lattice BGK method was introduced in the preceding chapter, nevertheless we call it lattice Boltzmann method in the sequel.

lattice Boltzmann methods. With these both enhancements it is possible to simulate for example gravity driven flows in cavities with obstacles. Nevertheless, the focus in the current chapter is on the extension of a (SC-SP) lattice Boltzmann method for fluid flows by a thermal component, this treatment is done in the third section. The fourth section describes how the thermal component can influence the evolution of the fluid in the sense of buoyancy.

2.1. Boundary Conditions

In this section we consider lattice Boltzmann models and the fluid on a bounded domain. Here, boundedness does not necessarily refer to a situation where the fluid is enclosed in an impenetrably boundary, but we consider the fluid on the domain of interest only. In simulations with such models we are not interested in proceedings which happen beyond the boundaries, explicitly. However, we have the opportunity to consider those proceedings as input data in our simulation in the form of boundary conditions. For instance we can prescribe the fluid's macroscopic velocity on boundaries which could be given as the results of those proceedings.
Imagine for example a motor in a car and let us assume we are interested in the motion of the exhaust gas through the exhaust system. In this case one boundary could be the connection to the engine where we could prescribe the pressure or velocity of the exhaust gas, the other boundaries of the domain would be the walls of the involved exhaust pipes. On the latter we could prescribe a different behavior of the exhaust gas. The passage where the exhaust gas passes out the exhaust system could be the final part of the boundary, and an specific prescription here is also possible.
In the latter example most likely the occurring boundaries are curved. As this section is thought as a brief impression of how boundaries can be considered in lattice Boltzmann models we restrict the description of boundary conditions here to straight boundaries which are aligned with the main lattice direction. For boundaries not aligned with lattice directions, schemes based on extrapolations like in [11] can be used [72]. A consideration of curved boundaries can be found e.g. in [44].

The restriction to a bounded domain makes an implementation of the lattice Boltzmann method possible, since then a finite number of lattice points is sufficient. An interior lattice point has the full number of neighbors, 18 in the case of the D3Q19 model. For these points the main concept of lattice Boltzmann method described in the previous chapter is still applicable. Nevertheless, there are lattice points which do not have the full number of neighbors, we denote these lattice points as boundary lattice points. Recapitulating the main concept, a streaming and a collision step are successively executed, in turns. After the streaming step almost all values of the density distribution (populations) are determined by pre-streaming distribution values of adjacent points[2]. Consequently, for boundary lattice points there are unknown populations after the streaming step. Fig-

[2]The only exception is the value corresponding to the rest particle.

ure 2.1 illustrates this situation in case of D2Q9 for a south boundary. Provided all populations are known the collision step can be executed as usual, especially for boundary lattice points.
A boundary condition in lattice Boltzmann models has the task to find the missing values of the density distribution, in a way which leads to a desired macroscopic behavior on the boundary. However, boundary conditions which replace not only the unknown populations can be constructed, for example the boundary conditions presented in [58] are nonlocal in the sense that information of neighboring lattice points is also used to recompute the density distribution including also the already known ones. When only the unknown populations are determined, the action of a boundary condition can be viewed as and additional streaming step from imaginary lattice points located outside of the actual numerical domain.

Choosing physical correct boundary conditions is necessary to achieve meaningful results. A simulation may gain or lose mass during time evolution [12]. This necessarily need not to fit with the real simulating process. Another effect is that incorrect density or velocity values on the boundary can eventually cause negative distribution values in the interior [68]. The lattice Boltzmann method itself is correct up to second order in velocity. Implementing inconsistent boundary conditions may affect the total accuracy of results obtained by that method [38]. It follows that boundary conditions have an immediate influence of the stability and accuracy of the entire method.

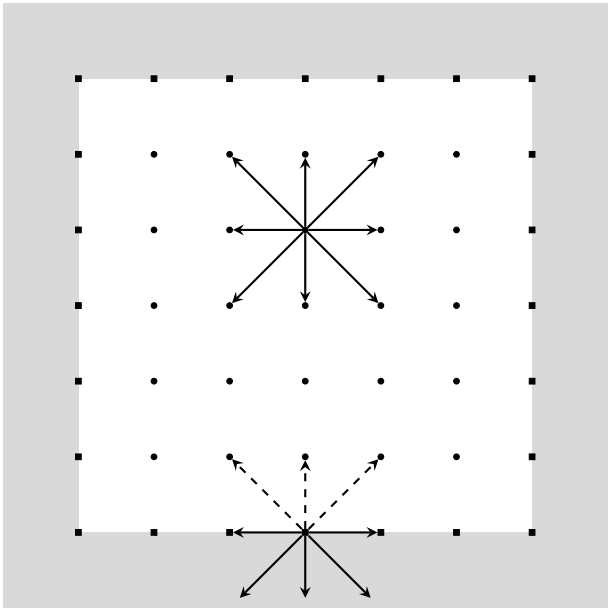

Figure 2.1.: Comparison of interior and boundary lattice points after streaming step. Circles refer to interior lattice points and squares to boundary lattice points. Dashed arrows indicate unknown values, whereas solid arrows refer to known ones.

2.1.1. Periodic Boundary Conditions

Periodic boundary conditions are in our opinion the simplest boundary conditions one can think of. For boundary lattice points they remove the drawback of not having the complete amount of adjacent lattice points in a straightforward manner. Periodic boundary conditions are applied to a boundary and a corresponding boundary counterpart. The missing neighboring lattice points are replaced with boundary lattice points of the corresponding boundary counterpart, and vice versa. Consider the domain illustrated in figure 2.1, a possible application of periodic boundary condition could be to link parallel the west boundary with the east one as well as the north with the south one. Thus, the effective numerical domain can in this example be viewed as a torus. In figure 2.2 the streaming step in D2Q9 is illustrated, where periodic boundary conditions are assumed for the west and east boundary. The extension to 3D models is straightforward.
Periodic boundary conditions are usually applied if the domain of interest and the physical process have a regular symmetry. They are also typically applied in order to get rid of actual physical boundaries, e.g. if one is interested in the behavior of a multi-component mixture for a given initial state where surface effects play a negligible role [61, 63].
Implementation of periodic boundary conditions is not a difficult task, the only difference to interior lattice points is that for boundary lattice points in equation (1.42) the post-stream position $\hat{\boldsymbol{x}} + \boldsymbol{c}_i \Delta\hat{t}$, if it is nonexistent, has to be replaced by a corresponding lattice point of the boundary counterpart.

2.1.2. Bounceback Boundary Conditions

The second type of boundary condition we present are bounceback conditions which in lattice Boltzmann methods are usually implemented if no-slip boundaries are present. They are also commonly used for consideration of solid walls and obstacles. The basic idea is relatively simple and states that the unknown populations of the density distribution are adopted from those of opposite directions. When a bounceback condition is applied the collision step is omitted at the lattice points with incomplete amount of distribution values. Hence they distinguish from the boundary lattice points and therefore we call them with a new term as bounceback lattice points.
The bounceback boundary condition with wall placed through the bounceback lattice points has an inconsistent accuracy with the lattice Boltzmann method, if instead the effective physical boundary lies half way between the bounceback lattice points and the first interior lattice points, the method still has a second order accuracy [29]. Figure 2.3 illustrates the position of the effective physical boundary. Remark that boundary lattice points are not part of the fluid domain which is why they are also called dry points, whereas boundary lattice points are called wet points.

More detailed the principle of bounceback boundary conditions is the following. The streaming step transports the density distribution from an interior lattice point to a bounceback lattice point. In the following collision step the collision operator is ordinary

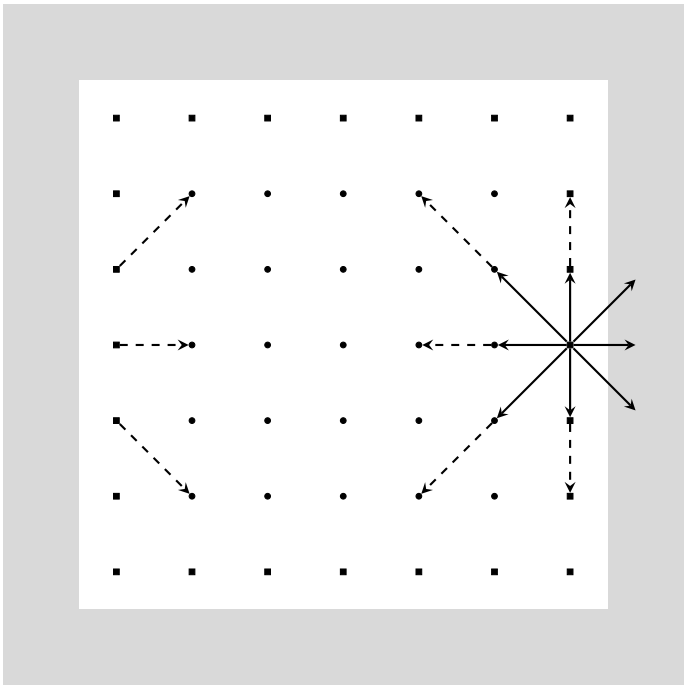

Figure 2.2.: Periodic boundary conditions in D2Q9. Solid arrows depict the pre-streaming state for an easter boundary lattice point, whereas the dashed arrows show the post-streaming state.

evaluated for interior lattice points and, if existent, also for boundary lattice points. The latter exist when besides of bounceback type different boundary conditions are applied for other boundaries. For bounceback lattice points, in place of the collision step, unknown values of the density distribution are replaced with the value of opposite direction. Since only the values streaming back into the fluid domain are important in the subsequent streaming step, a replacement of all values is also possible. This extremely simplifies an implementation, because the algorithm is then independent of the orientation of the boundary. Figure 2.4 illustrates the description above. Boundary lattice points have to be initialized with an appropriate density distribution.
From a mathematical point of view the principle of bounceback boundary conditions alters the lattice BGK equation (1.42) into

$$F_i(\hat{\boldsymbol{x}} + \boldsymbol{c}_i\Delta\hat{t}, \hat{t} + \Delta\hat{t}) - F_{i^-}(\hat{\boldsymbol{x}}, \hat{t}) = 0, \text{ for all } i = 0, \ldots, n_v, \tag{2.1}$$

whenever the position $\hat{\boldsymbol{x}}$ refers to a bounceback lattice point. In the latter equation i^- denotes the index of lattice velocity with opposite direction to lattice velocity $\boldsymbol{c}_i$, i.e. $\boldsymbol{c}_{i^-} = -\boldsymbol{c}_i$. This point of view shows that bounceback boundary conditions work in the two-dimensional case as well as in the three-dimensional one. In both cases they are often used for the handling of stationary walls and obstacles.

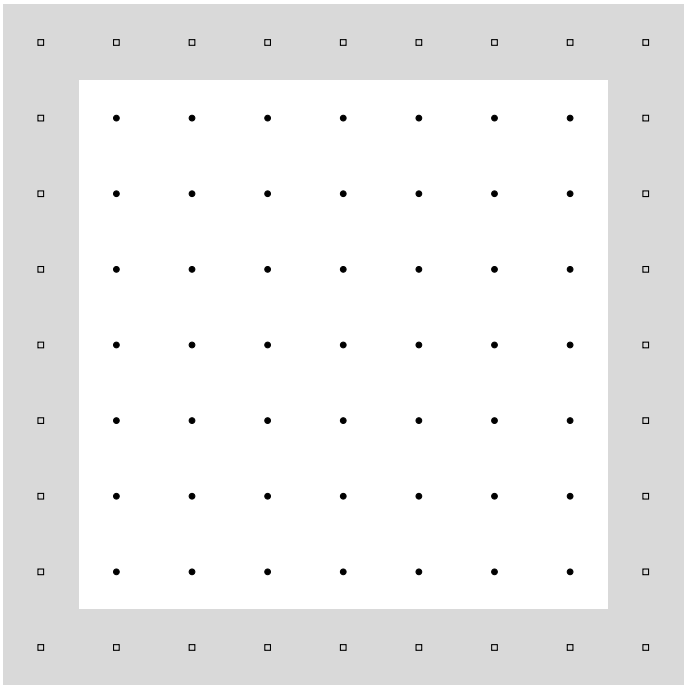

Figure 2.3.: Effective physical boundary when bounceback boundary conditions are applied to D2Q9. Empty squares refer to bounceback lattice points.

2.1.3. Velocity Boundary Conditions

In this subsection we deal with more sophisticated boundary conditions which prescribe the fluid's macroscopic velocity on a boundary. We have to convey that macroscopic condition to the microscopic model.
In the preceding chapter, we already defined the macroscopic quantities in dependence of the microscopic distribution (cf. (1.43) and (1.44)), thus it is natural to use these relations in the consideration of velocity boundary conditions. In contrast to the case of bounceback boundary conditions, we assume that the effective physical boundary passes through boundary lattice points, like shown in figure 2.1. For a boundary lattice point $\hat{\boldsymbol{x}}^0$ we prescribe the macroscopic velocity $\hat{\underline{\boldsymbol{u}}}(\hat{\boldsymbol{x}}^0, \hat{t})$ for a given time point $\hat{t}$. The velocity vector consists of two and three components in the two- and three-dimensional case, respectively. The linkage of the macroscopic velocity to the microscopic density distribution uses the current macroscopic mass density which is not and cannot[3] prescribed for the boundary. Since the mass density is an unknown quantity we first show in the following paragraph how it can be calculated from the given quantities. Afterwards, we return to our main task of calculating the missing populations.

[3] In addition to the velocity the density cannot be prescribed for the boundary as long as one calculates only the unknown values of the density distribution. The reason is that the prescribed velocity and the known values of the distribution uniquely imply a mass density.

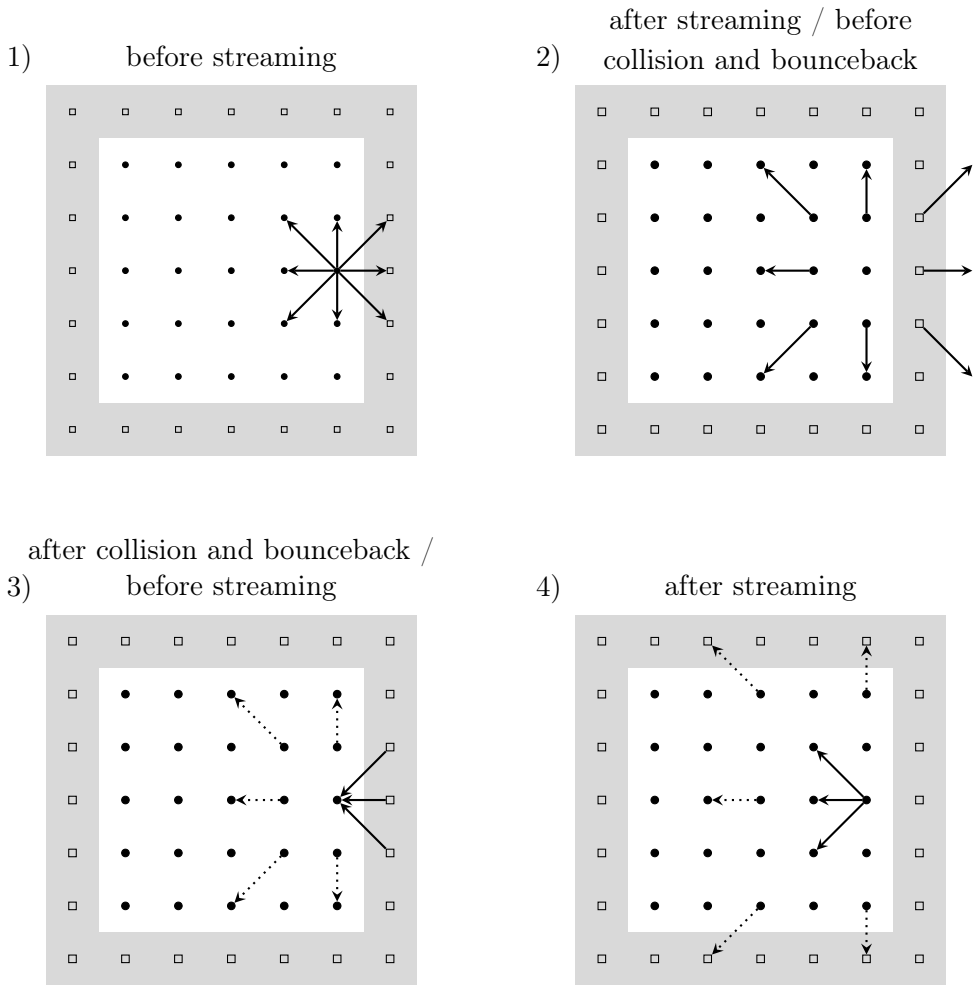

Figure 2.4.: Principle of bounceback boundary conditions. Dotted arrows indicate that values of density distribution were recalculated in the collision step.

Computation of Mass Density

The mass density is an independent variable in lattice Boltzmann methods and can be computed for interior lattice points by equation (1.43). For a boundary lattice points (1.43) is not feasible, since some necessary values for the calculation are missing, nevertheless we can calculate the density out of the known populations in addition with the prescribed velocity. This procedure can be found in [35] and reads as follows. We denote the sum of post-stream unknown populations by $\hat{\rho}_-(\hat{\boldsymbol{x}}^0, \hat{t})$, i.e.

$$\hat{\rho}_-(\hat{\boldsymbol{x}}^0, \hat{t}) = \sum_{i \in \mathcal{I}_-} F_i(\hat{\boldsymbol{x}}^0, \hat{t}),$$

where $\mathcal{I}_- = \{i = 0, \ldots, n_v \mid F_i(\hat{\boldsymbol{x}}^0, \hat{t}) \text{ unknown after streaming step}\}$ is the set of indices of unknown density distribution values. Similarly, $\hat{\rho}_+(\hat{\boldsymbol{x}}^0, \hat{t})$ denotes the sum over directions opposite to the unknown ones, meaning

$$\hat{\rho}_+(\hat{\boldsymbol{x}}^0, \hat{t}) = \sum_{i \in \mathcal{I}_+} F_i(\hat{\boldsymbol{x}}^0, \hat{t}) \quad \text{with} \quad \mathcal{I}_+ = \left\{i = 0, \ldots, n_v \mid i^- \in \mathcal{I}_-\right\},$$

where i^- is explained in (2.1). The remaining populations which are those whose corresponding lattice velocities are tangential to the boundary or zero are summed up and denoted by $\hat{\rho}_0(\hat{\boldsymbol{x}}^0, \hat{t})$. With this notation the mass density decomposes, due to (1.43), into

$$\hat{\rho}(\hat{\boldsymbol{x}}^0, \hat{t}) = \hat{\rho}_-(\hat{\boldsymbol{x}}^0, \hat{t}) + \hat{\rho}_+(\hat{\boldsymbol{x}}^0, \hat{t}) + \hat{\rho}_0(\hat{\boldsymbol{x}}^0, \hat{t}). \tag{2.2}$$

The prescribed velocity can be used to determine the velocity normal to the boundary $\hat{\underline{u}}_n(\hat{\boldsymbol{x}}^0, \hat{t})$, where the vector normal to the boundary is assumed to point outside of the fluid in direction of the boundary. Alternatively from (1.44) we get the relation

$$\hat{\rho}(\hat{\boldsymbol{x}}^0, \hat{t})\hat{\underline{u}}_n(\hat{\boldsymbol{x}}^0, \hat{t}) = \hat{\rho}_+(\hat{\boldsymbol{x}}^0, \hat{t}) - \hat{\rho}_-(\hat{\boldsymbol{x}}^0, \hat{t}). \tag{2.3}$$

Hence, we can compute $\hat{\rho}(\hat{\boldsymbol{x}}^0, \hat{t})$ by combining (2.2) and (2.3), thus it follows

$$\hat{\rho}(\hat{\boldsymbol{x}}^0, \hat{t}) = \frac{1}{1 + \hat{\underline{u}}_n(\hat{\boldsymbol{x}}^0, \hat{t})} \left(2 \cdot \hat{\rho}_+(\hat{\boldsymbol{x}}^0, \hat{t}) + \hat{\rho}_0(\hat{\boldsymbol{x}}^0, \hat{t})\right), \tag{2.4}$$

where on the right hand side only known quantities appear.

Computation of Unknown Density Distribution

We still aim finding the unknown values of the density distribution, such that the macroscopic velocity matches the prescribed one. The number of components the prescribed velocity vector consists of gives, by using (1.44), an equal number of constraints for the unknown values. This means in the two-dimensional case we have two constraints and in the three-dimensional one we achieve three constraints. The number of unknown values depends on the discretization model. Using the D2Q9 model we have three unknowns, compare with figure 2.1, and in the D3Q19 model we have five unknowns like shown in figure 2.5. In both cases we have more unknown populations than constraints, hence additional relations are required.
Zou and He [72] suggest as an additional relation that the non-equilibrium part of the distribution normal to the boundary fulfills a bounceback condition. In the literature the resulting kind of boundary condition is sometimes called Zou and He velocity boundary condition. Following this suggestion, we get

$$F_n(\hat{\boldsymbol{x}}^0, \hat{t}) - F_n^{(eq)}(\hat{\boldsymbol{x}}^0, \hat{t}) = F_{n^-}(\hat{\boldsymbol{x}}^0, \hat{t}) - F_{n^-}^{(eq)}(\hat{\boldsymbol{x}}^0, \hat{t}), \tag{2.5}$$

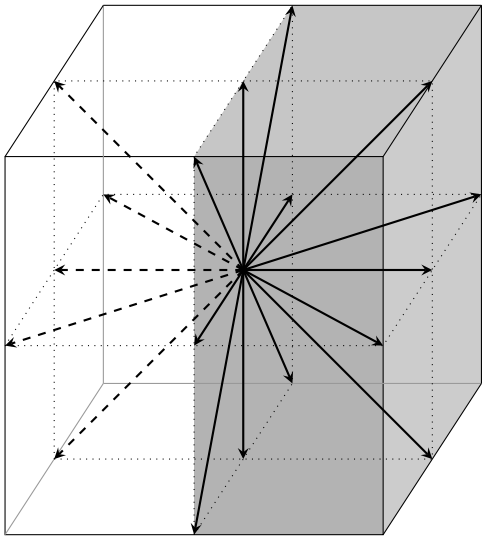

Figure 2.5.: Illustration of a boundary lattice point in D3Q19 after streaming step. Dashed arrows indicate unknown values, whereas solid arrows are referred to known ones.

where n and n^- is the index of lattice velocity normal to the boundary and opposite to the former, respectively. Note that there exist a lattice velocity $\boldsymbol{c}_i$ normal to the boundary, since we assumed that boundaries are aligned with the main lattice direction. For the two-dimensional case we have three equations for three unknown values, hence we can easily determine the unknown populations.
The three-dimensional case is not covered by the foregoing consideration, since we still have more unknowns than equations. Here we focus exclusively on the D3Q19 model, hence we need to find another appropriate relation to achieve a well constrained system of linear equations. Finding this relation can however be avoided by basically extending the bounceback condition of the non-equilibrium part of the distribution normal to the boundary to all unknowns. Afterwards, a redistribution of the density like in [38] adjusts the distribution to match the prescribed velocity. We outline this procedure more detailed now.
In the previous paragraph, we have computed the mass density which appears in (1.44) on the left hand side. Together with the prescribed velocity the complete left hand side is given, we denote the thus prescribed momentum density by

$$\underline{\boldsymbol{j}}(\hat{\boldsymbol{x}}^0, \hat{t}) = \hat{\rho}(\hat{\boldsymbol{x}}^0, \hat{t})\underline{\hat{\boldsymbol{u}}}(\hat{\boldsymbol{x}}^0, \hat{t}).$$

Without loss of generality we assume the boundary to be aligned such that $n = 1$ holds, meaning lattice velocity $\boldsymbol{c}_1 = (1, 0, 0)$ gives the direction of the vector normal to the boundary (cf. (1.48)). After a streaming step $F_3(\hat{\boldsymbol{x}}^0, \hat{t})$, $F_8(\hat{\boldsymbol{x}}^0, \hat{t})$, $F_9(\hat{\boldsymbol{x}}^0, \hat{t})$, $F_{12}(\hat{\boldsymbol{x}}^0, \hat{t})$ and $F_{13}(\hat{\boldsymbol{x}}^0, \hat{t})$ are unknown populations. The value of $F_3(\hat{\boldsymbol{x}}^0, \hat{t})$ can be determined by

(2.5) with $n = 1$ and $n^- = 3$,

$$F_3(\hat{\boldsymbol{x}}^0, \hat{t}) = F_3^{(eq)}(\hat{\boldsymbol{x}}^0, \hat{t}) + F_1^{(neq)}(\hat{\boldsymbol{x}}^0, \hat{t}). \tag{2.6}$$

We have written in the latter equation and will also write in the following the non-equilibrium part of the population corresponding to lattice velocity $\boldsymbol{c}_i$ by

$$F_i^{(neq)}(\hat{\boldsymbol{x}}, \hat{t}) := F_i(\hat{\boldsymbol{x}}, \hat{t}) - F_i^{(eq)}(\hat{\boldsymbol{x}}, \hat{t}). \tag{2.7}$$

A bounceback condition for the non-equilibrium part is used to compute the remaining four unknowns, too, which yields

$$\begin{aligned} F_8(\hat{\boldsymbol{x}}^0, \hat{t}) &= F_8^{(eq)}(\hat{\boldsymbol{x}}^0, \hat{t}) + F_{10}^{(neq)}(\hat{\boldsymbol{x}}^0, \hat{t}), \\ F_9(\hat{\boldsymbol{x}}^0, \hat{t}) &= F_9^{(eq)}(\hat{\boldsymbol{x}}^0, \hat{t}) + F_7^{(neq)}(\hat{\boldsymbol{x}}^0, \hat{t}), \\ F_{12}(\hat{\boldsymbol{x}}^0, \hat{t}) &= F_{12}^{(eq)}(\hat{\boldsymbol{x}}^0, \hat{t}) + F_{14}^{(neq)}(\hat{\boldsymbol{x}}^0, \hat{t}), \\ F_{13}(\hat{\boldsymbol{x}}^0, \hat{t}) &= F_{13}^{(eq)}(\hat{\boldsymbol{x}}^0, \hat{t}) + F_{11}^{(neq)}(\hat{\boldsymbol{x}}^0, \hat{t}). \end{aligned} \tag{2.8}$$

With this choice the momentum density normal to the boundary matches the prescribed one, as shown next. Due to (1.44) we obtain

$$\begin{aligned} \rho(\hat{\boldsymbol{x}}^0, \hat{t})\hat{u}^1(\hat{\boldsymbol{x}}^0, \hat{t}) = &\big(F_1(\hat{\boldsymbol{x}}^0, \hat{t}) + F_7(\hat{\boldsymbol{x}}^0, \hat{t}) + F_{10}(\hat{\boldsymbol{x}}^0, \hat{t}) + F_{11}(\hat{\boldsymbol{x}}^0, \hat{t}) + F_{14}(\hat{\boldsymbol{x}}^0, \hat{t})\big) \\ &- \big(F_3(\hat{\boldsymbol{x}}^0, \hat{t}) + F_8(\hat{\boldsymbol{x}}^0, \hat{t}) + F_9(\hat{\boldsymbol{x}}^0, \hat{t}) + F_{12}(\hat{\boldsymbol{x}}^0, \hat{t}) + F_{13}(\hat{\boldsymbol{x}}^0, \hat{t})\big). \end{aligned}$$

After inserting (2.6) and (2.8) for the subtracting terms, we get with use of a rearranged version of (2.7),

$$\begin{aligned} \rho(\hat{\boldsymbol{x}}^0, \hat{t})\hat{u}^1(\hat{\boldsymbol{x}}^0, \hat{t}) &= F_1^{(eq)}(\hat{\boldsymbol{x}}^0, \hat{t}) - F_3^{(eq)}(\hat{\boldsymbol{x}}^0, \hat{t}) + F_7^{(eq)}(\hat{\boldsymbol{x}}^0, \hat{t}) - F_8^{(eq)}(\hat{\boldsymbol{x}}^0, \hat{t}) \\ &\quad - F_9^{(eq)}(\hat{\boldsymbol{x}}^0, \hat{t}) + F_{10}^{(eq)}(\hat{\boldsymbol{x}}^0, \hat{t}) + F_{11}^{(eq)}(\hat{\boldsymbol{x}}^0, \hat{t}) - F_{12}^{(eq)}(\hat{\boldsymbol{x}}^0, \hat{t}) \\ &\quad - F_{13}^{(eq)}(\hat{\boldsymbol{x}}^0, \hat{t}) + F_{14}^{(eq)}(\hat{\boldsymbol{x}}^0, \hat{t}) \\ &= \sum_{i=0}^{18} c_i^1 F_i^{(eq)}(\hat{\boldsymbol{x}}^0, \hat{t}), \end{aligned}$$

where the sum exactly computes to the prescribed momentum density normal to the boundary, i.e. to the first component of $\underline{\boldsymbol{j}}(\hat{\boldsymbol{x}}^0, \hat{t})$. Denoting the difference between $\underline{\boldsymbol{j}}(\hat{\boldsymbol{x}}^0, \hat{t})$ and the momentum density implied by the distribution with

$$\Delta\boldsymbol{j}(\hat{\boldsymbol{x}}^0, \hat{t}) = \begin{pmatrix} \Delta j^1(\hat{\boldsymbol{x}}^0, \hat{t}) \\ \Delta j^2(\hat{\boldsymbol{x}}^0, \hat{t}) \\ \Delta j^3(\hat{\boldsymbol{x}}^0, \hat{t}) \end{pmatrix} := \sum_{i=0}^{18} \boldsymbol{c}_i F_i(\hat{\boldsymbol{x}}^0, \hat{t}) - \underline{\boldsymbol{j}}(\hat{\boldsymbol{x}}^0, \hat{t}), \tag{2.9}$$

it holds

$$\Delta j^1(\hat{\boldsymbol{x}}^0, \hat{t}) = 0.$$

In the foregoing calculation the upper right index 1 always refers to the first component of the corresponding vector, note that for the given orientation of the boundary this component corresponds to the normal direction.
The prescribed momentum density tangential to the boundary is in general not obtained by the choice (2.8). The final step adjusts the formerly four unknown values, such that the momentum density gets consistent with the prescription. For this reason we first compute $\Delta j^2(\hat{\boldsymbol{x}}^0, \hat{t})$ and $\Delta j^3(\hat{\boldsymbol{x}}^0, \hat{t})$, we get

$$\begin{aligned}
\Delta j^2(\hat{\boldsymbol{x}}^0, \hat{t}) &= \sum_{i=0}^{18} c_i^2 F_i(\hat{\boldsymbol{x}}^0, \hat{t}) - \underline{j}^2(\hat{\boldsymbol{x}}^0, \hat{t}) \\
&= \sum_{i=0}^{18} c_i^2 F_i(\hat{\boldsymbol{x}}^0, \hat{t}) - \sum_{i=0}^{18} c_i^2 F_i^{(eq)}(\hat{\boldsymbol{x}}^0, \hat{t}) \\
&= \sum_{i=0}^{18} c_i^2 \left(F_i(\hat{\boldsymbol{x}}^0, \hat{t}) - F_i^{(eq)}(\hat{\boldsymbol{x}}^0, \hat{t}) \right) \\
&= \sum_{i=0}^{18} c_i^2 F_i^{(neq)}(\hat{\boldsymbol{x}}^0, \hat{t}), \\
\Delta j^3(\hat{\boldsymbol{x}}^0, \hat{t}) &= \sum_{i=0}^{18} c_i^3 F_i^{(neq)}(\hat{\boldsymbol{x}}^0, \hat{t}).
\end{aligned}$$

We try to redistribute $\Delta j^2(\hat{\boldsymbol{x}}^0, \hat{t})$ and $\Delta j^3(\hat{\boldsymbol{x}}^0, \hat{t})$ over the formerly four unknown populations, such that follows $\Delta \boldsymbol{j}(\hat{\boldsymbol{x}}^0, \hat{t}) = 0$. Since $c_8^2 = 1$ and $c_9^2 = -1$ holds, increasing $F_8^{(neq)}(\hat{\boldsymbol{x}}^0, \hat{t})$ and decreasing $F_9^{(neq)}(\hat{\boldsymbol{x}}^0, \hat{t})$ leads to an increase of $\Delta j^2(\hat{\boldsymbol{x}}^0, \hat{t})$. The other way round, decreasing $F_8^{(neq)}(\hat{\boldsymbol{x}}^0, \hat{t})$ and increasing and $F_9^{(neq)}(\hat{\boldsymbol{x}}^0, \hat{t})$ leads to a decrease of $\Delta j^2(\hat{\boldsymbol{x}}^0, \hat{t})$. An analogue effect is given for $F_{12}^{(neq)}(\hat{\boldsymbol{x}}^0, \hat{t})$, $F_{13}^{(neq)}(\hat{\boldsymbol{x}}^0, \hat{t})$ and $\Delta j^3(\hat{\boldsymbol{x}}^0, \hat{t})$. Hence, the redistributed non-equilibrium values $F_i^{\star(neq)}$ with the desired property are obtained by the general equation

$$F_i^{\star(neq)}(\hat{\boldsymbol{x}}^0, \hat{t}) = F_i^{(neq)}(\hat{\boldsymbol{x}}^0, \hat{t}) - \frac{1}{2} c_i^2 \Delta j^2(\hat{\boldsymbol{x}}^0, \hat{t}) - \frac{1}{2} c_i^3 \Delta j^3(\hat{\boldsymbol{x}}^0, \hat{t}), \tag{2.10}$$

with $i = 8, 9, 12, 13$ for the given orientation. $\Delta j^1(\hat{\boldsymbol{x}}^0, \hat{t})$ is not influenced by this redistribution. Boundaries of different orientations, still aligned with the main lattice direction, are treated analogue. The procedure described by equation (2.10) redistributes the excess momentum (2.9) uniformly over the unknown populations.

Summarizing, velocity boundary conditions can be realized by computing the macroscopic density with (2.4), replacing the unknown population normal to the boundary with help of (2.5) and the remaining four unknown populations by appropriate equa-

tions referring to (2.10). Implementing velocity boundary conditions therefore demands a distinction of the orientation of the boundary.

2.1.4. Pressure Boundary Conditions

The last type of boundary conditions we present in the current section are those which prescribe, similar to velocity boundary conditions, a different macroscopic quantity on the boundary, namely the pressure. Actually, this means that a macroscopic mass density is prescribed on the boundary, since the pressure is proportional to the density, see especially (1.57) for D3Q19. A pressure boundary condition can be combined with additional constraints for the macroscopic velocity, but only the components tangential to the boundary can be prescribed. The velocity normal to the boundary $\hat{u}_n(\hat{\boldsymbol{x}}^0, \hat{t})$ instead is already uniquely determined by the pressure condition, as one can see in (2.4). Rearranging this equation leads to

$$\hat{u}_n(\hat{\boldsymbol{x}}^0, \hat{t}) = \frac{2 \cdot \hat{\rho}_+(\hat{\boldsymbol{x}}^0, \hat{t}) + \hat{\rho}_0(\hat{\boldsymbol{x}}^0, \hat{t})}{\underline{\hat{\rho}}(\hat{\boldsymbol{x}}^0, \hat{t})} - 1,$$

where $\underline{\hat{\rho}}(\hat{\boldsymbol{x}}^0, \hat{t})$ denotes the prescribed density. Hence, the task reads to determine the unknown values of the distribution. Again a bounceback condition (2.5) for the non-equilibrium part of the distribution normal to the boundary is used [72].

In D2Q9 it remains to solve for two unknowns and provided additionally a velocity tangential to the boundary is prescribed this task is not a difficult one, since it means to solve a well constrained system of linear equations. If no velocity tangential to the boundary is prescribed we have only one condition to be fulfilled, but since two populations need to be determined this cannot be solved uniquely. The only condition is given by

$$\underline{\hat{\rho}}(\hat{\boldsymbol{x}}^0, \hat{t}) = \sum_{i=0}^{8} F_i(\hat{\boldsymbol{x}}^0, \hat{t}),$$

and the problem can be solved for instance by further assuming the two unknown populations are equal.

The task in the three-dimensional (D3Q19) case is to determine four populations. When we suppose that the pressure boundary condition is given in addition with tangential velocities, the idea described in the second paragraph of the preceding subsection can adopted here [35, 38]. However, if no additional velocity conditions are imposed one can extend the principle described above for D2Q9 to the three-dimensional, analogue.

2.2. Additional Force Terms

When considering the motion of a fluid, the fluid would come to rest after some time due to the viscosity if there are no forces driving the fluid. For instance, these forces can result from a pressure gradient or an external force like gravity acting on the fluid. There are also other situations where an external or internal force has to be considered. Anyway, the demand of extending the simulation by effects resulting from forces acting on the fluid is given.
On the macroscopic scale the Navier-Stokes equations describe the motion of the fluid. We already know from the results in the preceding chapter that lattice Boltzmann methods simulate fluid motions described by the incompressible Navier-Stokes equations (cf. (1.81)) provided the density variation is small. An additional force can be incorporated to these equations by simply adding a term expressing the acceleration due to that force on the right hand side of the momentum equation [60]. Therefore, the complete set of incompressible Navier-Stokes equations which takes into account additional forces reads

$$\begin{aligned} \vec{\nabla} \cdot \vec{u} &= 0, \\ \frac{\partial \vec{u}}{\partial t} + \left(\vec{u} \cdot \vec{\nabla}\right) \vec{u} &= -\vec{\nabla}\hat{p} + \hat{\nu}\Delta\vec{u} + \vec{k}, \end{aligned} \tag{2.11}$$

where $\vec{k}$ is the acceleration due to the additional force density $\vec{K} = \rho\vec{k}$.

The lattice Boltzmann method has to be altered in such a way that their hydrodynamical behavior is described by equations (2.11). Then the model considers effects coming from additional forces in a physical correct manner. Guo et al. state that in order to obtain the correct continuity equation, the fluid velocity must be defined such that the effect of the external force is included, and to obtain the correct momentum equation, the contributions of the force to the momentum flux must be canceled [24]. They also propose an approach fulfilling these both conditions. In the following, we briefly present their model in the current section and use it for the consideration of buoyancy effects below in section 2.4.

Basically, we can incorporate additional forces by simply modifying the collision step and using a slightly differing formula for the calculation of the macroscopic velocity. Hence, the consideration of additional forces can be done without much effort.
Recapitulating the equilibrium distribution (1.55) of D3Q19

$$F_i^{(eq)}(\hat{\boldsymbol{x}}, \hat{t}) = \omega_i \hat{\rho}(\hat{\boldsymbol{x}}, \hat{t}) \left[1 + 3(\boldsymbol{c}_i \cdot \hat{\boldsymbol{u}}(\hat{\boldsymbol{x}}, \hat{t})) + \frac{9}{2}(\boldsymbol{c}_i \cdot \hat{\boldsymbol{u}}(\hat{\boldsymbol{x}}, \hat{t}))^2 - \frac{3}{2}|\hat{\boldsymbol{u}}(\hat{\boldsymbol{x}}, \hat{t})|^2\right],$$

$i = 0, \ldots, 18$. We can rewrite this equation to

$$F_i^{(eq)}(\hat{\boldsymbol{x}}, \hat{t}) = \omega_i \hat{\rho}(\hat{\boldsymbol{x}}, \hat{t}) \left[1 + \frac{\boldsymbol{c}_i \cdot \hat{\boldsymbol{u}}(\hat{\boldsymbol{x}}, \hat{t})}{c_s^2} + \frac{\left[\hat{\boldsymbol{u}}(\hat{\boldsymbol{x}}, \hat{t})\hat{\boldsymbol{u}}(\hat{\boldsymbol{x}}, \hat{t})^T\right] : \left[\boldsymbol{c}_i\boldsymbol{c}_i^T - c_s^2 I\right]}{2c_s^4}\right], \tag{2.12}$$

with $c_s = \frac{1}{\sqrt{3}}$, I being the identity matrix and the twice contraction product as follows[4]:

Notation. *Let A and B be two matrices of same dimension, say*

$$A = (a_{ij})_{i,j=1,\dots,n} \text{ and } B = (b_{ij})_{i,j=1,\dots,n}.$$

Then the twice contraction product $A : B$ is computed as follows

$$A : B = \sum_{i=1}^{n} \sum_{j=1}^{n} a_{ij} b_{ij}.$$

This means the twice contraction is the summation of the component wise multiplication.

Equation (2.12) is a general expression of the equilibrium equation.
Assuming a discrete forcing term is given in a similar more generalized form

$$K_i(\hat{\boldsymbol{x}}, \hat{t}) = \omega_i \left[l_1 + \frac{\boldsymbol{l}_2 \cdot \boldsymbol{c}_i}{c_s^2} + \frac{l_3 : \left[\boldsymbol{c}_i \boldsymbol{c}_i^T - c_s^2 I \right]}{2 c_s^4} \right], \tag{2.13}$$

with unknown scalar l_1, vector $\boldsymbol{l}_2$ and matrix l_3 each depending on the force density $\boldsymbol{K}(\hat{\boldsymbol{x}}, \hat{t})$ which need to be determined. The weights ω_i are equal with those of the equilibrium distribution.
On the one hand the modification of the collision term adds $K_i(\hat{\boldsymbol{x}}, \hat{t})$ to the known collision term from the previous chapter. Hence, this modification changes (1.42) into

$$F_i(\hat{\boldsymbol{x}} + \boldsymbol{c}_i \Delta\hat{t}, \hat{t} + \Delta\hat{t}) - F_i(\hat{\boldsymbol{x}}, \hat{t}) = -\frac{1}{\hat{\tau}_c} \left[F_i(\hat{\boldsymbol{x}}, \hat{t}) - F_i^{(eq)}(\hat{\boldsymbol{x}}, \hat{t}) \right] + K_i(\hat{\boldsymbol{x}}, \hat{t}). \tag{2.14}$$

On the other hand we use the altered equation

$$\boldsymbol{u}^\star(\hat{\boldsymbol{x}}, \hat{t}) = \frac{1}{\rho(\hat{\boldsymbol{x}}, \hat{t})} \left(\sum_{i=0}^{n_v} \boldsymbol{c}_i F_i(\hat{\boldsymbol{x}}, \hat{t}) + \frac{\boldsymbol{K}(\hat{\boldsymbol{x}}, \hat{t})}{2} \right) \tag{2.15}$$

to compute the macroscopic velocity which is especially used in the computation of the equilibrium distribution in the collision step.
The unknowns in (2.13) have to be determined such that the modified model leads to the correct macroscopic equations in a multi-scale expansion. This is done in [24], the authors conclude that a feasible choice is given by

$$l_1 = 0, \quad \boldsymbol{l}_2 = \left(1 - \frac{1}{2\hat{\tau}_c} \right) \boldsymbol{K}(\hat{\boldsymbol{x}}, \hat{t}), \quad \boldsymbol{l}_3 = \left(1 - \frac{1}{2\hat{\tau}_c} \right) 2\boldsymbol{u}^\star(\hat{\boldsymbol{x}}, \hat{t}) \boldsymbol{K}(\hat{\boldsymbol{x}}, \hat{t})^T.$$

[4]Remark: The pressure/density relation (1.57) can be written as $p(\hat{\boldsymbol{x}}, \hat{t}) = c_s^2 \rho(\hat{\boldsymbol{x}}, \hat{t})$, valid not only for D3Q19. c_s gives the speed of sound in the corresponding model.

Inserting $c_s = \frac{1}{\sqrt{3}}$ and the latter values in (2.13), it follows

$$K_i(\hat{\boldsymbol{x}}, \hat{t}) = \left(1 - \frac{1}{2\hat{\tau}_c}\right) \omega_i \left[3\left(\boldsymbol{c}_i - \boldsymbol{u}^\star(\hat{\boldsymbol{x}}, \hat{t})\right) + 9\left(\boldsymbol{c}_i \cdot \boldsymbol{u}^\star(\hat{\boldsymbol{x}}, \hat{t})\right)\boldsymbol{c}_i\right] \cdot \boldsymbol{K}(\hat{\boldsymbol{x}}, \hat{t}).$$

Using this discrete force term and the little model changes (2.14) and (2.15) the resulting equations in a Chapman-Enskog approximation match the incompressible Navier-Stokes equations including additional forces. Therefore, the model incorporates additional forces in a physical correct manner. Note that if no forces are present, meaning $\boldsymbol{K}(\hat{\boldsymbol{x}}, \hat{t}) = 0$, the modified model is equivalent to that presented in the previous chapter.

2.3. Incorporation of a Thermal Component

The lattice Boltzmann method or more precisely the lattice BGK method presented in the previous chapter is a numerical approach to simulate incompressible fluid flows. Although the method presented in the previous chapter satisfies the incompressible Navier-Stokes equations, an application of the LBGK method to a variety of physical problems is often possible not until one considers corresponding boundary and surface conditions. We touched that topic at the beginning of the current chapter. Despite the consideration of boundary and surface conditions enables an application to a variety of problems, the method is still only capable of simulating isothermal flows.
The goal of this section is to develop a numerical method to simulate the temperature evolution. Therefore we propose a method which extends the lattice BGK method such that the temperature is advected by the fluid's flow and diffuses in it, meaning the temperature obeys an advection-diffusion equation. Like viscosity in the lattice BGK method, a parameter which can be chosen to tune the thermal diffusivity is available. The fluid itself behaves like an isothermal fluid, that means in areas of different temperatures the fluid's viscosity does not distinguish. Consequently, the latter fact limits the application of the proposed method to problems in which only a relatively small temperature range appears or at least to those in which the influence from the temperature on the viscosity is small. Furthermore, the compression work done by the pressure and the viscous heat dissipation are neglected. When simulating the motion of real incompressible fluids in applications these terms are (very often) negligible. A less simple method which incorporates also the compression work done by the pressure and the viscous heat dissipation can be found in [26].

In literature, the existing approaches to add a thermal component to lattice BGK methods can be grouped in at least two categories. On the one hand there is a multispeed approach which uses only the density distribution function (e.g. [1, 41]). In these approaches a higher order approximation of the equilibrium distribution is necessary to obtain the energy evolution equation and thus an energy conservating method [40].
On the other hand there is the category of approaches which do not use the density distribution of the fluid alone. One possibility is to use so called passive-scalar ap-

proaches which are based on multiple component models [56], where the temperature is regarded as an additional component without mass which behaves like an passive diffusing one only advected by the flow [55, 57]. These procedures have the advantage that the thermal diffusivity can be tuned independently of the viscosity, whereas in multispeed approaches a fixed Prandtl number of usually $Pr = \frac{1}{2}$ appears. The Prandtl number is a dimensionless quantity describing the ratio of kinematic viscosity and thermal diffusivity. Another possibility is given by multi-distribution approaches, these schemes are similar to the passive-scalar approaches because they also use a separate distribution function to simulate the temperature evolution. The numerical method we propose in the following is classified to them.
In this procedure, the LBGK method simulating the density and velocity evolution can theoretically be decoupled from the temperature evolution, thus for instance a classical Navier-Stokes solver can be used to simulate the density and velocity evolution instead.

Although we have already mentioned above that the proposed method will satisfy an advection-diffusion equation, we determine the desired temperature evolution equation in the subsequent subsection extensively.

2.3.1. Determination of Macroscopic Equation

In the previous chapter we dealt with the LBGK method, where we could show that the numerical method obeys the well known incompressible Navier-Stokes equations. This subsection discusses the determination of the general macroscopic equation the temperature obeys, and thus clears up the question how the evolution equation for the temperature looks like. The determination uses the Boltzmann equation directly and is analogue to [26]. Here, we focus on the three-dimensional case exclusively, the generalization to $\mathbb{R}^d$, $d \in \{2, 3\}$, is straightforward.

Since we already know a relation between the temperature and the density distribution $f(\boldsymbol{x}, \boldsymbol{v}, t)$ satisfying the Boltzmann equation, it is naturally to start with this relation. Recapitulating that relation (cf. (1.8)) gives

$$\rho(\boldsymbol{x}, t)E(\boldsymbol{x}, t) = \int_{\mathbb{R}^3} \frac{|\boldsymbol{v} - \boldsymbol{u}(\boldsymbol{x}, t)|^2}{2} f(\boldsymbol{x}, \boldsymbol{v}, t)\,\mathrm{d}\boldsymbol{v}, \tag{2.16}$$

with the internal energy $E(\boldsymbol{x}, t) = \frac{3}{2}\frac{k_B T(\boldsymbol{x},t)}{m}$ in $\mathbb{R}^3$. We define a new distribution, calling it the energy distribution, by

$$g(\boldsymbol{x}, \boldsymbol{v}, t) = \frac{|\boldsymbol{v} - \boldsymbol{u}(\boldsymbol{x}, t)|^2}{2} f(\boldsymbol{x}, \boldsymbol{v}, t).$$

For the new distribution we derive a PDE similar to the Boltzmann equation. The desired macroscopic temperature evolution equation is then obtained from this PDE via a Chapman-Enskog expansion.

PDE for energy distribution

A derivation of the energy distribution with respect to time results in

$$\begin{aligned}\frac{\partial g(\boldsymbol{x},\boldsymbol{v},t)}{\partial t} &= \frac{\partial}{\partial t}\left(\frac{|\boldsymbol{v}-\boldsymbol{u}(\boldsymbol{x},t)|^2}{2} f(\boldsymbol{x},\boldsymbol{v},t)\right)\\ &= \frac{1}{2}\left[|\boldsymbol{v}-\boldsymbol{u}(\boldsymbol{x},t)|^2 \frac{\partial f(\boldsymbol{x},\boldsymbol{v},t)}{\partial t} + f(\boldsymbol{x},\boldsymbol{v},t)\frac{\partial |\boldsymbol{v}-\boldsymbol{u}(\boldsymbol{x},t)|^2}{\partial t}\right].\end{aligned}$$

Similarly, we obtain for the advection term

$$\begin{aligned}\boldsymbol{v}\cdot\boldsymbol{\nabla} g(\boldsymbol{x},\boldsymbol{v},t) &= \boldsymbol{v}\cdot\boldsymbol{\nabla}\left(\frac{1}{2}|\boldsymbol{v}-\boldsymbol{u}(\boldsymbol{x},t)|^2 f(\boldsymbol{x},\boldsymbol{v},t)\right)\\ &= \frac{1}{2}\left[f(\boldsymbol{x},\boldsymbol{v},t)\boldsymbol{v}\cdot\boldsymbol{\nabla}\left(|\boldsymbol{v}-\boldsymbol{u}(\boldsymbol{x},t)|^2\right) + |\boldsymbol{v}-\boldsymbol{u}(\boldsymbol{x},t)|^2 \boldsymbol{v}\cdot\boldsymbol{\nabla} f(\boldsymbol{x},\boldsymbol{v},t)\right].\end{aligned}$$

Combining both equations results in

$$\begin{aligned}\frac{\partial g(\boldsymbol{x},\boldsymbol{v},t)}{\partial t} + \boldsymbol{v}\cdot\boldsymbol{\nabla} g(\boldsymbol{x},\boldsymbol{v},t) = \frac{|\boldsymbol{v}-\boldsymbol{u}(\boldsymbol{x},t)|^2}{2}&\left[\frac{\partial f(\boldsymbol{x},\boldsymbol{v},t)}{\partial t} + \boldsymbol{v}\cdot\boldsymbol{\nabla} f(\boldsymbol{x},\boldsymbol{v},t)\right]\\ &- f(\boldsymbol{x},\boldsymbol{v},t)\left[-\frac{1}{2}\frac{\partial |\boldsymbol{v}-\boldsymbol{u}(\boldsymbol{x},t)|^2}{\partial t} - \frac{1}{2}\boldsymbol{v}\cdot\boldsymbol{\nabla}\left(|\boldsymbol{v}-\boldsymbol{u}(\boldsymbol{x},t)|^2\right)\right],\end{aligned}$$

where the left hand side of the Boltzmann equation (1.4) appears in the square bracket on the first line of the right hand side. Since the density distribution $f(\boldsymbol{x},\boldsymbol{v},t)$ satisfies the Boltzmann equation, the square bracket can be substituted by the corresponding right hand side $Q(f,f)$ of the Boltzmann equation.
A new collision term is introduced which corresponds to a substitution of the square bracket by the right hand side of the BGK equation (1.29), where a new relaxation parameter τ_d is used, meaning that

$$\begin{aligned}\frac{|\boldsymbol{v}-\boldsymbol{u}(\boldsymbol{x},t)|^2}{2} Q(f,f) \rightsquigarrow \frac{|\boldsymbol{v}-\boldsymbol{u}(\boldsymbol{x},t)|^2}{2}&\left(-\frac{1}{\tau_d}\left[f(\boldsymbol{x},\boldsymbol{v},t) - f^{(eq)}(\boldsymbol{x},\boldsymbol{v},t)\right]\right)\\ &= -\frac{1}{\tau_d}\left[g(\boldsymbol{x},\boldsymbol{v},t) - g^{(eq)}(\boldsymbol{x},\boldsymbol{v},t)\right],\end{aligned}$$

with

$$\begin{aligned}g^{(eq)}(\boldsymbol{x},\boldsymbol{v},t) &:= \frac{|\boldsymbol{v}-\boldsymbol{u}(\boldsymbol{x},t)|^2}{2} f^{(eq)}(\boldsymbol{x},\boldsymbol{v},t) \qquad (2.17)\\ &= \frac{|\boldsymbol{v}-\boldsymbol{u}(\boldsymbol{x},t)|^2 \rho(\boldsymbol{x},t)}{2}\left(\frac{m}{2\pi k_B T(\boldsymbol{x},t)}\right)^{3/2} \exp\left(\frac{-m}{2k_B T(\boldsymbol{x},t)}|\boldsymbol{v}-\boldsymbol{u}(\boldsymbol{x},t)|^2\right).\end{aligned}$$

It follows a first PDE for the energy distribution:

$$\frac{\partial g(\boldsymbol{x},\boldsymbol{v},t)}{\partial t} + \boldsymbol{v}\cdot\boldsymbol{\nabla} g(\boldsymbol{x},\boldsymbol{v},t) = -\frac{1}{\tau_d}\left[g(\boldsymbol{x},\boldsymbol{v},t) - g^{(eq)}(\boldsymbol{x},\boldsymbol{v},t)\right] \\ - f(\boldsymbol{x},\boldsymbol{v},t)\left[-\frac{1}{2}\frac{\partial|\boldsymbol{v}-\boldsymbol{u}(\boldsymbol{x},t)|^2}{\partial t} - \frac{1}{2}\boldsymbol{v}\cdot\boldsymbol{\nabla}\left(|\boldsymbol{v}-\boldsymbol{u}(\boldsymbol{x},t)|^2\right)\right]. \tag{2.18}$$

However, this equation can be simplified, especially the square bracket on the second line. For this reason, we compute the derivative with respect to time as follows

$$\begin{aligned} -\frac{1}{2}\frac{\partial|\boldsymbol{v}-\boldsymbol{u}(\boldsymbol{x},t)|^2}{\partial t} &= -\frac{1}{2}\frac{\partial|\boldsymbol{v}|^2}{\partial t} + \frac{\partial\left(\boldsymbol{v}\cdot\boldsymbol{u}(\boldsymbol{x},t)\right)}{\partial t} - \frac{1}{2}\frac{\partial|\boldsymbol{u}(\boldsymbol{x},t)|^2}{\partial t} \\ &= \boldsymbol{v}\cdot\frac{\partial\boldsymbol{u}(\boldsymbol{x},t)}{\partial t} - \boldsymbol{u}(\boldsymbol{x},t)\cdot\frac{\partial\boldsymbol{u}(\boldsymbol{x},t)}{\partial t} \\ &= (\boldsymbol{v}-\boldsymbol{u}(\boldsymbol{x},t))\cdot\frac{\partial\boldsymbol{u}(\boldsymbol{x},t)}{\partial t}. \end{aligned}$$

The second term in the square bracket of (2.18) is simplified with help of

$$\boldsymbol{\nabla}\left(\boldsymbol{v}\cdot\boldsymbol{u}(\boldsymbol{x},t)\right) = \left[(\boldsymbol{v}\cdot\boldsymbol{\nabla})\boldsymbol{u}(\boldsymbol{x},t)\right]$$

and

$$\begin{aligned} &\frac{1}{2}\left[\boldsymbol{v}\cdot\boldsymbol{\nabla}\left(|\boldsymbol{u}(\boldsymbol{x},t)|^2\right)\right] \\ &\quad= \frac{1}{2}\left[\boldsymbol{v}\cdot\boldsymbol{\nabla}(u^1(\boldsymbol{x},t)^2) + \boldsymbol{v}\cdot\boldsymbol{\nabla}(u^2(\boldsymbol{x},t)^2) + \boldsymbol{v}\cdot\boldsymbol{\nabla}(u^3(\boldsymbol{x},t)^2)\right] \\ &\quad= u^1(\boldsymbol{x},t)\left[\boldsymbol{v}\cdot\left(\boldsymbol{\nabla}u^1(\boldsymbol{x},t)\right)\right] + u^2(\boldsymbol{x},t)\left[\boldsymbol{v}\cdot\left(\boldsymbol{\nabla}u^2(\boldsymbol{x},t)\right)\right] + u^3(\boldsymbol{x},t)\left[\boldsymbol{v}\cdot\left(\boldsymbol{\nabla}u^3(\boldsymbol{x},t)\right)\right] \\ &\quad= u^1(\boldsymbol{x},t)\left[(\boldsymbol{v}\cdot\boldsymbol{\nabla})\,u^1(\boldsymbol{x},t)\right] + u^2(\boldsymbol{x},t)\left[(\boldsymbol{v}\cdot\boldsymbol{\nabla})\,u^2(\boldsymbol{x},t)\right] + u^3(\boldsymbol{x},t)\left[(\boldsymbol{v}\cdot(\boldsymbol{\nabla})\,u^3(\boldsymbol{x},t)\right] \\ &\quad= \boldsymbol{u}(\boldsymbol{x},t)\cdot\left[(\boldsymbol{v}\cdot\boldsymbol{\nabla})\boldsymbol{u}(\boldsymbol{x},t)\right]. \end{aligned}$$

Using the latter two equations, the mentioned second term can be simplified as follows

$$\begin{aligned} -\frac{1}{2}\boldsymbol{v}\cdot\boldsymbol{\nabla}\left(|\boldsymbol{v}-\boldsymbol{u}(\boldsymbol{x},t)|^2\right) &= -\frac{1}{2}\boldsymbol{v}\cdot\boldsymbol{\nabla}\left(|\boldsymbol{v}|^2 - 2\boldsymbol{v}\cdot\boldsymbol{u}(\boldsymbol{x},t) + |\boldsymbol{u}(\boldsymbol{x},t)|^2\right) \\ &= \boldsymbol{v}\cdot\boldsymbol{\nabla}\left(\boldsymbol{v}\cdot\boldsymbol{u}(\boldsymbol{x},t)\right) - \frac{1}{2}\left[\boldsymbol{v}\cdot\boldsymbol{\nabla}\left(|\boldsymbol{u}(\boldsymbol{x},t)|^2\right)\right] \\ &= \boldsymbol{v}\cdot\left[(\boldsymbol{v}\cdot\boldsymbol{\nabla})\boldsymbol{u}(\boldsymbol{x},t)\right] - \boldsymbol{u}(\boldsymbol{x},t)\cdot\left[(\boldsymbol{v}\cdot\boldsymbol{\nabla})\boldsymbol{u}(\boldsymbol{x},t)\right] \\ &= (\boldsymbol{v}-\boldsymbol{u}(\boldsymbol{x},t))\cdot\left[(\boldsymbol{v}\cdot\boldsymbol{\nabla})\boldsymbol{u}(\boldsymbol{x},t)\right]. \end{aligned}$$

By using all simplifications together, the simplified form of (2.18) becomes our final PDE for the energy distribution. It reads

$$\frac{\partial g(\boldsymbol{x},\boldsymbol{v},t)}{\partial t} + \boldsymbol{v}\cdot\boldsymbol{\nabla} g(\boldsymbol{x},\boldsymbol{v},t) = -\frac{1}{\tau_d}\left[g(\boldsymbol{x},\boldsymbol{v},t) - g^{(eq)}(\boldsymbol{x},\boldsymbol{v},t)\right] - f(\boldsymbol{x},\boldsymbol{v},t)q(\boldsymbol{x},t), \tag{2.19}$$

with

$$q(\boldsymbol{x},\boldsymbol{v},t) = (\boldsymbol{v}-\boldsymbol{u}(\boldsymbol{x},t))\cdot\left[\frac{\partial \boldsymbol{u}(\boldsymbol{x},t)}{\partial t} + (\boldsymbol{v}\cdot\boldsymbol{\nabla})\boldsymbol{u}(\boldsymbol{x},t)\right]. \tag{2.20}$$

Chapman-Enskog Approximation

Following [26], the last equation in the previous paragraph, (2.19), is used in a Chapman-Enskog approximation to determine the macroscopic temperature evolution equation. Therefore, we denote the equilibria of the density and energy distribution by $f^{(0)}(\boldsymbol{x},\boldsymbol{v},t)$ and $g^{(0)}(\boldsymbol{x},\boldsymbol{v},t)$, respectively. The distributions are expanded around their corresponding equilibrium, it follows

$$\begin{aligned} f(\boldsymbol{x},\boldsymbol{v},t) &= f^{(0)}(\boldsymbol{x},\boldsymbol{v},t) + \delta f^{(1)}(\boldsymbol{x},\boldsymbol{v},t) + \delta^2 f^{(2)}(\boldsymbol{x},\boldsymbol{v},t) + \dots, \\ g(\boldsymbol{x},\boldsymbol{v},t) &= g^{(0)}(\boldsymbol{x},\boldsymbol{v},t) + \delta g^{(1)}(\boldsymbol{x},\boldsymbol{v},t) + \delta^2 g^{(2)}(\boldsymbol{x},\boldsymbol{v},t) + \dots, \end{aligned} \tag{2.21}$$

with δ being the expansion parameter. We also expand or scale the occuring operators by

$$\begin{aligned} \frac{\partial}{\partial t} &= \delta\frac{\partial^{(1)}}{\partial t} + \delta^2\frac{\partial^{(2)}}{\partial t} + \dots, \\ \boldsymbol{\nabla} &= \delta\boldsymbol{\nabla}^{(1)}. \end{aligned} \tag{2.22}$$

Considering the definition (2.20) and the operators (2.22), we observe that $q(\boldsymbol{x},\boldsymbol{v},t)$ has the following expression

$$q(\boldsymbol{x},\boldsymbol{v},t) = \delta q^{(1)}(\boldsymbol{x},\boldsymbol{v},t) + \delta^2 q^{(2)}(\boldsymbol{x},\boldsymbol{v},t) + \dots, \tag{2.23}$$

with

$$\begin{aligned} q^{(1)}(\boldsymbol{x},\boldsymbol{v},t) &= (\boldsymbol{v}-\boldsymbol{u}(\boldsymbol{x},t))\cdot\left[\frac{\partial^{(1)}\boldsymbol{u}(\boldsymbol{x},t)}{\partial t} + (\boldsymbol{v}\cdot\boldsymbol{\nabla}^{(1)})\boldsymbol{u}(\boldsymbol{x},t)\right], \\ q^{(k)}(\boldsymbol{x},\boldsymbol{v},t) &= (\boldsymbol{v}-\boldsymbol{u}(\boldsymbol{x},t))\cdot\left[\frac{\partial^{(k)}\boldsymbol{u}(\boldsymbol{x},t)}{\partial t}\right], \quad 2\leq k\in\mathbb{N}. \end{aligned}$$

Substitution of (2.21), (2.22) and (2.23) into (2.19) yields the Chapman-Enskog expansion. The first order terms give the following equation

$$\frac{\partial^{(1)} g^{(0)}(\boldsymbol{x},\boldsymbol{v},t)}{\partial t} + \boldsymbol{v}\cdot\boldsymbol{\nabla}^{(1)} g^{(0)}(\boldsymbol{x},\boldsymbol{v},t) = -\frac{g^{(1)}(\boldsymbol{x},\boldsymbol{v},t)}{\tau_d} - f^{(0)}(\boldsymbol{x},\boldsymbol{v},t) q^{(1)}(\boldsymbol{x},\boldsymbol{v},t), \tag{2.24}$$

whereas those of order two read

$$\frac{\partial^{(2)} g^{(0)}(\boldsymbol{x},\boldsymbol{v},t)}{\partial t} + \left[\frac{\partial^{(1)}}{\partial t} + \boldsymbol{v}\cdot\boldsymbol{\nabla}^{(1)}\right] g^{(1)}(\boldsymbol{x},\boldsymbol{v},t) = -\frac{g^{(2)}(\boldsymbol{x},\boldsymbol{v},t)}{\tau_d} - f^{(0)}(\boldsymbol{x},\boldsymbol{v},t) q^{(2)}(\boldsymbol{x},\boldsymbol{v},t) - f^{(1)}(\boldsymbol{x},\boldsymbol{v},t) q^{(1)}(\boldsymbol{x},\boldsymbol{v},t). \tag{2.25}$$

Higher order terms are disregarded. Integration of (2.24) and (2.25) over velocity space leads to the temperature evolution equation. Before we integrate, we split $q^{(1)}(\boldsymbol{x},\boldsymbol{v},t)$ in (2.23) into two terms

$$q^{(1)}(\boldsymbol{x},\boldsymbol{v},t) = q_1^{(1)}(\boldsymbol{x},\boldsymbol{v},t) + q_2^{(1)}(\boldsymbol{x},\boldsymbol{v},t), \tag{2.26}$$

where only $q_1^{(1)}(\boldsymbol{x},\boldsymbol{v},t)$ contributes to the thermal conduction term in the evolution equation resulting below, whereas $q_2^{(1)}(\boldsymbol{x},\boldsymbol{v},t)$ only affects the terms of the compression work done by pressure and the viscous heat dissipation. We set

$$q_1^{(1)}(\boldsymbol{x},\boldsymbol{v},t) = (\boldsymbol{v}-\boldsymbol{u}(\boldsymbol{x},t))\cdot\left[\frac{\partial^{(1)}\boldsymbol{u}(\boldsymbol{x},t)}{\partial t} + (\boldsymbol{u}(\boldsymbol{x},t)\cdot\boldsymbol{\nabla}^{(1)})\boldsymbol{u}(\boldsymbol{x},t)\right],$$

thus the term in the square bracket corresponds to the first order left hand side of the incompressible Navier-Stokes equations, therefore we can substitute it by the corresponding right hand side. We obtain

$$q_1^{(1)}(\boldsymbol{x},\boldsymbol{v},t) = (\boldsymbol{v}-\boldsymbol{u}(\boldsymbol{x},t))\cdot\left[-\boldsymbol{\nabla}^{(1)}\frac{p(\boldsymbol{x},t)}{\rho(\boldsymbol{x},t)}\right].$$

The remaining unknown term $q_2^{(1)}(\boldsymbol{x},\boldsymbol{v},t)$ is then given by the difference of $q^{(1)}(\boldsymbol{x},\boldsymbol{v},t)$ and $q_1^{(1)}(\boldsymbol{x},\boldsymbol{v},t)$. The notation explained on page 61 is used in the expression of this

difference.

$$\begin{aligned} q_2^{(1)}(\boldsymbol{x},\boldsymbol{v},t) &= q^{(1)}(\boldsymbol{x},\boldsymbol{v},t) - q_1^{(1)}(\boldsymbol{x},\boldsymbol{v},t) \\ &= (\boldsymbol{v}-\boldsymbol{u}(\boldsymbol{x},t)) \cdot \left[\frac{\partial^{(1)}\boldsymbol{u}(\boldsymbol{x},t)}{\partial t} + (\boldsymbol{v}\cdot\boldsymbol{\nabla}^{(1)})\boldsymbol{u}(\boldsymbol{x},t) \right] \\ &= (\boldsymbol{v}-\boldsymbol{u}(\boldsymbol{x},t)) \cdot \left[(\boldsymbol{v}-\boldsymbol{u}(\boldsymbol{x},t))\cdot\boldsymbol{\nabla}^{(1)} \right] \boldsymbol{u}(\boldsymbol{x},t) \\ &= \left[(\boldsymbol{v}-\boldsymbol{u}(\boldsymbol{x},t))\,(\boldsymbol{v}-\boldsymbol{u}(\boldsymbol{x},t))^T \right] : \left[\boldsymbol{\nabla}^{(1)}\boldsymbol{u}(\boldsymbol{x},t) \right]. \end{aligned}$$

Now we integrate (2.24) and (2.25), for the sake of clarity we only give the results here. More information to the calculation can be found in appendix A.3. Integrating the first order equation (2.24) over velocity space yields

$$\frac{\partial^{(1)}}{\partial t}\left(\rho(\boldsymbol{x},t)E(\boldsymbol{x},t)\right) + \boldsymbol{\nabla}^{(1)}\cdot\left(\rho(\boldsymbol{x},t)\boldsymbol{u}(\boldsymbol{x},t)E(\boldsymbol{x},t)\right) = -p(\boldsymbol{x},t)\boldsymbol{\nabla}^{(1)}\cdot\boldsymbol{u}(\boldsymbol{x},t). \tag{2.27}$$

When integrating the second order terms (2.25), one obtains [26]

$$\frac{\partial^{(2)}}{\partial t}(\rho(\boldsymbol{x},t)E(\boldsymbol{x},t)) = \boldsymbol{\nabla}^{(1)}\cdot\Big(\rho(\boldsymbol{x},t)\kappa\boldsymbol{\nabla}^{(1)}E(\boldsymbol{x},t)\Big) + \boldsymbol{\Lambda}^{(1)}(\boldsymbol{x},t) : \left[\boldsymbol{\nabla}^{(1)}\boldsymbol{u}(\boldsymbol{x},t)\right], \tag{2.28}$$

where the coefficient κ is the thermal conductivity and

$$\boldsymbol{\Lambda}^{(1)}(\boldsymbol{x},t) = \left[\rho(\boldsymbol{x},t)\nu\left(\boldsymbol{\nabla}^{(1)}\boldsymbol{u}(\boldsymbol{x},t) + \Big(\boldsymbol{\nabla}^{(1)}\boldsymbol{u}(\boldsymbol{x},t)\Big)^T\right)\right].$$

Finally, combining (2.27) and (2.28) leads to the complete evolution equation up to second order

$$\begin{aligned} \frac{\partial}{\partial t}(\rho(\boldsymbol{x},t)E(\boldsymbol{x},t)) + \boldsymbol{\nabla}\cdot(\rho(\boldsymbol{x},t)\boldsymbol{u}(\boldsymbol{x},t)E(\boldsymbol{x},t)) &= \boldsymbol{\nabla}\cdot(\rho(\boldsymbol{x},t)\kappa\boldsymbol{\nabla}E(\boldsymbol{x},t)) \\ &\quad + \boldsymbol{\Lambda}^{(1)}(\boldsymbol{x},t) : \left[\boldsymbol{\nabla}\boldsymbol{u}(\boldsymbol{x},t)^T\right] - p(\boldsymbol{x},t)\boldsymbol{\nabla}\cdot\boldsymbol{u}(\boldsymbol{x},t). \end{aligned} \tag{2.29}$$

The both terms in the second line refer to the viscous heat dissipation and the compression work done by the pressure, respectively. As explained above, we assume these terms are negligible, thus (2.29) reduces to

$$\frac{\partial}{\partial t}(\rho(\boldsymbol{x},t)E(\boldsymbol{x},t)) + \boldsymbol{\nabla}\cdot(\rho(\boldsymbol{x},t)\boldsymbol{u}(\boldsymbol{x},t)E(\boldsymbol{x},t)) = \chi\Delta\left(\rho(\boldsymbol{x},t)E(\boldsymbol{x},t)\right), \tag{2.30}$$

with Laplacian Δ and thermal diffusivity χ. We have treated $\rho(\boldsymbol{x},t)$ as a constant, i.e. assumed again that changes in mass density are negligible. Equation (2.30) is the desired advection-diffusion equation we have already spoken about at the beginning of the current section.

2.3.2. Numerical Scheme

In this subsection, we propose a numerical scheme to simulate the temperature evolution, like in [48, 49]. Like in section 2.3.1 we focus again on the three-dimensional case taking the D3Q19 discretization model explicitly. The method originates in solving

$$\frac{\partial g(\boldsymbol{x},\boldsymbol{v},t)}{\partial t} + \boldsymbol{v}\cdot\boldsymbol{\nabla} g(\boldsymbol{x},\boldsymbol{v},t) = -\frac{1}{\tau_d}\left[g(\boldsymbol{x},\boldsymbol{v},t) - g^{(eq)}(\boldsymbol{x},\boldsymbol{v},t)\right], \tag{2.31}$$

where the equilibrium distribution $g^{(eq)}(\boldsymbol{x},t)$ depends on the macroscopic density and velocity. One possibility to simulate the density and velocity evolution is the lattice BGK method, presented in chapter 1. Hence, we understand the numerical scheme for the temperature evolution as an extension to the lattice BGK method (cf. especially (1.42)) which should be solved simultaneously. For our purpose, approximating the solution of (2.31) numerically demands a discretization of space. Using the same discretization as for the lattice BGK method is a natural choice. We propose to use the method given by [49]

$$g_i(\boldsymbol{x}+\boldsymbol{c}_i\Delta t, t+\Delta t) - g_i(\boldsymbol{x},t) = -\frac{1}{\tau_d}\left[g_i(\boldsymbol{x},t) - g_i^{(eq)}(\boldsymbol{x},t)\right], \quad i=0,\dots,18, \tag{2.32}$$

where the velocities $\boldsymbol{c}_i$ are those of the lattice BGK equation and the equilibrium distribution $g_i^{(eq)}(\boldsymbol{x},t)$ is a discretized approximation of the continuous equilibrium distribution (2.17). The quantities $g_i(\boldsymbol{x},t)$ describe the associated discrete energy distribution which is characterized by

$$\sum_{i=0}^{18} g_i(\boldsymbol{x},t) = \rho(\boldsymbol{x},t)E(\boldsymbol{x},t). \tag{2.33}$$

In the following two paragraphs, we deduce the discrete equilibrium distribution and use a Chapman-Enskog expansion to verify that the method (2.32) recovers the macroscopic equation, (2.30), determined in the previous subsection.

Discrete Energy Equilibrium Distribution

The discrete energy equilibrium distribution is a discretized approximation of the continuous equilibrium distribution (2.17). Observing the calculations in section 2.3.1, we see that only integrations up to first order of the equilibrium distribution were necessary to derive the macroscopic energy equation, i.e. the integrals

$$\int_{\mathbb{R}^3} g^{(eq)}(\boldsymbol{x},\boldsymbol{v},t)\,\mathrm{d}\boldsymbol{v} \quad \text{and} \quad \int_{\mathbb{R}^3} \boldsymbol{v} g^{(eq)}(\boldsymbol{x},\boldsymbol{v},t)\,\mathrm{d}\boldsymbol{v}. \tag{2.34}$$

The discrete equilibrium distribution originates in a Taylor expansion of the continuous distribution in $\boldsymbol{u}$ around zero up to second order, this expansion reads (cf. (1.46))

$$\begin{aligned}
g^{(eq)} &= \frac{1}{2}|\boldsymbol{v}-\boldsymbol{u}|^2 f^{(eq)} \\
&= \frac{Em}{3k_BT}|\boldsymbol{v}-\boldsymbol{u}|^2 f^{(eq)} \\
&= \rho E \left(\frac{m}{2\pi k_B T}\right)^{3/2} \exp\left(\frac{-m}{2k_BT}|\boldsymbol{v}|^2\right) \left[\frac{m|\boldsymbol{v}-\boldsymbol{u}|^2}{3k_BT} \exp\left(\frac{m}{k_BT}(\boldsymbol{v}\cdot\boldsymbol{u}) - \frac{m}{2k_BT}|\boldsymbol{u}|^2\right)\right] \\
&= \rho E \left(\frac{m}{2\pi k_B T}\right)^{3/2} \exp\left(\frac{-m}{2k_BT}|\boldsymbol{v}|^2\right) \\
&\qquad \left[\frac{m|\boldsymbol{v}|^2}{3k_BT} + \left(\frac{m|\boldsymbol{v}|^2}{3k_BT} - \frac{2}{3}\right)\frac{m(\boldsymbol{v}\cdot\boldsymbol{u})}{k_BT} + \left(\frac{m|\boldsymbol{v}|^2}{3k_BT} - \frac{4}{3}\right)\left(\frac{m}{k_BT}\right)^2 \frac{(\boldsymbol{v}\cdot\boldsymbol{u})^2}{2}\right. \\
&\qquad\qquad \left. - \left(\frac{m|\boldsymbol{v}|^2}{3k_BT} - \frac{2}{3}\right)\frac{m}{2k_BT}|\boldsymbol{u}|^2\right] + \mathcal{O}(|\boldsymbol{u}|^3),
\end{aligned}$$

where function arguments were omitted for the sake of clarity. Splitting the terms of the square bracket yields

$$\begin{aligned}
g^{(eq)} &= \rho E \left(\frac{m}{2\pi k_B T}\right)^{3/2} \exp\left(\frac{-m}{2k_BT}|\boldsymbol{v}|^2\right) \\
&\qquad \left[\frac{m|\boldsymbol{v}|^2}{3k_BT} + \left(\frac{m|\boldsymbol{v}|^2}{3k_BT} - \frac{2}{3}\right)\frac{m(\boldsymbol{v}\cdot\boldsymbol{u})}{k_BT} + \left(\frac{m}{k_BT}\right)^2 \frac{(\boldsymbol{v}\cdot\boldsymbol{u})^2}{2} - \frac{m}{2k_BT}|\boldsymbol{u}|^2\right] \\
&\quad + \rho E \left(\frac{m}{2\pi k_B T}\right)^{3/2} \exp\left(\frac{-m}{2k_BT}|\boldsymbol{v}|^2\right) \\
&\qquad \left[\left(\frac{m|\boldsymbol{v}|^2}{3k_BT} - \frac{7}{3}\right)\left(\frac{m}{k_BT}\right)^2 \frac{(\boldsymbol{v}\cdot\boldsymbol{u})^2}{2} - \left(\frac{m|\boldsymbol{v}|^2}{3k_BT} - \frac{5}{3}\right)\frac{m}{2k_BT}|\boldsymbol{u}|^2\right] + \mathcal{O}(|\boldsymbol{u}|^3),
\end{aligned}$$

where then the second addend can be neglected, since the integrals (2.34) are not affected by this term, meaning that

$$\begin{aligned}
\int_{\mathbb{R}^3} \rho E \left(\frac{m}{2\pi k_B T}\right)^{3/2} \exp\left(\frac{-m}{2k_BT}|\boldsymbol{v}|^2\right) \left[\left(\frac{m|\boldsymbol{v}|^2}{3k_BT} - \frac{7}{3}\right)\left(\frac{m}{k_BT}\right)^2 \frac{(\boldsymbol{v}\cdot\boldsymbol{u})^2}{2}\right. \\
\left. - \left(\frac{m|\boldsymbol{v}|^2}{3k_BT} - \frac{5}{3}\right)\frac{m}{2k_BT}|\boldsymbol{u}|^2\right] \mathrm{d}\boldsymbol{v} = 0
\end{aligned}$$

and

$$\int_{\mathbb{R}^3} \boldsymbol{v}\rho E \left(\frac{m}{2\pi k_B T}\right)^{3/2} \exp\left(\frac{-m}{2k_B T}|\boldsymbol{v}|^2\right) \left[\left(\frac{m|\boldsymbol{v}|^2}{3k_B T} - \frac{7}{3}\right)\left(\frac{m}{k_B T}\right)^2 \frac{(\boldsymbol{v}\cdot\boldsymbol{u})^2}{2} - \left(\frac{m|\boldsymbol{v}|^2}{3k_B T} - \frac{5}{3}\right)\frac{m}{2k_B T}|\boldsymbol{u}|^2\right] \mathrm{d}\boldsymbol{v} = 0.$$

We are looking for a discrete equilibrium distribution, and since the remaining term is of similar shape as the density equilibrium distribution (1.46), we use the same ansatz function for the discrete energy equilibrium distribution. This means, we try to determine coefficients A_i, B_i, C_i and D_i in

$$g_i^{(eq)}(\boldsymbol{x},t) = \omega_i \rho(\boldsymbol{x},t) E(\boldsymbol{x},t) \left[A_i + B_i(\boldsymbol{c}_i\cdot\boldsymbol{u}(\boldsymbol{x},t)) + C_i(\boldsymbol{c}_i\cdot\boldsymbol{u}(\boldsymbol{x},t))^2 + D_i|\boldsymbol{u}(\boldsymbol{x},t)|^2\right], \tag{2.35}$$

for $i = 0,\dots,18$, such that the discrete energy equilibrium satisfies

$$\sum_{i=0}^{18} g_i^{(eq)}(\boldsymbol{x},t) = \rho(\boldsymbol{x},t)E(\boldsymbol{x},t). \tag{2.36}$$

In (2.35), the appearing weights ω_i are given by (1.56) and lattice velocities are given by (1.48). We can avoid a direct computation of the coefficients A_i, B_i, C_i and D_i which would be similar to the computation in subsection 1.5.4. Namely, by comparison of (1.46) and (1.55) we conclude that it holds $\frac{m}{k_B T} = 3$, hence we try to use

$$g_i^{(eq)}(\boldsymbol{x},t) = \omega_i \rho(\boldsymbol{x},t) E(\boldsymbol{x},t) \left[|\boldsymbol{c}_i|^2 + \left(|\boldsymbol{c}_i|^2 - \frac{2}{3}\right) 3(\boldsymbol{c}_i\cdot\boldsymbol{u}(\boldsymbol{x},t)) + \frac{9}{2}(\boldsymbol{c}_i\cdot\boldsymbol{u}(\boldsymbol{x},t))^2 - \frac{3}{2}|\boldsymbol{u}(\boldsymbol{x},t)|^2\right],$$

which leads by considering the lattice velocities (1.48) for D3Q19 to

$$\begin{aligned}
g_0^{(eq)}(\boldsymbol{x},t) &= \frac{1}{3}\rho(\boldsymbol{x},t)E(\boldsymbol{x},t) \left[-\frac{3}{2}|\boldsymbol{u}(\boldsymbol{x},t)|^2\right] = -\frac{1}{2}\rho(\boldsymbol{x},t)E(\boldsymbol{x},t)|\boldsymbol{u}(\boldsymbol{x},t)|^2,\\
g_j^{(eq)}(\boldsymbol{x},t) &= \frac{1}{18}\rho(\boldsymbol{x},t)E(\boldsymbol{x},t) \left[1 + (\boldsymbol{c}_j\cdot\boldsymbol{u}(\boldsymbol{x},t)) + \frac{9}{2}(\boldsymbol{c}_j\cdot\boldsymbol{u}(\boldsymbol{x},t))^2 - \frac{3}{2}|\boldsymbol{u}(\boldsymbol{x},t)|^2\right],\\
g_k^{(eq)}(\boldsymbol{x},t) &= \frac{1}{36}\rho(\boldsymbol{x},t)E(\boldsymbol{x},t) \left[2 + 4(\boldsymbol{c}_k\cdot\boldsymbol{u}(\boldsymbol{x},t)) + \frac{9}{2}(\boldsymbol{c}_k\cdot\boldsymbol{u}(\boldsymbol{x},t))^2 - \frac{3}{2}|\boldsymbol{u}(\boldsymbol{x},t)|^2\right],
\end{aligned} \tag{2.37}$$

for $j = 1, \dots, 6$ and $k = 7, \dots, 18$. Summing up verifies that (2.36) is fulfilled and moreover it also holds

$$\sum_{i=0}^{18} \boldsymbol{c}_i g_i^{(eq)}(\boldsymbol{x}, t) = \rho(\boldsymbol{x}, t)\boldsymbol{u}(\boldsymbol{x}, t)E(\boldsymbol{x}, t). \tag{2.38}$$

Hence, the numerical scheme (2.32) is now well defined, in the subsequent paragraph we show that it is also meaningful.

Verification of Macroscopic Equation

Like in section 1.6, a Chapman-Enskog expansion can be used here to recover the advection-diffusion equation, and therefore to prove that the proposed method is meaningful from a physical point of view. Most of the calculations within this verification are analogue to those of section 1.6. In order to understand the procedure in the current paragraph well, we recommend the reader to recapitulate the calculations of section 1.6.

We begin the procedure in the same way as we did when recovering the Navier-Stokes equations in the previous chapter. This means we employ a Taylor expansion of (2.32), leading to (cf. (1.58))

$$\hat{\varepsilon}\left(\frac{\partial}{\partial t} + \boldsymbol{c}_i \cdot \boldsymbol{\nabla}\right) g_i(\boldsymbol{x}, t) + \frac{1}{2}\hat{\varepsilon}^2\left(\frac{\partial}{\partial t} + \boldsymbol{c}_i \cdot \boldsymbol{\nabla}\right)^2 g_i(\boldsymbol{x}, t) = -\frac{1}{\tau_d}\left[g_i(\boldsymbol{x}, t) - g_i^{(eq)}(\boldsymbol{x}, t)\right], \tag{2.39}$$

where $\Delta t = \hat{\varepsilon}$ was replaced by a parameter $\hat{\varepsilon}$, similar to the computation leading to (1.58). The energy distribution is expanded as

$$g_i(\boldsymbol{x}, t) = g_i^{(0)}(\boldsymbol{x}, t) + \hat{\varepsilon} g_i^{(1)}(\boldsymbol{x}, t) + \hat{\varepsilon}^2 g_i^{(2)}(\boldsymbol{x}, t) + \mathcal{O}(\hat{\varepsilon}^3), \tag{2.40}$$

where $g_i^{(0)}(\boldsymbol{x}, t)$ denotes the equilibrium distribution $g_i^{(eq)}(\boldsymbol{x}, t)$. Furthermore, we use the expanded time differential operator (cf. (1.62))

$$\frac{\partial}{\partial \hat{t}} = \frac{\partial^{(1)}}{\partial \hat{t}} + \hat{\varepsilon}\frac{\partial^{(2)}}{\partial \hat{t}} + \mathcal{O}(\hat{\varepsilon}^2)$$

and the scaled spatial differential operator (1.63)

$$\boldsymbol{\nabla} = \boldsymbol{\nabla}^{(1)}.$$

By substituting these three expansions into (2.39), we can deduce the first and second

order expansion, respectively. They are given analogue to (1.64) and (1.66) by

$$\left(\frac{\partial^{(1)}}{\partial t} + \boldsymbol{c}_i \cdot \boldsymbol{\nabla}^{(1)}\right) g_i^{(0)}(\boldsymbol{x}, t) = -\frac{1}{\tau_d} g_i^{(1)}(\boldsymbol{x}, t), \tag{2.41}$$

and

$$\left[\left(1 - \frac{1}{2\tau_d}\right)\left(\frac{\partial^{(1)}}{\partial t} + \boldsymbol{c}_i \cdot \boldsymbol{\nabla}^{(1)}\right) g_i^{(1)}(\boldsymbol{x}, t) + \frac{\partial^{(2)}}{\partial t} g_i^{(0)}(\boldsymbol{x}, t)\right] = -\frac{1}{\tau_d} g_i^{(2)}(\boldsymbol{x}, t), \tag{2.42}$$

respectively. Due to (2.36) and (2.38), summation of (2.41) over all $i = 0, \ldots, 18$ yields the first order approximation

$$\frac{\partial^{(1)}}{\partial t}\left(\rho(\boldsymbol{x}, t) E(\boldsymbol{x}, t)\right) + \boldsymbol{\nabla}^{(1)} \cdot \left(\rho(\boldsymbol{x}, t) \boldsymbol{u}(\boldsymbol{x}, t) E(\boldsymbol{x}, t)\right) = 0, \tag{2.43}$$

where we assume (cf. (1.61))

$$\sum_{i=0}^{18} g_i^{(1)}(\boldsymbol{x}, t) = \sum_{i=0}^{18} g_i^{(2)}(\boldsymbol{x}, t) = 0. \tag{2.44}$$

The corresponding second order approximation is obtained by taking summation of (2.42), thus we obtain

$$\frac{\partial^{(2)}}{\partial t}\left(\rho(\boldsymbol{x}, t) E(\boldsymbol{x}, t)\right) + \left(1 - \frac{1}{2\tau_d}\right) \Pi^{(2)}(\boldsymbol{x}, t) = 0, \tag{2.45}$$

with

$$\Pi^{(2)}(\boldsymbol{x}, t) = \sum_{i=0}^{18} \left(\frac{\partial^{(1)}}{\partial t} + \boldsymbol{c}_i \cdot \boldsymbol{\nabla}^{(1)}\right) g_i^{(1)}(\boldsymbol{x}, t).$$

A further investigation of $\Pi^{(2)}(\boldsymbol{x}, t)$ is necessary for our purpose. The authors of [49] state, that one can obtain

$$\Pi^{(2)}(\boldsymbol{x}, t) = -\frac{5}{9} \tau_d \Delta^{(2)}\left(\rho(\boldsymbol{x}, t) E(\boldsymbol{x}, t)\right), \tag{2.46}$$

after neglecting some appropriate terms, where $\Delta^{(2)} = \Delta$ is a scaled Laplace operator. Using this equation we rewrite (2.45) as

$$\frac{\partial^{(2)}}{\partial t}\left(\rho(\boldsymbol{x}, t) E(\boldsymbol{x}, t)\right) = \frac{5}{9}\left(\tau_d - \frac{1}{2}\right) \Delta^{(2)}\left(\rho(\boldsymbol{x}, t) E(\boldsymbol{x}, t)\right).$$

The latter equation combined with (2.43) gives the Chapman-Enskog approximation up

to second order which reads

$$\frac{\partial}{\partial t}\left(\rho(\boldsymbol{x},t)E(\boldsymbol{x},t)\right)+\boldsymbol{\nabla}\cdot\left(\rho(\boldsymbol{x},t)\boldsymbol{u}(\boldsymbol{x},t)E(\boldsymbol{x},t)\right)=\chi\Delta\left(\rho(\boldsymbol{x},t)E(\boldsymbol{x},t)\right),$$

with $\chi=\frac{5}{9}\left(\tau_d-\frac{1}{2}\right)$ being the coefficient of thermal diffusivity. The latter equation matches with the desired advection-diffusion equation (2.30). Note that an idea of the derivation of equation (2.46) is given in appendix A.4.

In the preceding calculations we have shown that the numerical method given by (2.32) can be used to simulate the evolution of the energy $E(\boldsymbol{x},t)$ which diffuses and is advected by the fluid flow. The rate of diffusion can be tuned by the relaxation parameter τ_d. The energy is related to the temperature $T(\boldsymbol{x},t)$ by $E(\boldsymbol{x},t)=\frac{3}{2}\frac{k_BT(\boldsymbol{x},t)}{m}$ in $\mathbb{R}^3$. All in all, we are capable to simulate the evolution of the temperature.

2.4. Buoyancy Effects

It is well known that warmer air rises which for instance enables a hot-air balloon to fly. This phenomenon results from the fact that warmer air has a lower mass density than colder one and in addition with gravity this leads to an effective force directed upwards. In the last section, we have developed a model simulating the temperature evolution. The temperature in this model is advected by the fluid and diffuses in it. Therefore, the temperature evolution is directly influenced by the fluid flow, but the other way round, we do not consider the fact that temperature, or more precisely temperature difference, affects the motion of the fluid, yet. In the current section, we describe fluid flows involving buoyancy effects due to temperature differences on the macroscopic scale and demonstrate how one can simulate them easily with lattice Boltzmann methods.

2.4.1. Adjustment of the Macroscopic Equation

In the current subsection we describe fluid flows involving buoyancy effects due to temperature differences on the macroscopic scale. We focus on the second equation of (2.11), the momentum equation, in the following [16, 50]. If the occurring force term results from gravity, then the momentum equation can be written as follows

$$\frac{\partial\vec{u}}{\partial t}+\left(\vec{u}\cdot\vec{\nabla}\right)\vec{u}=-\vec{\nabla}\hat{p}+\hat{\nu}\Delta\vec{u}+\vec{g}, \tag{2.47}$$

where $\vec{g}$ is the vector of acceleration due to gravity. Multiplying (2.47) with mass density ρ yields

$$\rho\frac{\partial\vec{u}}{\partial t}+\rho\left(\vec{u}\cdot\vec{\nabla}\right)\vec{u}=-\vec{\nabla}p+\mu\Delta\vec{u}+\rho\vec{g}, \tag{2.48}$$

where μ is the dynamic viscosity. Inspecting this equation if the fluid is in a stationary equilibrium without any motion or at least with a homogeneous velocity, it reduces to

$$\vec{\nabla} p_e = \rho_e \vec{g} \quad \Leftrightarrow \quad 0 = -\vec{\nabla} p_e + \rho_e \vec{g}, \tag{2.49}$$

where p_e and ρ_e are the pressure and density in that equilibrium state, respectively. We can write the pressure as

$$p = p_e + p_m, \tag{2.50}$$

with an appropriate p_m. Actually, the incompressible Navier-Stokes equations (2.11), especially (2.48), are satisfied only by fluids with a constant density, nevertheless if present density variations are small and therefore negligible we also can take these equations. Hence, we may assume that the density can be written in the form

$$\rho = \rho_e + \rho_m, \tag{2.51}$$

with an appropriate $\rho_m \ll 1$. By inserting (2.50) and (2.51) into (2.48) and adding (2.49), one obtains

$$(\rho_e + \rho_m) \frac{\partial \vec{u}}{\partial t} + (\rho_e + \rho_m) \left(\vec{u} \cdot \vec{\nabla} \right) \vec{u} = -\vec{\nabla} p_m + \mu \Delta \vec{u} + \rho_m \vec{g}. \tag{2.52}$$

The approach presented in the current section uses the Boussinesq approximation which is based on the assumption that in the governing macroscopic equations variations in mass density and temperature are negligible everywhere except in the term describing the gravitational force [14]. This means $\rho_m = 0$, and thus $\rho_e = \rho$ is used except in the latter term, where the density is assumed to depend exclusively on the temperature but only in the sense of a first order truncated Taylor series expansion. This linear relation is expressed by

$$\rho = \rho_e \left(1 - \beta (T - T_e)\right), \tag{2.53}$$

with β the coefficient of thermal expansion and T_e the temperature measured in stationary equilibrium. The Boussinesq approximation simplifies (2.52) into

$$\rho \frac{\partial \vec{u}}{\partial t} + \rho \left(\vec{u} \cdot \vec{\nabla} \right) \vec{u} = -\vec{\nabla} p_m + \mu \Delta \vec{u} + \rho_m \vec{g}. \tag{2.54}$$

The assumption of linear relation (2.53) implies

$$\underbrace{\rho - \rho_e}_{=\rho_m} = -\rho_e \beta (T - T_e) \approx -\rho \beta (T - T_e),$$

since $\rho_e \approx \rho$. ρ_m in (2.54) can be substituted by the approximation $-\rho\beta(T - T_e)$. Doing so and after dividing by ρ, we achieve

$$\frac{\partial \vec{u}}{\partial t} + \left(\vec{u} \cdot \vec{\nabla}\right) \vec{u} = -\vec{\nabla}\hat{p}_m + \hat{\nu}\Delta\vec{u} - \beta(T - T_e)\vec{g}, \tag{2.55}$$

with $\hat{p}_m = \frac{p_m}{\rho}$ and $\hat{\nu} = \frac{\mu}{\rho}$ as in (1.81).
Eventually, on the macroscopic scale the buoyancy term is fully described as an additional force depending on the temperature difference. We remark that the pressure gradient was altered and distinguishes from the one in (2.11).

2.4.2. Realization in LBM

In this subsection, we show how the buoyancy term described in the preceding subsection can be considered in lattice Boltzmann methods. On the one hand, we have a description of the buoyancy term on the macroscopic scale. On the other hand, we have seen in section 2.2 how force terms can be incorporated in lattice Boltzmann methods. Both facts can be combined to realize an incorporation to the numerical method. As remarked at the end of the previous subsection, equations (2.11) and (2.55) differ also in the pressure gradient, hence the task is to bring both sides in line.

We begin this task with an investigation of the pressure gradient in (2.55) multiplied by ρ. With use of (2.49) and (2.50), it follows

$$-\vec{\nabla}\left(\rho\hat{p}_m\right) = -\vec{\nabla}p_m = -\vec{\nabla}\left(p - p_e\right) = -\vec{\nabla}p + \rho_e\vec{g}.$$

Hence, (2.55) is equivalent to

$$\frac{\partial \vec{u}}{\partial t} + \left(\vec{u} \cdot \vec{\nabla}\right) \vec{u} = -\vec{\nabla}\hat{p} + \hat{\nu}\Delta\vec{u} + \left(\frac{\rho_e}{\rho} - \beta(T - T_e)\right)\vec{g}, \tag{2.56}$$

and a reasonable approximation reads

$$\frac{\partial \vec{u}}{\partial t} + \left(\vec{u} \cdot \vec{\nabla}\right) \vec{u} = -\vec{\nabla}\hat{p} + \hat{\nu}\Delta\vec{u} + \left(1 - \beta(T - T_e)\right)\vec{g}, \tag{2.57}$$

since $\frac{\rho_e}{\rho}$ is close to 1.
Equation (2.56) can also be achieved directly by substituting (2.53) into the last term in (2.48). Then, the approximation (2.57) is obtained out of of (2.56) by the same step which besides is consistent with the calculation in the derivation of the incompressible Navier-Stokes equations in the preceding chapter. There, we also assumed that variations of mass density are negligible.

Finally, the governing equation respecting the buoyancy effect (2.57) is in line with (2.11). Choosing $\vec{k} = \left(1 - \beta(T - T_e)\right)\vec{g}$ and using the modified model presented in section 2.2, we can incorporate buoyancy effects due to temperature differences in lattice Boltzmann methods.

CHAPTER 3

Numerical Tests for Enhanced Lattice Boltzmann

In the preceding two chapters we have developed the lattice Boltzmann method and some useful enhancements to it. The current chapter deals with the practical issue of the developed numerical method, meaning the application of it. The considerations in the last two chapters were kept general in such a way that the lattice Boltzmann method was not constructed for a given physical problem. Certainly, this limits the application to less sophisticated problems.

If we take only the main concept of the lattice Boltzmann method into account together with appropriate boundary conditions, we are able to simulate Poiseuille flow (e.g. [4, 60]) through a channel. Despite we dedicated our calculations more to the three-dimensional case, we simulate Poiseuille flow in each two and three dimensions below. This shows the models capability to handle free fluid flows. Inserting obstacles into the channel, we can also demonstrate the capability to simulate flow past an obstacle. Both simulations are done in section 3.1. Taking not only the main concept and boundary conditions into account but also the second numerical scheme, we can simulate a temperature evolution in a given domain. In the absence of a temperature influenced flow, i.e. without considering buoyancy effects, we can initialize the flow in an equilibrium state without any motion, then the temperature only diffuses in the fluid. The resulting process is mathematically described by the heat equation. This simulation and its results are given in section 3.2. Moreover, we simulate Rayleigh-Bénard convection (e.g. [17, 21]) in the same section.

3.1. Channel Flow

In the current subsection, we consider flows through a channel in two dimensions as well as three dimensions. Figure 3.1 illustrates the channels and the arrows show the direction of flow. On the open sides of the channel we impose boundary conditions which drive the fluid through the channel. In detail, we use Zou and He pressure boundary conditions [72] for both ends of the channel. Prescribing two different pressures yields a pressure gradient driving the fluid. Thus, we obtain an inflow at the open side with higher pressure and an outflow at the other side. The pressure gradient is equivalent to an external body force acting on the fluid. Hence, the simulation is equivalent to a simulation

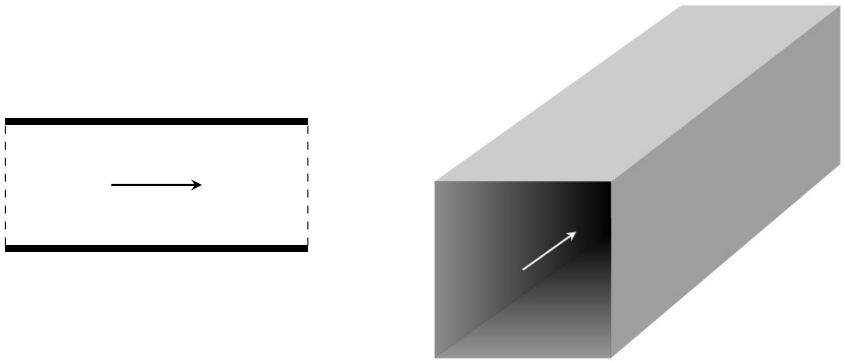

Figure 3.1.: Two- and three-dimensional channels. Arrows show the direction of flow and dashed lines illustrate the open sides of the channel.

with periodic boundary conditions and an appropriate force term. Although, in our opinion, the implementation with pressure boundary conditions is more sophisticated, we implement both possibilities. Thus, we emphasize the capability to simulate external forces correctly and demonstrate that also pressure boundary conditions work fine. For the channel walls a bounceback boundary condition is used.
The two dimensional simulation is based on the D2Q9 model, where the equilibrium distribution reads

$$F_0^{(eq)}(\hat{\boldsymbol{x}},\hat{t}) = \omega_0\hat{\rho}(\hat{\boldsymbol{x}},\hat{t})\left[1-\frac{3}{2}|\hat{\boldsymbol{u}}(\hat{\boldsymbol{x}},\hat{t})|^2\right]$$
$$F_i^{(eq)}(\hat{\boldsymbol{x}},\hat{t}) = \omega_i\hat{\rho}(\hat{\boldsymbol{x}},\hat{t})\left[1+3(\boldsymbol{c}_i\cdot\hat{\boldsymbol{u}}(\hat{\boldsymbol{x}},\hat{t}))+\frac{9}{2}(\boldsymbol{c}_i\cdot\hat{\boldsymbol{u}}(\hat{\boldsymbol{x}},\hat{t}))^2-\frac{3}{2}|\hat{\boldsymbol{u}}(\hat{\boldsymbol{x}},\hat{t})|^2\right],$$

with

$$\omega_i = \begin{cases} \frac{4}{9}, & i=0 \\ \frac{1}{9}, & i=1,\dots,4 \\ \frac{1}{36}, & i=5,\dots,8 \end{cases}$$

and lattice velocities

$$\begin{aligned} &\boldsymbol{c}_0=(0,0), \\ &\boldsymbol{c}_1=(1,0), && \boldsymbol{c}_2=(0,1), && \boldsymbol{c}_3=(-1,0), && \boldsymbol{c}_4=(0,-1), \\ &\boldsymbol{c}_5=(1,1), && \boldsymbol{c}_6=(-1,1), && \boldsymbol{c}_7=(-1,-1), && \boldsymbol{c}_8=(1,-1). \end{aligned}$$

For the three dimensional simulation, we use the D3Q19 model. The lattice velocities are given in (1.48) and the corresponding equilibrium distribution reads as above but

with different weights

$$\omega_i = \begin{cases} \frac{1}{3}, & i = 0 \\ \frac{1}{18}, & i = 1, \ldots, 6 \\ \frac{1}{36}, & i = 7, \ldots, 18 \end{cases} .$$

The kinematic viscosity is computed by $\nu = \frac{2\hat{\tau}_c - 1}{6}$ in both models.

3.1.1. Poiseuille Flow

The Poiseuille flow, also known as Hagen-Poiseuille flow, is a steady state flow in a long, straight channel, where the fluid is pressure-driven. In our simulations the channel is parallel to the x^1-axis and has an unchanged cross section along the x^1-axis. The cross section is a line segment in two dimensions and a rectangle in three dimensions, compare also with figure 3.1.

Analytical Solution

The Poiseuille flow is one of only few situations where an analytical solution of the Navier-Stokes equations is known [61]. We consider a two-dimensional channel of width $2L$ and flow in x^1-direction. The velocity component in direction tangential to the main flow direction is zero and the velocity component in main flow direction depends only on the position, meaning the distance to the walls, i.e.

$$\vec{u}(\vec{x}, t) = \begin{pmatrix} u^1(\vec{x}, t) \\ u^2(\vec{x}, t) \end{pmatrix} = \begin{pmatrix} u^1(x^2) \\ 0 \end{pmatrix} . \tag{3.1}$$

The complete Navier-Stokes equations (1.81) reduce to

$$0 = \nu \Delta \vec{u}(\vec{x}, t) - \vec{\nabla} \tilde{p}(\vec{x}, t)$$

and the divergence equation of (1.81) vanishes, since it is automatically fulfilled by (3.1). In general a pressure gradient is equivalent to a force density, in the present case we obtain

$$-\vec{\nabla} \tilde{p}(\vec{x}, t) = \vec{k}, \tag{3.2}$$

with $\vec{k}$ being the acceleration corresponding to the force. Note, $\tilde{p}$ is the pressure divided by the mass density ρ_0 which is assumed constant in the incompressible Navier-Stokes equations. The solution of the Poiseuille flow then reads [4, 61]

$$\vec{u}(\vec{x}, t) = \frac{L^2 - (x^2)^2}{2\nu} \vec{k}, \tag{3.3}$$

where ν denotes the kinematic viscosity and the second space component $x^2 = 0$ is assumed to be in center of the channel's cross section. The walls are located at $x^2 = -L$ and $x^2 = L$, respectively, thus the velocity profile in flow direction is a parabola with zero velocity on the boundaries. Note that the second component of $\vec{k}$, tangential to main flow direction, is zero, thus same for the velocity component in this direction.

2D Simulation

The two-dimensional simulation of Poiseuille flow is done on a lattice with $n_{x^1} = 151$ lattice points in x^1-direction and $n_{x^2} = 32$ in x^2-direction. The first, $x^2 = 1$, and last row, $x^2 = 32$, are bounceback lattice points and the effective boundaries lie half way between the bounceback lattice points and the first interior lattice points. Hence, the walls are located at $x^2 = 1 + \frac{1}{2}$ and $x^2 = 32 - \frac{1}{2}$. It follows a channel width of $L = 15$. On the left opening, the inlet at $x^1 = 1$, we impose a pressure boundary condition prescribing a constant density of $\rho_{in} = 1.03$ where the according pressure-density relation reads $p = \frac{1}{3}\rho$. The outflow boundary condition prescribes a density of $\rho_{out} = 1$ at lattice points with $x^1 = n_{x^1}$. All other lattice points are initialized with zero velocity and constant density $\rho = 1$. The pressure gradient reads

$$\boldsymbol{\nabla} p(\boldsymbol{x}, t) = \begin{pmatrix} \frac{1}{3}\frac{\rho_{out} - \rho_{in}}{n_{x^1} - 1} \\ 0 \end{pmatrix} = \begin{pmatrix} -\frac{1}{15000} \\ 0 \end{pmatrix},$$

which implies, by (3.2), an acceleration of

$$\boldsymbol{k} = -\frac{1}{\rho_0}\boldsymbol{\nabla} p(\boldsymbol{x}, t) = -\frac{1}{1.015}\begin{pmatrix} -\frac{1}{15000} \\ 0 \end{pmatrix} = \begin{pmatrix} \frac{1}{15225} \\ 0 \end{pmatrix}, \tag{3.4}$$

where the average density was used for ρ_0. Furthermore, in the simulation a relaxation parameter $\hat{\tau}_c = 0.9$ is used which implies a kinematic viscosity of $\nu = \frac{2}{15}$.

Both, the analytical solution and the result of the lattice Boltzmann simulation are shown in figure 3.2. The numerically computed velocities match very well with the analytical solution. The sole exception is near the walls, but note that the effective channel walls lie half way between the bounceback lattice points and the first row of interior lattice points. The first and last marker in the figures corresponds to bounceback lattice points which lie outside of the effective domain, and therefore a velocity given in these points is actually meaningless. Nevertheless, using the velocity in the bounceback lattice point to compute the velocity on the boundary by linear interpolation, the zero velocity at the walls is not obtained by the lattice Boltzmann simulation.

In figure 3.3 the results of the lattice Boltzmann simulation with periodic boundary conditions and a body force according to (3.4) is shown. Not striking, the two velocity profiles in figures 3.2 and 3.3 are equal. The difference between the two simulations becomes visible when inspecting the mass density field. When pressure boundary conditions are applied, the more one approaches to the outflow the lower gets the density, as

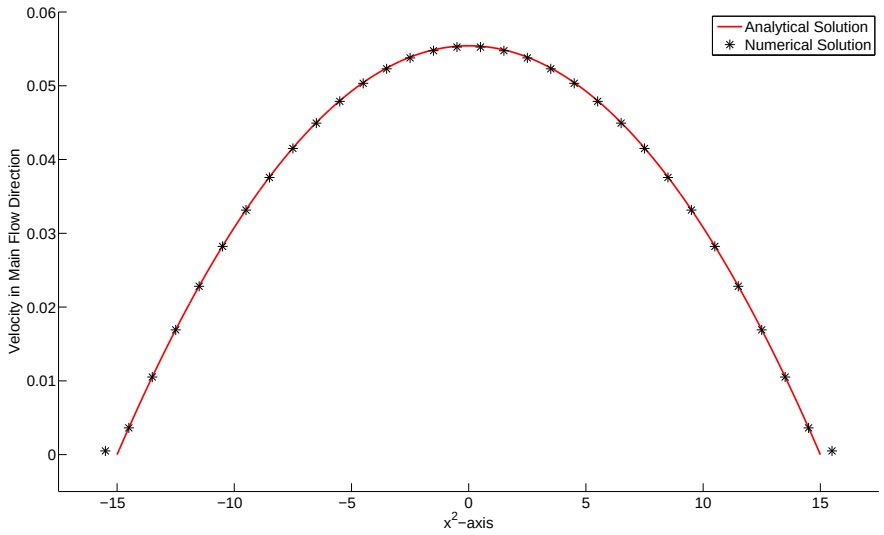

Figure 3.2.: Velocity profile in a two-dimensional Poiseuille flow simulation with pressure boundary conditions.

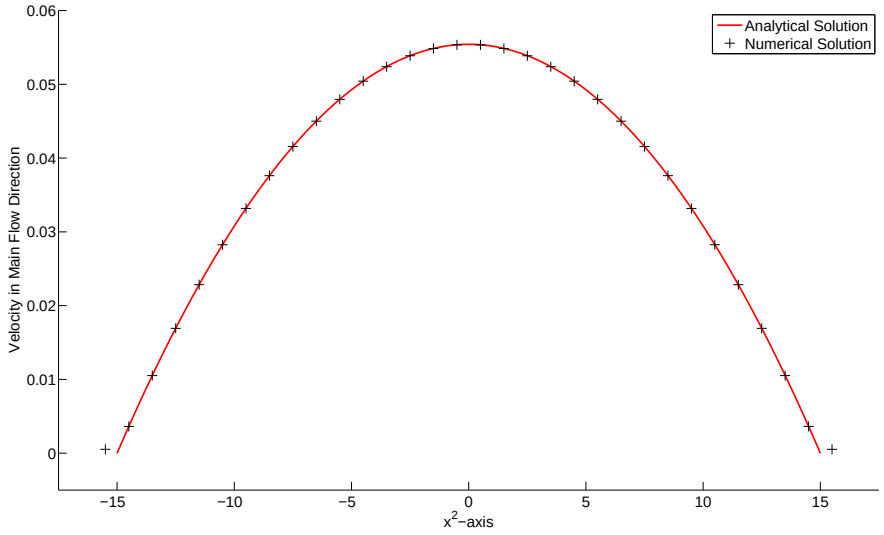

Figure 3.3.: Velocity profile in a two-dimensional Poiseuille flow simulation with periodic boundary conditions and a force acting on the fluid.

shown in figure 3.4. This is an immediate consequence from the fact that the pressure in lattice Boltzmann methods is proportional to the density. In the simulation with periodic boundary conditions and an additional force, the density is equally constant $\rho = 1$. The assumption of a constant density which, as shown in chapter 1, led to the Navier-Stokes equations is therefore only satisfied in the simulation with periodic boundary conditions. For this reason, we prefer the realization with periodic boundary conditions and an acting body force driving the fluid.

3D Simulation

For the three-dimensional Poiseuille flow in a channel with square cross section, as shown in figure 3.1, there is no analytical solution known [4]. Testing the D3Q19 lattice Boltzmann method, we expand the simulation of the previous paragraph to three dimensions. Hence, we have 151 lattice points in x^1-direction and each 32 lattice points in x^2- and x^3-direction. The relaxation parameter is kept at $\hat{\tau}_c = 0.9$, thus the kinematic viscosity is $\nu = \frac{2}{15}$. At the channel inflow a Zou and He pressure boundary condition is applied. Like in the two-dimensional simulation, we prescribe a density of $\rho_{in} = 1.03$. The outflow boundary condition is of same kind as the inflow, but it prescribes a density of $\rho_{out} = 1$. The pressure-density relation in D3Q19 is $p = \frac{1}{3}\rho$, see also (1.57).
In figures 3.5, 3.6 and 3.7 the velocity profile of the simulation is presented. From the simulation we get the velocity profile in discrete points, the surface given in figure 3.5 is obtained by linear interpolation. We observe the highest velocity in the center of the channel, however this was expected from the results of the two-dimensional investiga-

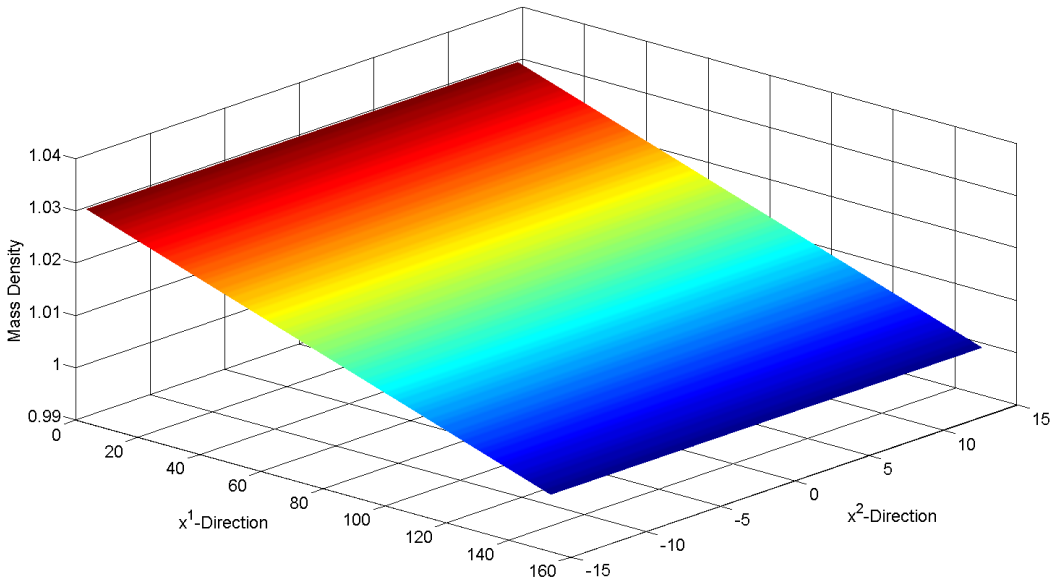

Figure 3.4.: Density field in a two-dimensional Poiseuille flow with pressure boundary conditions.

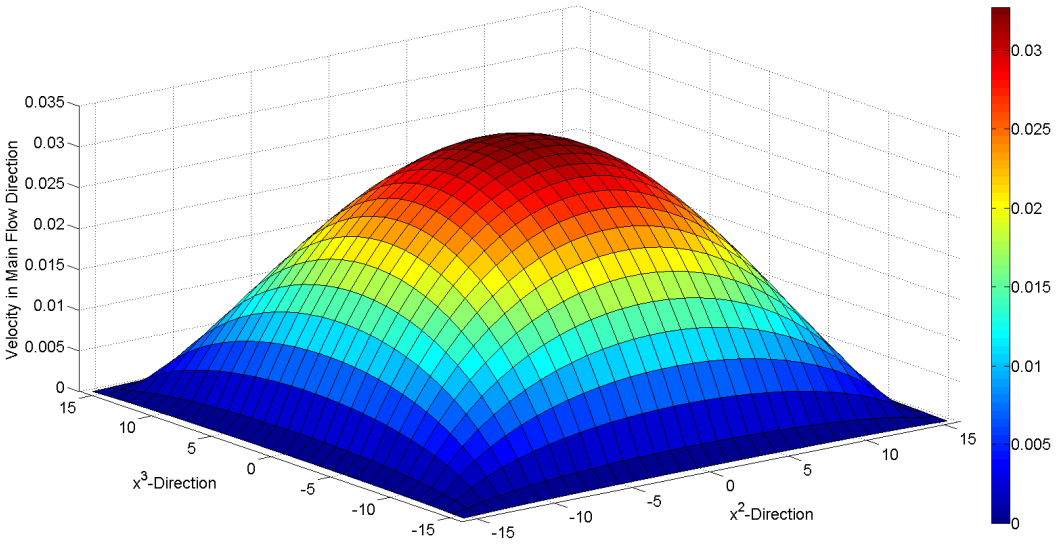

Figure 3.5.: Velocity profile in a three-dimensional Poiseuille flow simulation with pressure boundary conditions.

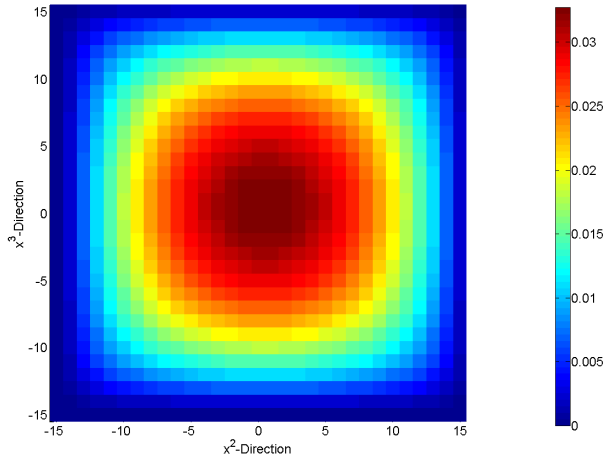

Figure 3.6.: Velocity profile in a three-dimensional Poiseuille flow simulation with pressure boundary conditions. View from top of the graph in figure 3.5.

tion and from physical reasoning. The velocity profile reflects the result of the two-dimensional case, cutting the profile along lines parallel to the x^2- or x^3-axis the cut-out is a parabola with the properties of the two-dimensional velocity profile, see figure 3.8 and compare the structure with figure 3.2. Due to friction at walls the velocity on the wall should be equal to zero, like in two dimensions. The simulation above had a square cross section. Additionally, we simulate a Poiseuille flow in a channel with an oblong cross section. The parameters are 60 lattice points in x^1-direction, 16 in x^2-direction and 26 in x^3-direction. The chosen relaxation parameter is $\hat{\tau}_c = 1.1$ and boundary conditions as given above. Figure 3.9 shows a contour plot of the resulting velocity profile.

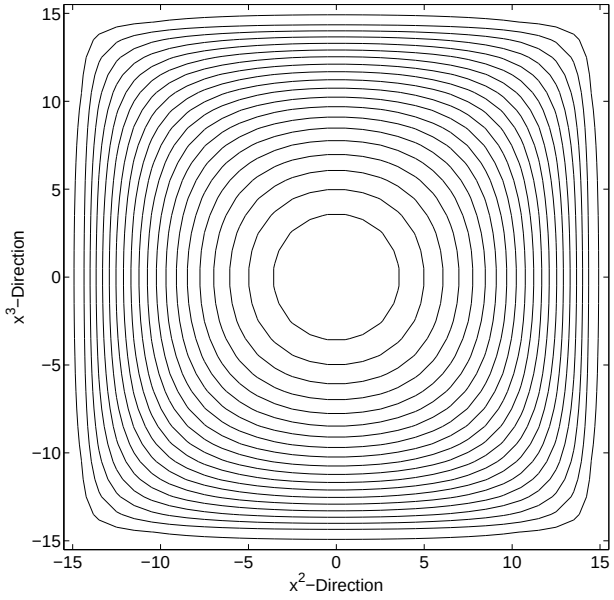

Figure 3.7.: Contour plot of velocity profile in a three-dimensional Poiseuille flow simulation with pressure boundary conditions.

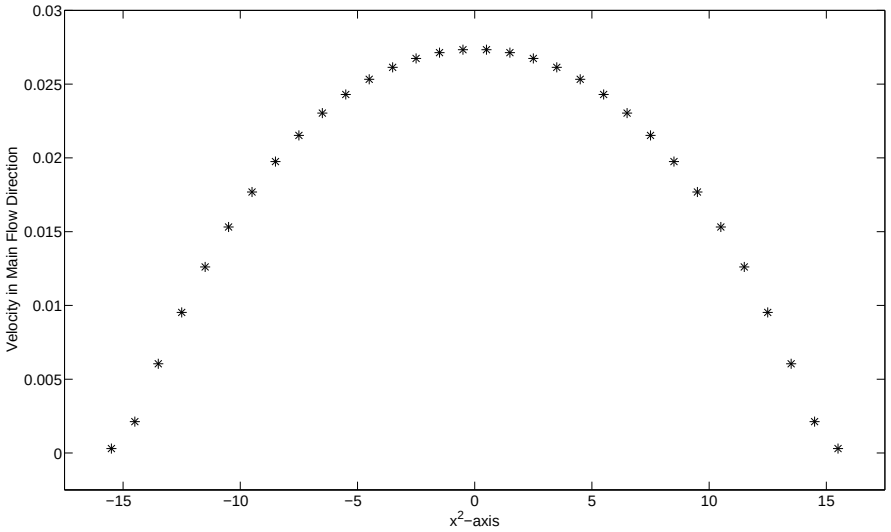

Figure 3.8.: Cut-out of the velocity profile given in preceding figures along the tenth row which corresponds to the line with $x^3 = 6.5$.

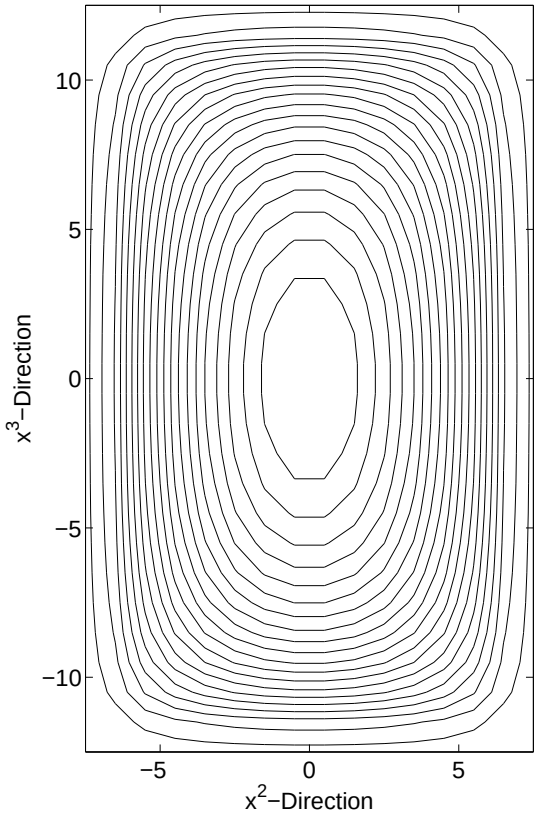

Figure 3.9.: Contour plot of the velocity profile of a three-dimensional Poiseuille flow in a channel with oblong cross section.

3.1.2. Flow Past an Obstacle

Considering channels in the shape of those illustrated in figure 3.1, we have seen in the previous subsection how fluids flow through them. In the current subsection, we add solid obstacles in the center of the channel. In detail we add a rectangular obstacle in the two-dimensional channel, see also figure 3.10. Analogue, we add a cuboid in the center of the three-dimensional channel.
In the simulation, the obstacles consists of bounceback lattice points, like the channel

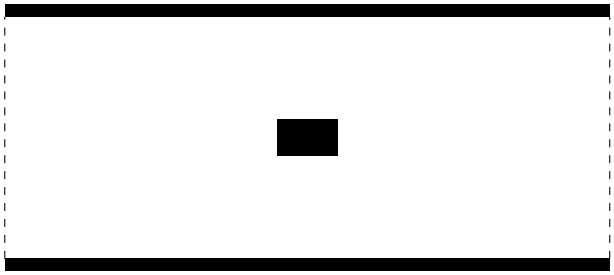

Figure 3.10.: Obstacle in a channel.

walls. In order to achieve a flow past the obstacle we again use a pressure driven flow realized by Zou and He pressure boundary conditions. A flow through a two-dimensional channel with 151 lattice points in x^1-direction and 32 in x^2-direction is simulated where an obstacle of 7 (in x^1-direction) times 4 (in x^2-direction) lattice points is inserted in the middle of the channel. Pressure boundary conditions like in the two-dimensional Poiseuille flow above are applied. The flow is illustrated with help of streamlines in figure 3.11 and the modulus of the velocity is presented in figure 3.12. In the latter we can see that the velocity increases when passing the obstacle. We also use this kind of visualizing the velocity to illustrate the three-dimensional flow past an obstacle.
The flow we simulated consists of a channel with 101x32x32 lattice points in x^1-, x^2- and x^3-direction, respectively. The measurements of the centrally inserted cuboid are 7x4x4, and the relaxation parameter is $\hat{\tau}_c = 1$. We use same pressure boundary conditions as for the Poiseuille flow above. The intuitive behavior of the fluid, passing the obstacle analogue to the two-dimensional simulation, can be observed in the lattice Boltzmann simulation. For sake of simplicity, we only illustrate the simulated flow with help of a velocity visualization. The graphic is given in figure 3.13. Comparing it with the two-dimensional flow of figure 3.13 underlines a generalized behavior which at least is intuitively correct.
Further study of flows past an obstacle can be found, for instance, in articles [2, 67] dealing with that topic in-depth.

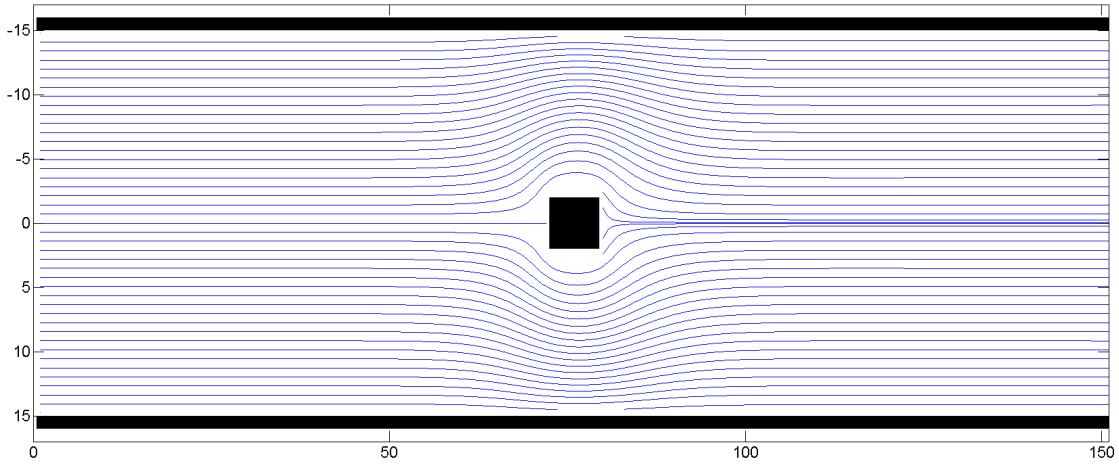

Figure 3.11.: Streamlines of a pressure driven flow past an obstacle. Additional streamlines start behind the obstacle for better illustration.

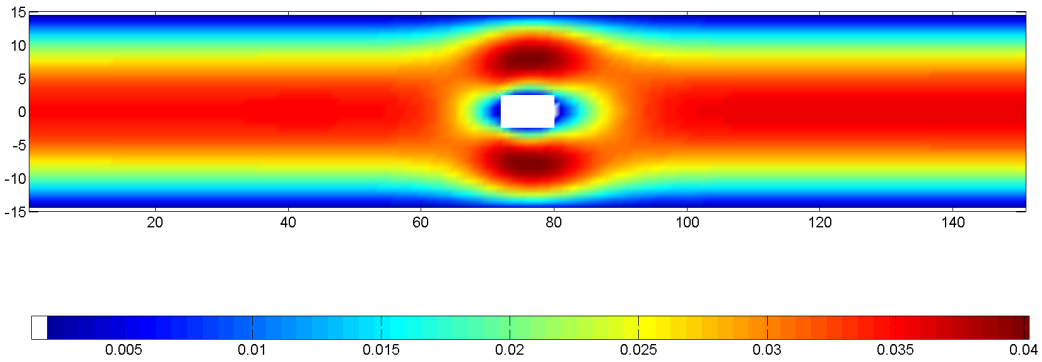

Figure 3.12.: Modulus of velocity for a pressure driven flow past an obstacle.

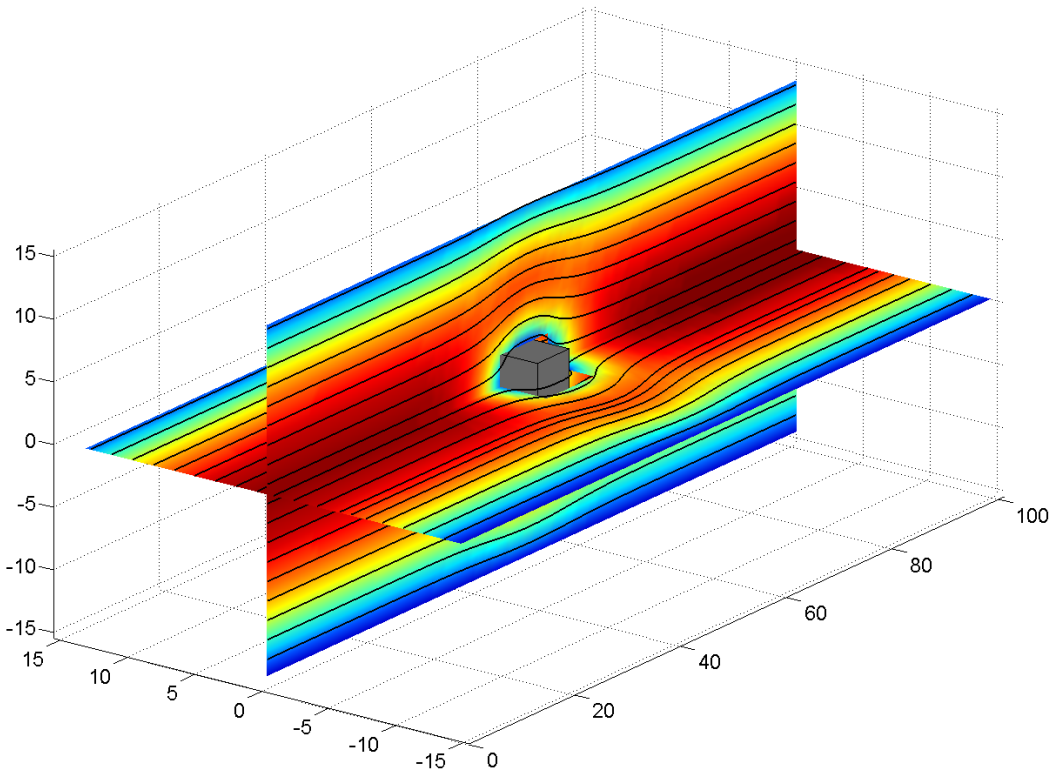

Figure 3.13.: Modulus of velocity for a pressure driven flow past an obstacle in three dimensions. Only two slices are plotted, on which streamlines are printed.

3.2. Temperature Evolution - Rayleigh-Bénard Convection

The previous section already addressed lattice Boltzmann simulations involving some of the enhancements we have presented in chapter 2. However, the main enhancement we have focused on in the preceding chapter, incorporation of a thermal component, has not been tested, yet.
In the current section, we simulate flows advecting temperature besides their diffusion. From a different point of view, we can say that we simulate the evolution of temperature. Furthermore in simulations below we also make use of the last enhancement we have presented in the previous chapter, the buoyancy effect. But the first simulation we begin with is a less sophisticated problem.
All simulations are performed with the temperature model derived in the previous chapter, this means we have implemented equation (2.32) with energy equilibrium distribution (2.37) for the three-dimensional D3Q19 model. The energy equilibrium distribution in the two-dimensional simulations (D2Q9) is [26, 48]

$$
\begin{aligned}
g_0^{(eq)}(\boldsymbol{x},t) &= -\frac{2}{3}\rho(\boldsymbol{x},t)E(\boldsymbol{x},t)|\boldsymbol{u}(\boldsymbol{x},t)|^2 \\
g_j^{(eq)}(\boldsymbol{x},t) &= \frac{1}{9}\rho(\boldsymbol{x},t)E(\boldsymbol{x},t)\left[\frac{3}{2}+\frac{3}{2}(\boldsymbol{c}_j\cdot\boldsymbol{u}(\boldsymbol{x},t))+\frac{9}{2}(\boldsymbol{c}_j\cdot\boldsymbol{u}(\boldsymbol{x},t))^2-\frac{3}{2}|\boldsymbol{u}(\boldsymbol{x},t)|^2\right], \\
g_k^{(eq)}(\boldsymbol{x},t) &= \frac{1}{36}\rho(\boldsymbol{x},t)E(\boldsymbol{x},t)\left[3+6(\boldsymbol{c}_k\cdot\boldsymbol{u}(\boldsymbol{x},t))+\frac{9}{2}(\boldsymbol{c}_k\cdot\boldsymbol{u}(\boldsymbol{x},t))^2-\frac{3}{2}|\boldsymbol{u}(\boldsymbol{x},t)|^2\right],
\end{aligned}
$$

with $j = 1,\ldots,4$, $k = 5,\ldots,8$ and lattice velocities $\boldsymbol{c}_i$ given for D2Q9 in section 1.5. The relaxation parameter τ_d in (2.32) tunes the thermal diffusivity χ, where the relations read

$$\chi = \frac{2}{3}(\tau_d - \frac{1}{2})$$

and

$$\chi = \frac{5}{9}(\tau_d - \frac{1}{2}),$$

for D2Q9 and D3Q19, respectively.

In the following, we simulate Rayleigh-Bénard convection (RBC), see, e.g., [21] for a detailed discussion of this problem. In our simulation we have two parallel rigid boundaries of infinite length aligned horizontal, as notion think of two plates. The temperature of both boundaries is maintained at two different temperatures, where the bottom boundary is assumed to be the colder one. In between the boundaries a viscous fluid is injected. The problem is stated under consideration of gravity which acts in direction from the upper boundary to the bottom one, compare also with figure 3.14.
At the beginning the fluid is initialized with a homogeneous density and zero velocity. Except the boundaries, the temperature is initialized constant, in our simulation equal

to the colder boundary temperature. In absence of a fluid's motion and consideration of gravity, the problem is described by the heat equation with corresponding boundary conditions which prescribe a constant temperature at the boundaries. Temperature diffusion would yield a linear increase of the temperature from top to bottom, see also figure 3.15. Roughly speaking, this coincides to a simulation of RBC where no influence of gravity and especially no buoyancy effects are considered. However, if buoyancy effects are considered besides diffusion also advection has to be taken into account. Since the fluid is initialized with zero velocity the complete fluid movement results from temperature differences. Thus, the fluid heats at the lower boundary and gravity drives it to the upper boundary, where it is cooled down. Since we consider incompressible fluids, the fluid cannot completely accumulate near the upper boundary, hence, not only an upward movement can be observed but also a downward one. Convection cells as shown in figure 3.14 appear.

In our simulation we use bounceback conditions for the interaction of the fluid with the boundaries. Due to the given symmetry of the problem we use periodic boundary conditions in horizontal direction, both for the density and the temperature distribution. The density distribution is initialized, such that for all lattice points the mass density ρ is equal to one, and the velocity $\boldsymbol{u}$ equal to zero. The temperature is supposed to maintain on the boundaries, corresponding boundary conditions for the energy distribution satisfying this property can be realized as follows.
In D2Q9 at the boundaries three values of the energy distribution have to be computed, such that (cf. (2.33))

$$\sum_{i=0}^{8} g_i(\boldsymbol{x}_b, t) = \rho(\boldsymbol{x}, t) E_b(\boldsymbol{x}_b, t)$$

is fulfilled for a given boundary point $\boldsymbol{x}_b$ and prescribed energy $E_b(\boldsymbol{x}_b, t)$. See also section 2.3 for more detailed investigation of the thermal model. Note the energy is proportional to the temperature. For simplicity we consider only a south boundary

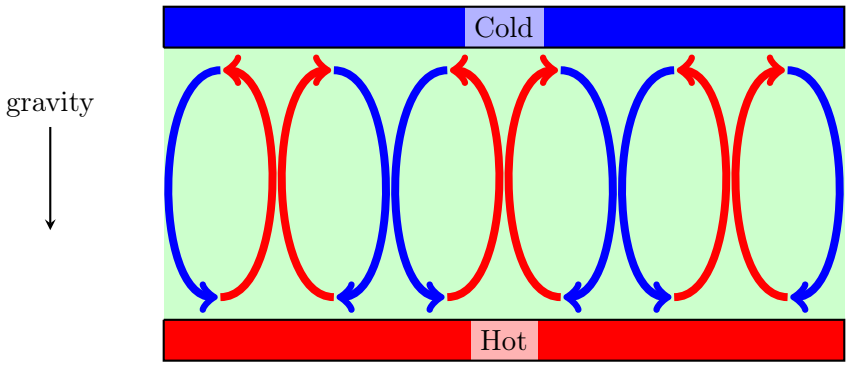

Figure 3.14.: Convection cells displayed at an image section of a two-dimensional Rayleigh-Bénard experiment.

where g_2, g_5 and g_6 have to be determined. Other boundaries can be treated analogue. By bringing the unknown values to the left hand side and all other terms to the right hand side, it follows for the above case

$$G(\boldsymbol{x}_b, t) := g_2(\boldsymbol{x}_b, t) + g_5(\boldsymbol{x}_b, t) + g_6(\boldsymbol{x}_b, t) = \rho(\boldsymbol{x}, t)E_b(\boldsymbol{x}_b, t) - \sum_{i\in\{1,3,4,7,8,9\}} g_i(\boldsymbol{x}_b, t),$$

where $G(\boldsymbol{x}_b, t)$ can be computed explicitly. With $G(\boldsymbol{x}_b, t)$ known, the unknown values can be calculated according to their relative weighting in the equilibrium, i.e.

$$\begin{aligned} g_2(\boldsymbol{x}_b, t) &= \frac{\omega_2}{\omega_2 + \omega_5 + \omega_8} G(\boldsymbol{x}_b, t), \\ g_5(\boldsymbol{x}_b, t) &= \frac{\omega_5}{\omega_2 + \omega_5 + \omega_8} G(\boldsymbol{x}_b, t), \\ g_8(\boldsymbol{x}_b, t) &= \frac{\omega_8}{\omega_2 + \omega_5 + \omega_8} G(\boldsymbol{x}_b, t). \end{aligned}$$

This kind of boundary conditions can be extended to three dimensions straightforward, and we use them in the three-dimensional simulation.
On the upper boundary we prescribe a temperature according to an energy of value $E_{cold} = 0$, whereas on the lower boundary we set $E_{hot} = 1$. The energy distribution is initialized in equilibrium state, such that $E = 0$ holds everywhere, except for the lower boundary. On the lower boundary initialization of the energy distribution is done by an equilibrium state with $E = E_{hot}$.

Firstly, we simulate the temperature evolution between the lower hot boundary and the upper cold one without considering buoyancy effects or gravity acting on the fluid at all. This means we approximate the solution of the heat equation with appropriate boundary conditions. The simulation is done in two dimensions on a 102 times 51 lattice, choosing relaxation parameters $\hat{\tau}_c = \tau_d = 0.75$[1]. Since the fluid is initialized in a rest state and no forces act on the fluid, the fluid stays at rest and need not to be simulated. Like expected, we obtain a stationary state for the temperature profile with an linear decrease from the warmer to the colder boundary. Figure 3.15 illustrates this result by a color plot of the corresponding energy.
Now, we add gravity to our simulation and we consider buoyancy effects. Using the modified model given in section 2.2, we add a force according to the acceleration

$$\boldsymbol{k}(\boldsymbol{x}, t) = \big(1 - \beta(T(\boldsymbol{x}, t) - T_e)\big)\boldsymbol{g},$$

with β the coefficient of thermal expansion, T_e a reference temperature and $\boldsymbol{g}$ the acceleration due to gravity. Instead of directly simulating the evolution of the temperature,

[1] At this point we appreciatively like to mention the web project on `http://www.LBMethod.org.org` which offers a good opportunity to swap ideas on topics around lattice Boltzmann methods. During the work on this thesis, we got several helpful hints by reading the discussions in the forum of this project. The choice of the lattice dimension was also inspired by reading on this web page.

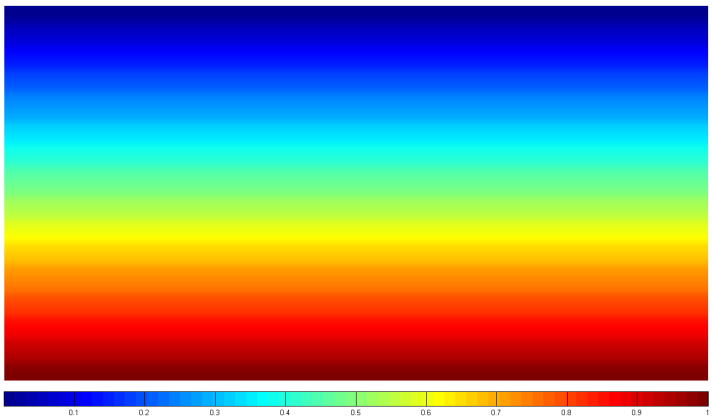

Figure 3.15.: Temperature profile between two boundaries maintained at two different temperatures without considering the influence of gravity. Boundary at the bottom is colder than the one at the top.

the algorithm simulates the evolution of the energy E proportional to the temperature, therefore we write the acceleration in terms of the energy as

$$\boldsymbol{k}(\boldsymbol{x},t) = \Big(1 - \hat{\beta}(E(\boldsymbol{x},t) - E_e)\Big)\,\boldsymbol{g}, \tag{3.5}$$

with an appropriate $\hat{\beta}$. We simulate Rayleigh-Bénard convection in two dimensions by taking

$$\boldsymbol{g} = \begin{pmatrix} 0 \\ -0.002 \end{pmatrix} \quad \text{and} \quad \hat{\beta} = 0.5.$$

Further, we set the reference energy E_e equal to the average energy corresponding to the temperature profile obtained in the simulation above when no gravity is considered, hence we choose $E_e = 0.5$. This simulation yields a result in the manner of the description above illustrated in figure 3.14. In figures 3.16 and 3.17 the simulation results are shown. Figure 3.16 shows the motion of the fluid between the two boundaries. We observe a circular movement. The resulting temperature profile is drawn in figure 3.17, here we also can see convection cells.

For the simulation of Rayleigh-Bénard convection in three dimensions a slightly modified force term is used. The force term according to the acceleration (3.5), used in the two-dimensional simulation, contains a constant term which yields a static pressure in the fluid. This is omitted in our three-dimensional simulation, instead of (3.5) a force according to the acceleration

$$\boldsymbol{k}(\boldsymbol{x},t) = -\hat{\beta}(E(\boldsymbol{x},t) - E_e)\boldsymbol{g},$$

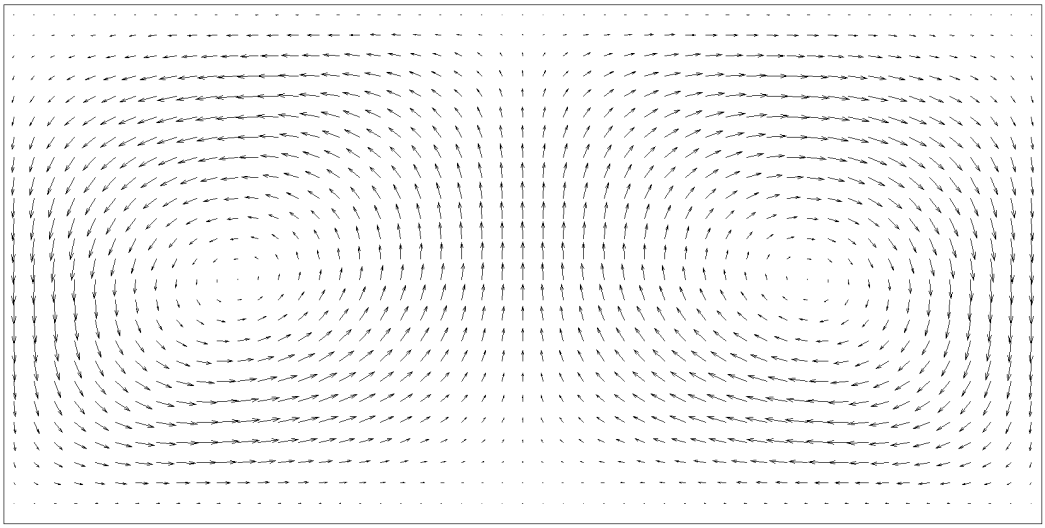

Figure 3.16.: Vector field illustrating the fluid's movement in a simulation of two-dimensional Rayleigh-Bénard convection.

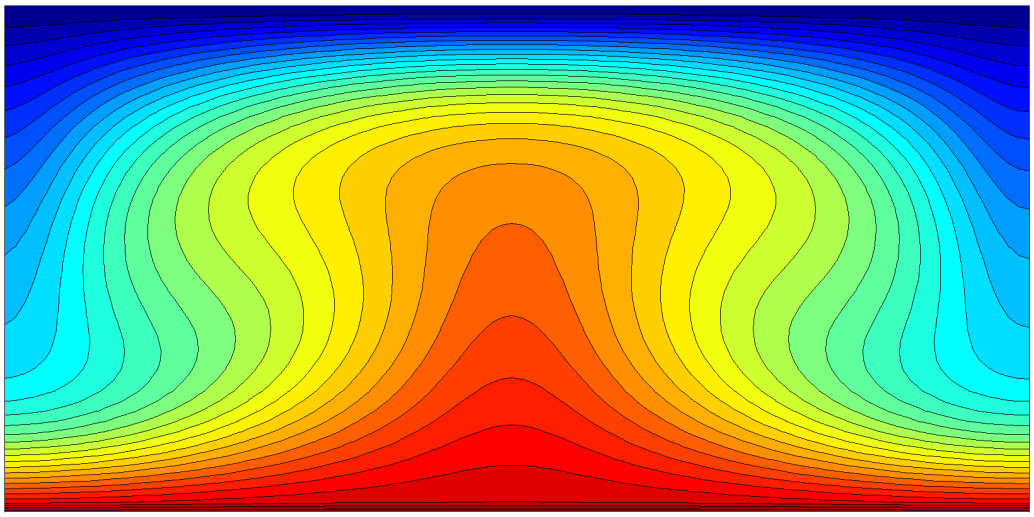

Figure 3.17.: Resulting temperature profile in a simulation of two-dimensional Rayleigh-Bénard convection. Lines are isotherms connecting points that have same temperature.

is used. Therefore, we simulate RBC only under the influence of changes in the acting force due to temperature variations. Compare this procedure also with the considerations in section 2.4.1 where the constant part was combined with the pressure gradient. We have chosen the following parameters

$$\hat{\beta} = 1, \quad \hat{\tau}_c = 0.75, \quad \tau_d = 0.75, \quad \boldsymbol{g} = \begin{pmatrix} 0 \\ 0 \\ -0.002 \end{pmatrix}$$

and we used a 60x60x50 lattice, thus the boundaries maintained at constant temperatures are squares of size 60x60. All other parameters are adopted from the two-dimensional RBC simulation above. Figure 3.18 illustrates the simulation, we again observe the presence of convection cells.

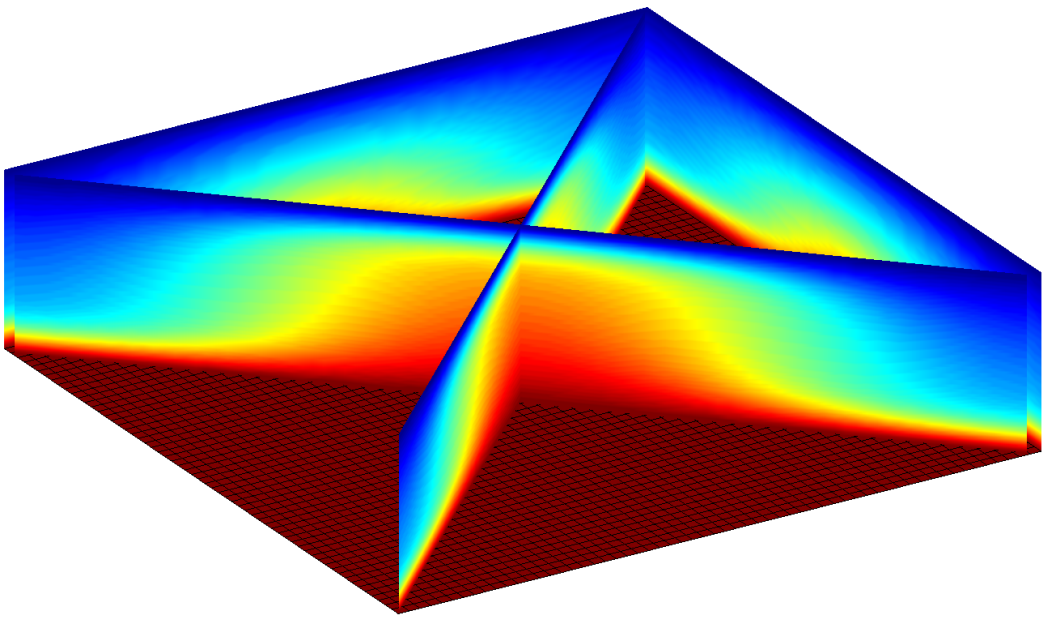

Figure 3.18.: Simulation of three-dimensional Rayleigh-Bénard convection with a lattice Boltzmann method.

Outlook

In this work we have developed numerical methods capable of simulating fluid flows in domains with straight boundaries. We further enhanced the main lattice Boltzmann method, such that we achieved a method capable to simulate problems described by the incompressible Navier-Stokes equations coupled to the advection-diffusion equation satisfied by the temperature. The consideration of complex boundaries would be an obvious enhancement to the presented method [43, 44].
In chapter 3 we have simulated flows past an obstacle. There, the obstacle was a solid object inserted in the flow which did not move its position due to the flow. One can also consider movable obstacles, this consideration is expressed by the generic term fluid structure interaction (FSI). In our opinion, FSI is an as powerful as fascinating enhancement. Fluid structure interaction describes the interaction of the fluid with a movable and deformable structure. Many possible applications arise when considering fluid structure interaction. To give only two examples, on the one hand the simulation of blood through veins would be possible, where the veins can be seen as flexible deformable tubes. On the other hand, the thermal model we have presented in chapter 2 enhanced with FSI would yield a method which could be used for the simulation of solar updraft towers. Solar updraft towers are a proposed type of renewable-energy power plants, where air within a greenhouse-like structure is heated by sunshine. The resulting convection causes the air to rise up through a chimney, the so moving air drives turbines. In this manner solar updraft towers produce energy. A simulation of solar updraft towers is an important step in optimization.
A further enhancement of the method presented in this work could be its coupling to existing circuit simulators. For instance, the efficiency of semiconductors is strongly depending on the temperature, hence also modeling the environment temperature is an important issue. The environment temperature close to the circuit changes due to heat loss of the electrical devices. The lattice Boltzmann method can be used for the consideration of cooling the circuit, where the heat loss of the electrical devices would be input data for the method, e.g. in the form of temperature boundary conditions. The other way round, the temperature evolution simulated by the lattice Boltzmann method gives input data for the circuit simulation.
The outlook demonstrated the existence of various problems where the lattice Boltzmann method can be used for. Further investigations and developments of the lattice Boltzmann method are therefore worthwhile.

APPENDIX A

Outsourced Calculations

The appendix is devoted to calculations omitted in the main part of this work. We catch up on some of the omitted calculations here. Whenever a calculation was moved into the appendix, we have noted it in the main chapters.

A.1. Dot Product of a Matrix Valued Function

In section 1.2.2 the momentum equation was computed. We used in the first step of (1.14) the following calculation.

$$\begin{aligned}
\boldsymbol{v}\left[\boldsymbol{v}\cdot\boldsymbol{\nabla}f(\boldsymbol{x},\boldsymbol{v},t)\right] &= \boldsymbol{v}\sum_{k=0}^{n} v_k \frac{\partial f(\boldsymbol{x},\boldsymbol{v},t)}{\partial x_k} \\
&= \begin{pmatrix} v_1 \displaystyle\sum_{k=0}^{n} \frac{\partial f(\boldsymbol{x},\boldsymbol{v},t)}{\partial x_k} v_k \\ \vdots \\ v_n \displaystyle\sum_{k=0}^{n} \frac{\partial f(\boldsymbol{x},\boldsymbol{v},t)}{\partial x_k} v_k \end{pmatrix} \\
&= \begin{pmatrix} \boldsymbol{\nabla}\cdot(v_1\boldsymbol{v}f(\boldsymbol{x},\boldsymbol{v},t)) \\ \vdots \\ \boldsymbol{\nabla}\cdot(v_n\boldsymbol{v}f(\boldsymbol{x},\boldsymbol{v},t)) \end{pmatrix} \\
&= \boldsymbol{\nabla}\cdot\begin{pmatrix} v_1v_1f(\boldsymbol{x},\boldsymbol{v},t) & v_1v_2f(\boldsymbol{x},\boldsymbol{v},t) & \dots & v_1v_nf(\boldsymbol{x},\boldsymbol{v},t) \\ \vdots & \vdots & & \vdots \\ v_nv_1f(\boldsymbol{x},\boldsymbol{v},t) & v_nv_2f(\boldsymbol{x},\boldsymbol{v},t) & \dots & v_nv_nf(\boldsymbol{x},\boldsymbol{v},t) \end{pmatrix} \\
&= \boldsymbol{\nabla}\cdot(\boldsymbol{v}\boldsymbol{v}^T f(\boldsymbol{x},\boldsymbol{v},t)).
\end{aligned}$$

A.2. Computation of a Time Derivative

In the current section, equation (1.76) is computed in detail. Thus, we show the validity of

$$\frac{\partial^{(1)}}{\partial \hat{t}}\left(\hat{\rho}(\hat{\boldsymbol{x}},\hat{t})\hat{u}^{\alpha}(\hat{\boldsymbol{x}},\hat{t})\hat{u}^{\beta}(\hat{\boldsymbol{x}},\hat{t})\right) = -\hat{u}^{\alpha}(\hat{\boldsymbol{x}},\hat{t})\frac{\partial^{(1)}}{\partial \hat{x}_{\beta}}p(\hat{\boldsymbol{x}},\hat{t}) - \hat{u}^{\beta}(\hat{\boldsymbol{x}},\hat{t})\frac{\partial^{(1)}}{\partial \hat{x}_{\alpha}}p(\hat{\boldsymbol{x}},\hat{t}) - \sum_{j=1}^{3}\frac{\partial^{(1)}}{\partial \hat{x}_{j}}\left(\hat{\rho}(\hat{\boldsymbol{x}},\hat{t})\hat{u}^{\alpha}(\hat{\boldsymbol{x}},\hat{t})\hat{u}^{\beta}(\hat{\boldsymbol{x}},\hat{t})\hat{u}^{j}(\hat{\boldsymbol{x}},\hat{t})\right). \tag{A.1}$$

For the time derivative on the left hand side of (A.1) the product rule implies

$$\begin{aligned}\frac{\partial^{(1)}}{\partial \hat{t}}&\left(\hat{\rho}(\hat{\boldsymbol{x}},\hat{t})\hat{u}^{\alpha}(\hat{\boldsymbol{x}},\hat{t})\hat{u}^{\beta}(\hat{\boldsymbol{x}},\hat{t})\right)\\ &= \hat{u}^{\alpha}(\hat{\boldsymbol{x}},\hat{t})\frac{\partial^{(1)}}{\partial \hat{t}}\left(\hat{\rho}(\hat{\boldsymbol{x}},\hat{t})\hat{u}^{\beta}(\hat{\boldsymbol{x}},\hat{t})\right) + \hat{\rho}(\hat{\boldsymbol{x}},\hat{t})\hat{u}^{\beta}(\hat{\boldsymbol{x}},\hat{t})\frac{\partial^{(1)}}{\partial \hat{t}}\hat{u}^{\alpha}(\hat{\boldsymbol{x}},\hat{t})\\ &= \hat{u}^{\alpha}(\hat{\boldsymbol{x}},\hat{t})\frac{\partial^{(1)}}{\partial \hat{t}}\left(\hat{\rho}(\hat{\boldsymbol{x}},\hat{t})\hat{u}^{\beta}(\hat{\boldsymbol{x}},\hat{t})\right) + \hat{u}^{\beta}(\hat{\boldsymbol{x}},\hat{t})\frac{\partial^{(1)}}{\partial \hat{t}}\left(\hat{\rho}(\hat{\boldsymbol{x}},\hat{t})\hat{u}^{\alpha}(\hat{\boldsymbol{x}},\hat{t})\right)\\ &\quad - \hat{u}^{\alpha}(\hat{\boldsymbol{x}},\hat{t})\hat{u}^{\beta}(\hat{\boldsymbol{x}},\hat{t})\frac{\partial^{(1)}}{\partial \hat{t}}\hat{\rho}(\hat{\boldsymbol{x}},\hat{t}).\end{aligned} \tag{A.2}$$

Writing (1.69) component wise reads

$$\frac{\partial^{(1)}}{\partial \hat{t}}\left(\hat{\rho}(\hat{\boldsymbol{x}},\hat{t})\hat{u}^{\gamma}(\hat{\boldsymbol{x}},\hat{t})\right) + \sum_{j=1}^{3}\frac{\partial^{(1)}}{\partial \hat{x}_{j}}\left(\hat{\rho}(\hat{\boldsymbol{x}},\hat{t})\hat{u}^{\gamma}(\hat{\boldsymbol{x}},\hat{t})\hat{u}^{j}(\hat{\boldsymbol{x}},\hat{t})\right) = -\frac{\partial^{(1)}}{\partial \hat{x}_{\gamma}}p(\hat{\boldsymbol{x}},\hat{t}).$$

Rearranged to the time derivative this equation can be substituted twice ($\gamma = \alpha$ and $\gamma = \beta$) in (A.2). Hence, we get with additional usage of (1.67) for the subtracting term on the right hand side of (A.2):

$$\begin{aligned}\frac{\partial^{(1)}}{\partial \hat{t}}\left(\hat{\rho}(\hat{\boldsymbol{x}},\hat{t})\hat{u}^{\alpha}(\hat{\boldsymbol{x}},\hat{t})\hat{u}^{\beta}(\hat{\boldsymbol{x}},\hat{t})\right) =& -\hat{u}^{\alpha}(\hat{\boldsymbol{x}},\hat{t})\sum_{j=1}^{3}\frac{\partial^{(1)}}{\partial \hat{x}_{j}}\left(\hat{\rho}(\hat{\boldsymbol{x}},\hat{t})\hat{u}^{\beta}(\hat{\boldsymbol{x}},\hat{t})\hat{u}^{j}(\hat{\boldsymbol{x}},\hat{t})\right)\\ &- \hat{u}^{\beta}(\hat{\boldsymbol{x}},\hat{t})\sum_{j=1}^{3}\frac{\partial^{(1)}}{\partial \hat{x}_{j}}\left(\hat{\rho}(\hat{\boldsymbol{x}},\hat{t})\hat{u}^{\alpha}(\hat{\boldsymbol{x}},\hat{t})\hat{u}^{j}(\hat{\boldsymbol{x}},\hat{t})\right)\\ &- \hat{u}^{\alpha}(\hat{\boldsymbol{x}},\hat{t})\frac{\partial^{(1)}}{\partial \hat{x}_{\beta}}p(\hat{\boldsymbol{x}},\hat{t}) - \hat{u}^{\beta}(\hat{\boldsymbol{x}},\hat{t})\frac{\partial^{(1)}}{\partial \hat{x}_{\alpha}}p(\hat{\boldsymbol{x}},\hat{t})\\ &+ \hat{u}^{\alpha}(\hat{\boldsymbol{x}},\hat{t})\hat{u}^{\beta}(\hat{\boldsymbol{x}},\hat{t})\sum_{j=1}^{3}\frac{\partial^{(1)}}{\partial \hat{x}_{j}}\left(\hat{\rho}(\hat{\boldsymbol{x}},\hat{t})\hat{u}^{j}(\hat{\boldsymbol{x}},\hat{t})\right).\end{aligned} \tag{A.3}$$

The latter equation can be simplified with help of the following equation

$$\begin{aligned}\hat{u}^\alpha(\hat{\boldsymbol{x}},\hat{t})\hat{u}^\beta(\hat{\boldsymbol{x}},\hat{t})\frac{\partial^{(1)}}{\partial\hat{x}_\gamma}\left(\hat{\rho}(\hat{\boldsymbol{x}},\hat{t})\hat{u}^\gamma(\hat{\boldsymbol{x}},\hat{t})\right) = &-\frac{\partial^{(1)}}{\partial\hat{x}_\gamma}\left(\hat{\rho}(\hat{\boldsymbol{x}},\hat{t})\hat{u}^\alpha(\hat{\boldsymbol{x}},\hat{t})\hat{u}^\beta(\hat{\boldsymbol{x}},\hat{t})\hat{u}^\gamma(\hat{\boldsymbol{x}},\hat{t})\right)\\ &+\hat{u}^\alpha(\hat{\boldsymbol{x}},\hat{t})\frac{\partial^{(1)}}{\partial\hat{x}_\gamma}\left(\hat{\rho}(\hat{\boldsymbol{x}},\hat{t})\hat{u}^\beta(\hat{\boldsymbol{x}},\hat{t})\hat{u}^\gamma(\hat{\boldsymbol{x}},\hat{t})\right)\\ &+\hat{u}^\beta(\hat{\boldsymbol{x}},\hat{t})\frac{\partial^{(1)}}{\partial\hat{x}_\gamma}\left(\hat{\rho}(\hat{\boldsymbol{x}},\hat{t})\hat{u}^\alpha(\hat{\boldsymbol{x}},\hat{t})\hat{u}^\gamma(\hat{\boldsymbol{x}},\hat{t})\right),\end{aligned}$$

which directly results by application of the product rule. The latter equation is substituted for each addend of the third sum in (A.3), doing so the terms of the first and second sum cancel out. Therefore, equation (A.3) reads

$$\begin{aligned}\frac{\partial^{(1)}}{\partial\hat{t}}\left(\hat{\rho}(\hat{\boldsymbol{x}},\hat{t})\hat{u}^\alpha(\hat{\boldsymbol{x}},\hat{t})\hat{u}^\beta(\hat{\boldsymbol{x}},\hat{t})\right) = &-\hat{u}^\alpha(\hat{\boldsymbol{x}},\hat{t})\frac{\partial^{(1)}}{\partial\hat{x}_\beta}p(\hat{\boldsymbol{x}},\hat{t})-\hat{u}^\beta(\hat{\boldsymbol{x}},\hat{t})\frac{\partial^{(1)}}{\partial\hat{x}_\alpha}p(\hat{\boldsymbol{x}},\hat{t})\\ &-\sum_{j=1}^{3}\frac{\partial^{(1)}}{\partial\hat{x}_j}\left(\hat{\rho}(\hat{\boldsymbol{x}},\hat{t})\hat{u}^\alpha(\hat{\boldsymbol{x}},\hat{t})\hat{u}^\beta(\hat{\boldsymbol{x}},\hat{t})\hat{u}^j(\hat{\boldsymbol{x}},\hat{t})\right),\end{aligned}$$

which is equivalent to (A.1).

A.3. Integration of PDE for Energy Distribution

In section 2.3.1, the integration of the first and second order terms, (2.24) and (2.25), of the Chapman-Enskog expansion was done by stating only the results. We catch up on this integration in the current section of the appendix:

Integration of First Order Terms

We integrate the approximation (2.24), for the sake of clarity we integrate the left and right hand side separately. For the left hand side we get

$$\begin{aligned}\int_{\mathbb{R}^3}\frac{\partial^{(1)}g^{(0)}(\boldsymbol{x},\boldsymbol{v},t)}{\partial t}\,\mathrm{d}\boldsymbol{v}+\int_{\mathbb{R}^3}\boldsymbol{v}\cdot\boldsymbol{\nabla}^{(1)}g^{(0)}(\boldsymbol{x},\boldsymbol{v},t)\,\mathrm{d}\boldsymbol{v}&\\ =\frac{\partial^{(1)}}{\partial t}\int_{\mathbb{R}^3}g^{(0)}(\boldsymbol{x},\boldsymbol{v},t)\,\mathrm{d}\boldsymbol{v}+\boldsymbol{\nabla}^{(1)}\cdot\int_{\mathbb{R}^3}\boldsymbol{v}g^{(0)}(\boldsymbol{x},\boldsymbol{v},t)\,\mathrm{d}\boldsymbol{v}.&\end{aligned}$$

In the latter equation the result of the first integral is given by (2.16) as an immediate consequence of the definition of the energy equilibrium distribution (2.17) and the fact that $f^{(eq)}(\boldsymbol{x},\boldsymbol{v},t)$ is satisfying the Boltzmann equation. The second integral can be

computed straightforward

$$\begin{aligned}\int_{\mathbb{R}^3} \boldsymbol{v} g^{(0)}(\boldsymbol{x},\boldsymbol{v},t)\,\mathrm{d}\boldsymbol{v} &= \int_{\mathbb{R}^3} \boldsymbol{v}\frac{|\boldsymbol{v}-\boldsymbol{u}(\boldsymbol{x},t)|^2\rho(\boldsymbol{x},t)}{2}\left(\frac{m}{2\pi k_B T(\boldsymbol{x},t)}\right)^{3/2} \\ &\qquad \exp\left(\frac{-m}{2k_B T(\boldsymbol{x},t)}|\boldsymbol{v}-\boldsymbol{u}(\boldsymbol{x},t)|^2\right)\,\mathrm{d}\boldsymbol{v} \\ &= \rho(\boldsymbol{x},t)\boldsymbol{u}(\boldsymbol{x},t)E(\boldsymbol{x},t),\end{aligned}$$

where $E(\boldsymbol{x},t) = \frac{3}{2}\frac{k_B T(\boldsymbol{x},t)}{m}$. Hence, it holds for the left hand side of (2.24)

$$\begin{aligned}&\int_{\mathbb{R}^3} \frac{\partial^{(1)} g^{(0)}(\boldsymbol{x},\boldsymbol{v},t)}{\partial t}\,\mathrm{d}\boldsymbol{v} + \int_{\mathbb{R}^3} \boldsymbol{v}\cdot\boldsymbol{\nabla}^{(1)} g^{(0)}(\boldsymbol{x},\boldsymbol{v},t)\,\mathrm{d}\boldsymbol{v} \\ &\qquad = \frac{\partial^{(1)}}{\partial t}\left(\rho(\boldsymbol{x},t)E(\boldsymbol{x},t)\right) + \boldsymbol{\nabla}^{(1)}\cdot\left(\rho(\boldsymbol{x},t)\boldsymbol{u}(\boldsymbol{x},t)E(\boldsymbol{x},t)\right).\end{aligned}$$

Now, we consider the right hand side of (2.24), integration yields two integrals

$$\int_{\mathbb{R}^3} -\frac{g^{(1)}(\boldsymbol{x},\boldsymbol{v},t)}{\tau_d}\,\mathrm{d}\boldsymbol{v} \quad \text{and} \quad \int_{\mathbb{R}^3} -f^{(0)}(\boldsymbol{x},\boldsymbol{v},t)q^{(1)}(\boldsymbol{x},\boldsymbol{v},t)\,\mathrm{d}\boldsymbol{v},$$

where the first one vanishes, because $\int_{\mathbb{R}^3} g(\boldsymbol{x},\boldsymbol{v},t)\,\mathrm{d}\boldsymbol{v}$ and $\int_{\mathbb{R}^3} g^{(0)}(\boldsymbol{x},\boldsymbol{v},t)\,\mathrm{d}\boldsymbol{v}$ yield the same result. And by further inspecting (2.21) one can conclude that the integrals $\int_{\mathbb{R}^3} g^{(k)}(\boldsymbol{x},\boldsymbol{v},t)\,\mathrm{d}\boldsymbol{v}$, $k \geq 1$, vanish. Further calculation of the second integral (using the split form (2.26) for $q^{(1)}(\boldsymbol{x},\boldsymbol{v},t)$) yields

$$\begin{aligned}&\int_{\mathbb{R}^3} -f^{(0)}(\boldsymbol{x},\boldsymbol{v},t)q^{(1)}(\boldsymbol{x},\boldsymbol{v},t)\,\mathrm{d}\boldsymbol{v} \\ &\quad = -\int_{\mathbb{R}^3} f^{(0)}(\boldsymbol{x},\boldsymbol{v},t)q_1^{(1)}(\boldsymbol{x},\boldsymbol{v},t)\,\mathrm{d}\boldsymbol{v} - \int_{\mathbb{R}^3} f^{(0)}(\boldsymbol{x},\boldsymbol{v},t)q_2^{(1)}(\boldsymbol{x},\boldsymbol{v},t)\,\mathrm{d}\boldsymbol{v} \\ &\quad = -\int_{\mathbb{R}^3} f^{(0)}(\boldsymbol{x},\boldsymbol{v},t)(\boldsymbol{v}-\boldsymbol{u}(\boldsymbol{x},t))\cdot\left[-\boldsymbol{\nabla}^{(1)}\frac{p(\boldsymbol{x},t)}{\rho(\boldsymbol{x},t)}\right]\,\mathrm{d}\boldsymbol{v} \\ &\qquad -\int_{\mathbb{R}^3} f^{(0)}(\boldsymbol{x},\boldsymbol{v},t)\left(\left[(\boldsymbol{v}-\boldsymbol{u}(\boldsymbol{x},t))\,(\boldsymbol{v}-\boldsymbol{u}(\boldsymbol{x},t))^T\right] : \left[\boldsymbol{\nabla}^{(1)}\boldsymbol{u}(\boldsymbol{x},t)\right]\right)\,\mathrm{d}\boldsymbol{v} \\ &\quad = \left[\boldsymbol{\nabla}^{(1)}\frac{p(\boldsymbol{x},t)}{\rho(\boldsymbol{x},t)}\right]\cdot\left(\int_{\mathbb{R}^3} f^{(0)}(\boldsymbol{x},\boldsymbol{v},t)\,(\boldsymbol{v}-\boldsymbol{u}(\boldsymbol{x},t))\,\mathrm{d}\boldsymbol{v}\right) \\ &\qquad -\left(\int_{\mathbb{R}^3} f^{(0)}(\boldsymbol{x},\boldsymbol{v},t)\,(\boldsymbol{v}-\boldsymbol{u}(\boldsymbol{x},t))\,(\boldsymbol{v}-\boldsymbol{u}(\boldsymbol{x},t))^T\,\mathrm{d}\boldsymbol{v}\right) : \left(\boldsymbol{\nabla}^{(1)}\boldsymbol{u}(\boldsymbol{x},t)\right),\end{aligned}$$

where one integral

$$\begin{aligned}\int_{\mathbb{R}^3} f^{(0)}(\boldsymbol{x},\boldsymbol{v},t)\,(\boldsymbol{v}-\boldsymbol{u}(\boldsymbol{x},t))\;\mathrm{d}\boldsymbol{v} &= \int_{\mathbb{R}^3} f^{(0)}(\boldsymbol{x},\boldsymbol{v},t)\boldsymbol{v}\,\mathrm{d}\boldsymbol{v} - \int_{\mathbb{R}^3} f^{(0)}(\boldsymbol{x},\boldsymbol{v},t)\boldsymbol{u}(\boldsymbol{x},t)\,\mathrm{d}\boldsymbol{v}\\ &= \rho(\boldsymbol{x},t)\boldsymbol{u}(\boldsymbol{x},t) - \rho(\boldsymbol{x},t)\boldsymbol{u}(\boldsymbol{x},t)\\ &= 0\end{aligned}$$

vanishes and the other

$$\int_{\mathbb{R}^3} f^{(0)}(\boldsymbol{x},\boldsymbol{v},t)\,(\boldsymbol{v}-\boldsymbol{u}(\boldsymbol{x},t))\,(\boldsymbol{v}-\boldsymbol{u}(\boldsymbol{x},t))^T\;\mathrm{d}\boldsymbol{v},$$

which is the zeroth order momentum flux tensor, reduces to $p(\boldsymbol{x},t)I$, with pressure $p(\boldsymbol{x},t)$ and identity matrix I. Compare with (1.15), the viscous terms vanish due to the state described by $f^{(0)}(\boldsymbol{x},\boldsymbol{v},t)$. It follows for the right hand side of (2.24)

$$\int_{\mathbb{R}^3} -f^{(0)}(\boldsymbol{x},\boldsymbol{v},t)q^{(1)}(\boldsymbol{x},\boldsymbol{v},t)\,\mathrm{d}\boldsymbol{v} = -p(\boldsymbol{x},t)\boldsymbol{\nabla}^{(1)}\cdot\boldsymbol{u}(\boldsymbol{x},t). \tag{A.4}$$

Furthermore, we see that only $q_2^{(1)}(\boldsymbol{x},\boldsymbol{v},t)$ contributes to the outcome (A.4). Combining both sides shows that integration of (2.24) leads to

$$\frac{\partial^{(1)}}{\partial t}\left(\rho(\boldsymbol{x},t)E(\boldsymbol{x},t)\right) + \boldsymbol{\nabla}^{(1)}\cdot\left(\rho(\boldsymbol{x},t)\boldsymbol{u}(\boldsymbol{x},t)E(\boldsymbol{x},t)\right) = -p(\boldsymbol{x},t)\boldsymbol{\nabla}^{(1)}\cdot\boldsymbol{u}(\boldsymbol{x},t).$$

This is the exactly the result (2.27) stated in section 2.3.1.

Integration of Second Order Terms

In this paragraph we integrate the second order Chapman-Enskog approximation (2.25) over velocity space. The integral over the first term on the left hand side of (2.25) can be computed directly to

$$\int_{\mathbb{R}^3} \frac{\partial^{(2)} g^{(0)}(\boldsymbol{x},\boldsymbol{v},t)}{\partial t}\,\mathrm{d}\boldsymbol{v} = \frac{\partial^{(2)}}{\partial t}\left(\rho(\boldsymbol{x},t)E(\boldsymbol{x},t)\right).$$

Due to the argument given in the previous paragraph, the integrated second term changes to

$$\begin{aligned}\int_{\mathbb{R}^3}\left[\frac{\partial^{(1)}}{\partial t}+\boldsymbol{v}\cdot\boldsymbol{\nabla}^{(1)}\right]g^{(1)}(\boldsymbol{x},\boldsymbol{v},t)\,\mathrm{d}\boldsymbol{v} &= \frac{\partial^{(1)}}{\partial t}\int_{\mathbb{R}^3}g^{(1)}(\boldsymbol{x},\boldsymbol{v},t)\,\mathrm{d}\boldsymbol{v}+\boldsymbol{\nabla}^{(1)}\cdot\int_{\mathbb{R}^3}\boldsymbol{v}g^{(1)}(\boldsymbol{x},\boldsymbol{v},t)\,\mathrm{d}\boldsymbol{v}\\ &= \boldsymbol{\nabla}^{(1)}\cdot\int_{\mathbb{R}^3}\boldsymbol{v}g^{(1)}(\boldsymbol{x},\boldsymbol{v},t)\,\mathrm{d}\boldsymbol{v}.\end{aligned}$$

With the same argument the first term on the right hand side of (2.25) vanishes when integrated. The second term also vanishes, as can be seen at follows

$$\begin{aligned}\int_{\mathbb{R}^3}f^{(0)}(\boldsymbol{x},\boldsymbol{v},t)q^{(2)}(\boldsymbol{x},\boldsymbol{v},t)\,\mathrm{d}\boldsymbol{v} &= \int_{\mathbb{R}^3}f^{(0)}(\boldsymbol{x},\boldsymbol{v},t)\,(\boldsymbol{v}-\boldsymbol{u}(\boldsymbol{x},t))\cdot\left[\frac{\partial^{(2)}}{\partial t}\boldsymbol{u}(\boldsymbol{x},t)\right]\,\mathrm{d}\boldsymbol{v}\\ &= \underbrace{\left[\int_{\mathbb{R}^3}f^{(0)}(\boldsymbol{x},\boldsymbol{v},t)\,(\boldsymbol{v}-\boldsymbol{u}(\boldsymbol{x},t))\,\mathrm{d}\boldsymbol{v}\right]}_{=0}\cdot\left[\frac{\partial^{(2)}}{\partial t}\boldsymbol{u}(\boldsymbol{x},t)\right]\\ &= 0.\end{aligned}$$

Hence, by integration of (2.25) we obtain

$$\frac{\partial^{(2)}}{\partial t}\left(\rho(\boldsymbol{x},t)E(\boldsymbol{x},t)\right)=-\boldsymbol{\nabla}^{(1)}\cdot\int_{\mathbb{R}^3}\boldsymbol{v}g^{(1)}(\boldsymbol{x},\boldsymbol{v},t)\,\mathrm{d}\boldsymbol{v}-\int_{\mathbb{R}^3}f^{(1)}(\boldsymbol{x},\boldsymbol{v},t)q^{(1)}(\boldsymbol{x},\boldsymbol{v},t)\,\mathrm{d}\boldsymbol{v}. \tag{A.5}$$

In order to achieve equation (2.28), a further investigation of the latter equation is necessary. We inspect the second integral on the right hand side and use the split form (2.26) for $q^{(1)}(\boldsymbol{x},\boldsymbol{v},t)$, thus we get

$$\begin{aligned}\int_{\mathbb{R}^3}f^{(1)}(\boldsymbol{x},\boldsymbol{v},t)q^{(1)}(\boldsymbol{x},\boldsymbol{v},t)\,\mathrm{d}\boldsymbol{v} &= \int_{\mathbb{R}^3}f^{(1)}(\boldsymbol{x},\boldsymbol{v},t)(\boldsymbol{v}-\boldsymbol{u}(\boldsymbol{x},t))\cdot\left[-\boldsymbol{\nabla}^{(1)}\frac{p(\boldsymbol{x},t)}{\rho(\boldsymbol{x},t)}\right]\,\mathrm{d}\boldsymbol{v}\\ &\quad+\int_{\mathbb{R}^3}f^{(1)}(\boldsymbol{x},\boldsymbol{v},t)\left[(\boldsymbol{v}-\boldsymbol{u}(\boldsymbol{x},t))\,(\boldsymbol{v}-\boldsymbol{u}(\boldsymbol{x},t))^T\right]:\left[\boldsymbol{\nabla}^{(1)}\boldsymbol{u}(\boldsymbol{x},t)\right]\,\mathrm{d}\boldsymbol{v}.\end{aligned} \tag{A.6}$$

The first integral on the right hand side vanishes, as we show next:

$$\begin{aligned}
&\int_{\mathbb{R}^3} f^{(1)}(\boldsymbol{x},\boldsymbol{v},t)(\boldsymbol{v}-\boldsymbol{u}(\boldsymbol{x},t))\cdot\left[-\boldsymbol{\nabla}^{(1)}\frac{p(\boldsymbol{x},t)}{\rho(\boldsymbol{x},t)}\right]\,\mathrm{d}\boldsymbol{v}\\
&\qquad=\int_{\mathbb{R}^3} f^{(1)}(\boldsymbol{x},\boldsymbol{v},t)(\boldsymbol{v}-\boldsymbol{u}(\boldsymbol{x},t))\,\mathrm{d}\boldsymbol{v}\cdot\left[-\boldsymbol{\nabla}^{(1)}\frac{p(\boldsymbol{x},t)}{\rho(\boldsymbol{x},t)}\right]\\
&\qquad=\left[\int_{\mathbb{R}^3} f^{(1)}(\boldsymbol{x},\boldsymbol{v},t)\boldsymbol{v}\,\mathrm{d}\boldsymbol{v}-\boldsymbol{u}(\boldsymbol{x},t)\int_{\mathbb{R}^3} f^{(1)}(\boldsymbol{x},\boldsymbol{v},t)\,\mathrm{d}\boldsymbol{v}\right]\cdot\left[-\boldsymbol{\nabla}^{(1)}\frac{p(\boldsymbol{x},t)}{\rho(\boldsymbol{x},t)}\right]
\end{aligned}$$

Both integrals in the square bracket are equal to zero, because of the validity of

$$\rho(\boldsymbol{x},t)=\int_{\mathbb{R}^3} f(\boldsymbol{x},\boldsymbol{v},t)\,\mathrm{d}\boldsymbol{v}=\int_{\mathbb{R}^3} f^{(0)}(\boldsymbol{x},\boldsymbol{v},t)\,\mathrm{d}\boldsymbol{v}$$

and the expansion

$$f(\boldsymbol{x},\boldsymbol{v},t)=f^{(0)}(\boldsymbol{x},\boldsymbol{v},t)+\delta f^{(1)}(\boldsymbol{x},\boldsymbol{v},t)+\delta^2 f^{(2)}(\boldsymbol{x},\boldsymbol{v},t)+\mathcal{O}(\delta^3), \tag{A.7}$$

from which one can then conclude

$$\int_{\mathbb{R}^3} f^{(k)}(\boldsymbol{x},\boldsymbol{v},t)\,\mathrm{d}\boldsymbol{v}=0,\quad k\geq 1.$$

Analogue it holds for the integrals

$$\int_{\mathbb{R}^3} \boldsymbol{v} f^{(k)}(\boldsymbol{x},\boldsymbol{v},t)\,\mathrm{d}\boldsymbol{v}=0,\quad k\geq 1.$$

It remains the investigation of the first order momentum flux tensor for the right hand side of (A.6). From chapter 1 we have (cf. (1.15))

$$\begin{aligned}
&\int_{\mathbb{R}^3} f(\boldsymbol{x},\boldsymbol{v},t)\left[(\boldsymbol{v}-\boldsymbol{u}(\boldsymbol{x},t))\,(\boldsymbol{v}-\boldsymbol{u}(\boldsymbol{x},t))^T\right]\,\mathrm{d}\boldsymbol{v}\\
&\qquad=p(\boldsymbol{x},t)I-\left[\rho(\boldsymbol{x},t)\nu\left(\boldsymbol{\nabla}\boldsymbol{u}(\boldsymbol{x},t)+(\boldsymbol{\nabla}\boldsymbol{u}(\boldsymbol{x},t))^T\right)\right].
\end{aligned} \tag{A.8}$$

Inserting the expansions (A.7) and $\boldsymbol{\nabla} = \delta \boldsymbol{\nabla}^{(1)}$ (cf. (2.22)) we see that the term in the square bracket is of first order, hence we conclude

$$\int_{\mathbb{R}^3} f^{(1)}(\boldsymbol{x}, \boldsymbol{v}, t) \left[(\boldsymbol{v} - \boldsymbol{u}(\boldsymbol{x}, t)) (\boldsymbol{v} - \boldsymbol{u}(\boldsymbol{x}, t))^T \right] \mathrm{d}\boldsymbol{v} \\ = -\left[\rho(\boldsymbol{x}, t) \nu \left(\boldsymbol{\nabla}^{(1)} \boldsymbol{u}(\boldsymbol{x}, t)^T + \left(\boldsymbol{\nabla}^{(1)} \boldsymbol{u}(\boldsymbol{x}, t)^T \right)^T \right) \right].$$

We denote the square bracket on the right hand side of (A.8) as $\Lambda(\boldsymbol{x}, t)$ and the corresponding first order term in the expansion

$$\Lambda(\boldsymbol{x}, t) = \Lambda^{(0)}(\boldsymbol{x}, t) + \delta \Lambda^{(1)}(\boldsymbol{x}, t) + \mathcal{O}(\delta^2)$$

is given by

$$\Lambda^{(1)}(\boldsymbol{x}, t) := \left[\rho(\boldsymbol{x}, t) \nu \left(\boldsymbol{\nabla}^{(1)} \boldsymbol{u}(\boldsymbol{x}, t)^T + \left(\boldsymbol{\nabla}^{(1)} \boldsymbol{u}(\boldsymbol{x}, t)^T \right)^T \right) \right].$$

Equation (A.5) then reads

$$\frac{\partial^{(2)}}{\partial t} \left(\rho(\boldsymbol{x}, t) E(\boldsymbol{x}, t) \right) = -\boldsymbol{\nabla}^{(1)} \cdot \int_{\mathbb{R}^3} \boldsymbol{v} g^{(1)}(\boldsymbol{x}, \boldsymbol{v}, t) \, \mathrm{d}\boldsymbol{v} + \Lambda^{(1)}(\boldsymbol{x}, t) : \left[\boldsymbol{\nabla}^{(1)} \boldsymbol{u}(\boldsymbol{x}, t) \right].$$

The remaining integral satisfies [26]

$$\int_{\mathbb{R}^3} \boldsymbol{v} g^{(1)}(\boldsymbol{x}, \boldsymbol{v}, t) \, \mathrm{d}\boldsymbol{v} = -\left(\rho(\boldsymbol{x}, t) \kappa \boldsymbol{\nabla}^{(1)} E(\boldsymbol{x}, t) \right),$$

where the coefficient κ is the thermal conductivity. Substitution in the preceding equation yields

$$\frac{\partial^{(2)}}{\partial t} (\rho(\boldsymbol{x}, t) E(\boldsymbol{x}, t)) = \boldsymbol{\nabla}^{(1)} \cdot \left(\rho(\boldsymbol{x}, t) \kappa \boldsymbol{\nabla}^{(1)} E(\boldsymbol{x}, t) \right) + \boldsymbol{\Lambda}^{(1)}(\boldsymbol{x}, t) : \left[\boldsymbol{\nabla}^{(1)} \boldsymbol{u}(\boldsymbol{x}, t) \right],$$

what is exactly (2.28).

A.4. Computation of $\Pi^{(2)}(\hat{\boldsymbol{x}}, \hat{t})$

The last section of the appendix aims to give an idea for the derivation of the approximation (see (2.46))

$$\Pi^{(2)}(\boldsymbol{x}, t) = \sum_{i=0}^{18} \left(\frac{\partial^{(1)}}{\partial t} + \boldsymbol{c}_i \cdot \boldsymbol{\nabla}^{(1)} \right) g_i^{(1)}(\boldsymbol{x}, t) \approx -\frac{5}{9} \tau_d \Delta^{(2)} \left(\rho(\boldsymbol{x}, t) E(\boldsymbol{x}, t) \right), \qquad (A.9)$$

which was used in section 2.3.2 to show that the numerical scheme approximately satisfies the advection-diffusion equation. The result was taken from [49] and the authors of [49] write that it follows by neglecting some appropriate terms. In the following we compute until the approximating term appears, the remaining terms are then neglected.

The time derivative can be omitted at once, due to (2.44), as one can see by

$$\begin{aligned}\Pi^{(2)}(\boldsymbol{x},t) &= \sum_{i=0}^{18} \frac{\partial^{(1)}}{\partial t} g_i^{(1)}(\boldsymbol{x},t) + \sum_{i=0}^{18} \left(\boldsymbol{c}_i \cdot \boldsymbol{\nabla}^{(1)}\right) g_i^{(1)}(\boldsymbol{x},t) \\ &= \frac{\partial^{(1)}}{\partial t} \sum_{i=0}^{18} g_i^{(1)}(\boldsymbol{x},t) + \sum_{i=0}^{18} \left(\boldsymbol{c}_i \cdot \boldsymbol{\nabla}^{(1)}\right) g_i^{(1)}(\boldsymbol{x},t) \\ &= \sum_{i=0}^{18} \left(\boldsymbol{c}_i \cdot \boldsymbol{\nabla}^{(1)}\right) g_i^{(1)}(\boldsymbol{x},t).\end{aligned}$$

In the remaining term we substitute $g_i^{(1)}(\boldsymbol{x},t)$ by

$$g_i^{(1)}(\boldsymbol{x},t) = -\tau_d \left[\frac{\partial^{(1)}}{\partial t} + \boldsymbol{c}_i \cdot \boldsymbol{\nabla}^{(1)}\right] g_i^{(0)}(\boldsymbol{x},t),$$

which follows by rearranging (2.41). Doing so we achieve

$$\begin{aligned}\Pi^{(2)}(\boldsymbol{x},t) &= -\tau_d \left[\sum_{i=0}^{18} \left(\boldsymbol{c}_i \cdot \boldsymbol{\nabla}^{(1)}\right) \frac{\partial^{(1)}}{\partial t} g_i^{(0)}(\boldsymbol{x},t) + \sum_{i=0}^{18} \left(\boldsymbol{c}_i \cdot \boldsymbol{\nabla}^{(1)}\right)\left(\boldsymbol{c}_i \cdot \boldsymbol{\nabla}^{(1)}\right) g_i^{(0)}(\boldsymbol{x},t)\right] \\ &= -\tau_d \left[\boldsymbol{\nabla}^{(1)} \frac{\partial^{(1)}}{\partial t} \cdot \sum_{i=0}^{18} \boldsymbol{c}_i g_i^{(0)}(\boldsymbol{x},t) + \sum_{i=0}^{18} \left(\boldsymbol{c}_i \cdot \boldsymbol{\nabla}^{(1)}\right)\left(\boldsymbol{c}_i \cdot \boldsymbol{\nabla}^{(1)}\right) g_i^{(0)}(\boldsymbol{x},t)\right] \\ &= -\tau_d \left[\boldsymbol{\nabla}^{(1)} \cdot \frac{\partial^{(1)}}{\partial t} \left(\rho(\boldsymbol{x},t)\boldsymbol{u}(\boldsymbol{x},t)E(\boldsymbol{x},t)\right) + \sum_{i=0}^{18} \left(\boldsymbol{c}_i \cdot \boldsymbol{\nabla}^{(1)}\right)\left(\boldsymbol{c}_i \cdot \boldsymbol{\nabla}^{(1)}\right) g_i^{(0)}(\boldsymbol{x},t)\right].\end{aligned} \tag{A.10}$$

The second term in the latter right hand side computes as follows

$$\begin{aligned}\sum_{i=0}^{18} \left(\boldsymbol{c}_i \cdot \boldsymbol{\nabla}^{(1)}\right)\left(\boldsymbol{c}_i \cdot \boldsymbol{\nabla}^{(1)}\right) g_i^{(0)}(\boldsymbol{x},t) &= \sum_{i=0}^{18} \left(\left[\boldsymbol{\nabla}^{(1)}\boldsymbol{\nabla}^{(1)T}\right] : \left[\boldsymbol{c}_i \boldsymbol{c}_i^T\right]\right) g_i^{(0)}(\boldsymbol{x},t) \\ &= \left[\boldsymbol{\nabla}^{(1)}\boldsymbol{\nabla}^{(1)T}\right] : \left[\sum_{i=0}^{18} \boldsymbol{c}_i \boldsymbol{c}_i^T g_i^{(0)}(\boldsymbol{x},t)\right]\end{aligned}$$

When using the lattice velocities (1.48) and the discrete energy equilibrium distribution

(2.37) explicitly, the following equation

$$\sum_{i=0}^{18} \boldsymbol{c}_i \boldsymbol{c}_i^T g_i^{(0)}(\boldsymbol{x}, t) = \rho(\boldsymbol{x}, t) E(\boldsymbol{x}, t) \boldsymbol{u}(\boldsymbol{x}, t) \boldsymbol{u}(\boldsymbol{x}, t)^T + \frac{5}{9} \rho(\boldsymbol{x}, t) E(\boldsymbol{x}, t) I,$$

with identity matrix I results from a straightforward computation. Thus we obtain

$$\begin{aligned}
&\sum_{i=0}^{18} \left(\boldsymbol{c}_i \cdot \boldsymbol{\nabla}^{(1)}\right) \left(\boldsymbol{c}_i \cdot \boldsymbol{\nabla}^{(1)}\right) g_i^{(0)}(\boldsymbol{x}, t) \\
&\quad = \left[\boldsymbol{\nabla}^{(1)} \boldsymbol{\nabla}^{(1)T}\right] : \left[\rho(\boldsymbol{x}, t) E(\boldsymbol{x}, t) \boldsymbol{u}(\boldsymbol{x}, t) \boldsymbol{u}(\boldsymbol{x}, t)^T + \frac{5}{9} \rho(\boldsymbol{x}, t) E(\boldsymbol{x}, t) I\right] \\
&\quad = \left[\boldsymbol{\nabla}^{(1)} \boldsymbol{\nabla}^{(1)T}\right] : \left[\rho(\boldsymbol{x}, t) E(\boldsymbol{x}, t) \boldsymbol{u}(\boldsymbol{x}, t) \boldsymbol{u}(\boldsymbol{x}, t)^T\right] + \left[\boldsymbol{\nabla}^{(1)} \boldsymbol{\nabla}^{(1)T}\right] : \left[\frac{5}{9} \rho(\boldsymbol{x}, t) E(\boldsymbol{x}, t) I\right] \\
&\quad = \left[\boldsymbol{\nabla}^{(1)} \boldsymbol{\nabla}^{(1)T}\right] : \left[\rho(\boldsymbol{x}, t) E(\boldsymbol{x}, t) \boldsymbol{u}(\boldsymbol{x}, t) \boldsymbol{u}(\boldsymbol{x}, t)^T\right] + \frac{5}{9} \Delta^{(2)} \left(\rho(\boldsymbol{x}, t) E(\boldsymbol{x}, t)\right), \qquad \text{(A.11)}
\end{aligned}$$

with scaled Laplace operator $\Delta^{(2)}$. The term we are looking for appears in the latter right hand side. After neglecting all other terms [49], we obtain

$$\Pi^{(2)}(\boldsymbol{x}, t) = -\frac{5}{9} \tau_d \Delta^{(2)} \left(\rho(\boldsymbol{x}, t) E(\boldsymbol{x}, t)\right).$$

References

[1] F. J. Alexander, S. Chen, and J. D. Sterling. Lattice Boltzmann thermohydrodynamics. *Physical Review E*, 47(4):R2249–R2252, April 1993.

[2] J. Bernsdorf, T. Zeiser, G. Brenner, and F. Durst. Simulation of a 2D Channel Flow Around a Square Obstacle with Laittce Boltzmann (BGK) Automata. *International Journal of Modern Physics C*, 9(8):1129–1141, 1998.

[3] P. L. Bhatnagar, E. P. Gross, and M. Krook. A Model for Collision Processes in Gases. I. Small Amplitude Processes in Charged and Neutral One-Component Systems. *Physical Review*, 94(3):511–525, May 1954.

[4] H. Bruus. *Theoretical Microfluidics*. Oxford University Press, 2008.

[5] C. Cercignani. *The Boltzmann equation and its applications*. Springer Verlag, New York, USA, 1988.

[6] C. Cercignani. *Rarefied gas dynamics: from basic concepts to actual calculations*. Cambridge University Press, Cambridge, UK, 2000.

[7] S. Chapman and T. Cowling. *The Mathematical Theory of Non-Uniform Gases*. Cambridge University Press, London, UK, 1970.

[8] S. Chen, H. Chen, D. Martínez, and W. Matthaeus. Lattice Boltzmann model for simulation of magnetohydrodynamics. *Physical Review Letters*, 67(27):3776–3779, Dec 1991.

[9] S. Chen, K. Diemer, G. D. Doolen, K. Eggert, C. Fu, S. Gutman, and B. J. Travis. Lattice gas automata for flow through porous media. *Physica D: Nonlinear Phenomena*, 47(1-2):72–84, 1991.

[10] S. Chen and G. D. Doolen. Lattice Boltzmann Method for Fluid Flows. *Annual Review of Fluid Mechanics*, 30(1):329–364, 1998.

[11] S. Chen, D. Martinez, and R. Mei. On boundary conditions in lattice Boltzmann methods. *Physics of Fluids*, 8(9):2527–2536, 1996.

[12] B. Chopard and A. Dupuis. A Mass Conserving Boundary Condition for Lattice Boltzmann Models. *International Journal of Modern Physics B*, 17:103–107, 2003.

[13] A. J. Chorin. Numerical Solution of the Navier-Stokes Equations. *Mathematics of Computation*, 22(104):745–762, 1968.

[14] I. G. Currie. *Fundamental mechanics of fluids*. Marcel Dekker Inc., 2003 - 3rd Edition.

[15] C. Curtiss, J. Hirschfelder, and B. Bird. *Molecular Theory of Gases and Liquids*. Wiley, New York, USA, 1954 (revised 1964).

[16] C. R. Doering and J. Gibbon. *Applied analysis of the Navier-Stokes equations*. Cambridge University Press, 1995.

[17] P. G. Drazin. *Introduction to Hydrodynamic Stability*. Cambridge University Press, 2002.

[18] S. Eliezer. *The interaction of high-power lasers with plasmas*. IOP Publishing Ltd, Bristol, UK, 2002.

[19] C. Fletcher. *Computational Techniques for Fluid Dynamics: Fundamental and general techniques*. Springer Verlag, Berlin, Germany, 2005.

[20] U. Frisch, B. Hasslacher, and Y. Pomeau. Lattice-Gas Automata for the Navier-Stokes Equation. *Physical Review Letters*, 56(14):1505–1508, Apr 1986.

[21] A. V. Getling. *Rayleigh-Bénard convection: Structures and Dynamics*. World Scientific, 1998 (2001).

[22] A. K. Gunstensen, D. H. Rothman, S. Zaleski, and G. Zanetti. Lattice Boltzmann model of immiscible fluids. *Physical Review A*, 43(8):4320–4327, Apr 1991.

[23] Z. Guo and T. S. Zhao. Lattice Boltzmann model for incompressible flows through porous media. *Physical Review E*, 66(3):036304, Sep 2002.

[24] Z. Guo, C. Zheng, and B. Shi. Discrete lattice effects on the forcing term in the lattice Boltzmann method. *Physical Review E*, 65(4):046308, Apr 2002.

[25] J. Hardy, Y. Pomeau, and O. de Pazzis. Time evolution of a two-dimensional model system. I. Invariant states and time correlation functions. *Journal of Mathematical Physics*, 14(12):1746–1759, 1973.

[26] X. He, S. Chen, and G. D. Doolen. A novel thermal model for the lattice Boltzmann method in incompressible limit. *Journal of Computational Physics*, 146(1):282–300, 1998.

[27] X. He and L.-S. Luo. Lattice Boltzmann Model for the Incompressible Navier Stokes Equation. *Journal of Statistical Physics*, 88:927–944, August 1997.

[28] X. He and L.-S. Luo. Theory of the lattice Boltzmann method: From the Boltzmann equation to the lattice Boltzmann equation. *Physical Review E*, 56(6):6811–6817, Dec 1997.

[29] X. He, Q. Zou, L.-S. Luo, and M. Dembo. Analytic solutions of simple flows and analysis of nonslip boundary conditions for the lattice Boltzmann BGK model. *Journal of Statistical Physics*, 87(1-2):115–136, 1997.

[30] D. Hänel. *Molekulare Gasdynamik*. Springer Verlag, 2004.

[31] R. Holme and D. H. Rothman. Lattice-gas and lattice-Boltzmann models of miscible fluids. *Journal of Statistical Physics*, 68:409–429, 1992.

[32] S. Hou, Q. Zou, S. Chen, G. Doolen, and A. C. Cogley. Simulation of cavity flow by the lattice Boltzmann method. *Journal of Computational Physics*, 118(2):329–347, 1995.

[33] J. Koelman. A Simple Lattice Boltzmann Scheme for Navier-Stokes Fluid Flow. *Europhysics Letters*, 15(6):603–607, 1991.

[34] M. Kutrib, R. Vollmar, and T. Worsch. Introduction to the special issue on cellular automata. *Parallel Computing*, 23(11):1567–1576, 1997.

[35] J. Latt, B. Chopard, O. Malaspinas, M. Deville, and A. Michler. Straight velocity boundaries in the lattice Boltzmann method. *Physical Review E*, 77(5):056703, May 2008.

[36] E. Laurien and H. Oertel. *Numerische Strömungsmechanik*. Vieweg Teubner, Wiesbaden, Germany, 2009 (3rd edition).

[37] C. Y. Lim, C. Shu, X. D. Niu, and Y. T. Chew. Application of lattice Boltzmann method to simulate microchannel flows. *Physics of Fluids*, 14(7):2299–2308, 2002.

[38] R. S. Maier, R. S. Bernard, and D. W. Grunau. Boundary conditions for the lattice Boltzmann method. *Physics of Fluids*, 8(7):1788–1801, 1996.

[39] N. S. Martys and H. Chen. Simulation of multicomponent fluids in complex three-dimensional geometries by the lattice Boltzmann method. *Physical Review E*, 53(1):743–750, Jan 1996.

[40] G. R. McNamara, A. L. Garcia, and A. B. J. Stabilization of thermal lattice Boltzmann models. *Journal of Statistical Physics*, 81(1-2):395–408, October 1995.

[41] G. R. McNamara, A. L. Garcia, and A. B. J. A Hydrodynamically Correct Thermal Lattice Boltzmann Model. *Journal of Statistical Physics*, 87(5-6):1111–1121, June 1997.

[42] G. R. McNamara and G. Zanetti. Use of the Boltzmann Equation to Simulate Lattice-Gas Automata. *Physical Review Letters*, 61(20):2332–2335, Nov 1988.

[43] R. Mei, L.-S. Luo, and W. Shyy. An Accurate Curved Boundary Treatment in the Lattice Boltzmann Method. *Journal of Computational Physics*, 155(2):307–330, 1999.

[44] R. Mei, W. Shyy, and D. Yu. Lattice Boltzmann Method for 3-D Flows with Curved Boundary. *Journal of Computational Physics*, 161:680–699, 2000.

[45] R. Nourgaliev, T. Dinh, T. Theofanous, and D. Joseph. The lattice Boltzmann equation method: theoretical interpretation, numerics and implications. *International Journal of Multiphase Flow*, 29:117–169, Jan 2003.

[46] A. Parmigiani, C. Huber, B. Chopard, J. Latt, and O. Bachmann. Application of the multi distribution function lattice Boltzmann approach to thermal flows. *The European Physical Journal - Special Topics*, 171(1):37–43, 2009.

[47] P. Pavlo, G. Vahala, and L. Vahala. Higher Order Isotropic Velocity Grids in Lattice Methods. *Physical Review Letters*, 80(18):3960–3963, May 1998.

[48] Y. Peng, C. Shu, and Y. T. Chew. Simplified thermal lattice Boltzmann model for incompressible thermal flows. *Physical Review E*, 68(2):026701–026709, Aug 2003.

[49] Y. Peng, C. Shu, and Y. T. Chew. A 3D incompressible thermal lattice Boltzmann model and its application to simulate natural convection in a cubic cavity. *Journal of Computational Physics*, 193(1):260–274, 2004.

[50] W. Polifke and J. Kopitz. *Wärmeübertragung: Grundlagen, analytische und numerische Methoden.* Pearson Studium, 2009.

[51] Y. Qian, D. d'Humieres, and P. Lallemand. Lattice BGK Models for Navier-Stokes Equation. *Europhysics Letters*, 17(6):479–484, 1992.

[52] L. Quartapelle. *Numerical solution of the incompressible Navier-Stokes equations.* Birkhäuser Verlag, Basel, Switzerland, 1993.

[53] P. Raiskinmäki, A. Shakib-Manesh, A. Jäsberg, A. Koponen, J. Merikoski, and J. Timonen. Lattice-Boltzmann Simulation of Capillary Rise Dynamics. *Journal of Statistical Physics*, 107:143–158, 2002.

[54] L. Saint-Raymond. *Hydrodynamic Limits of the Boltzmann Equation.* Springer Verlag, Berlin, Germany, 2009.

[55] X. Shan. Simulation of Rayleigh-Bénard convection using a lattice Boltzmann method. *Physical Review E*, 55(3):2780–2788, Mar 1997.

[56] X. Shan and H. Chen. Lattice Boltzmann model for simulating flows with multiple phases and components. *Physical Review E*, 47(3):1815–1819, Mar 1993.

[57] X. Shan and G. Doolen. Diffusion in a multicomponent lattice Boltzmann equation model. *Physical Review E*, 54(4):3614–3620, Oct 1996.

[58] P. A. Skordos. Initial and boundary conditions for the lattice Boltzmann method. *Physical Review E*, 48(6):4823–4842, Dec 1993.

[59] V. Sofonea and R. F. Sekerka. Viscosity of finite difference lattice Boltzmann models. *Journal of Computational Physics*, 184(2):422–434, 2003.

[60] J. Spurk and N. Aksel. *Strömungslehre*. Springer Verlag, 2007.

[61] S. Succi. *The Lattice Boltzmann Equation for Fluid Dynamics and Beyond*. Oxford University Press, Oxford, UK, 2001.

[62] M. C. Sukop and D. Or. Lattice Boltzmann method for modeling liquid-vapor interface configurations in porous media. *Water Resources Research*, 40:W01509, 2004.

[63] M. C. Sukop and D. T. Thorne Jr. *Lattice Boltzmann Modeling: An Introduction for Geoscientists and Engineers*. Springer Publishing Company, Incorporated, 2007.

[64] M. R. Swift, E. Orlandini, W. R. Osborn, and J. M. Yeomans. Lattice Boltzmann simulations of liquid-gas and binary fluid systems. *Physical Review E*, 54(5):5041–5052, Nov 1996.

[65] R. Temam. *Navier-Stokes equations: theory and numerical analysis*. AMS Chelsea Publishing, Providence, RI, USA, 2001.

[66] J. von Neumann. *Theory of Self-Reproducing Automata*. University of Illinois Press, Champaign, IL, USA, 1966.

[67] L. Wagner and F. Hayot. Lattice Boltzmann simulations of flow past a cylindrical obstacle. *Journal of Statistical Physics*, 81(1-2):63–70, 1995.

[68] X. Wei, X. Li, K. Mueller, and A. Kaufmann. The Lattice-Boltzmann Method for Simulating Gaseous Phenomena. *IEEE Trans. Visualization and Computer Graphics*, 10(2):164–176, 2004.

[69] D. Wolf-Gladrow. *Lattice-Gas Cellular Automata and Lattice Boltzmann Models*. Springer Verlag, Berlin, Germany, 2000.

[70] S. Wolfram. *A new kind of science*. Wolfram Media, Champaign, IL, USA, 2002.

[71] G. Zanetti. Hydrodynamics of lattice-gas automata. *Physical Review A*, 40(3):1539–1548, Aug 1989.

[72] Q. Zou and X. He. On pressure and velocity boundary conditions for the lattice Boltzmann BGK model. *Physics of Fluids*, 9(6):1591–1598, 1997.